TECHNICAL REPORT NO. 3

ANALYSIS OF STRUCTURES IN JOINTED ROCK

RESEARCH ON ROCK BOLT REINFORCEMENT AND INTEGRAL LINED TUNNELS

SEPTEMBER, 1967

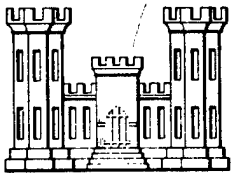

OMAHA DISTRICT, CORPS OF ENGINEERS
OMAHA, NEBRASKA 68102

THIS RESEARCH HAS BEEN FUNDED BY OFFICE, CHIEF OF ENGINEERS AND THE DEFENSE ATOMIC SUPPORT AGENCY

PREPARED UNDER DACA-45-67-C-0015 by
RICHARD E. GOODMAN, BERKELEY CAIFORNIA

Destroy this report when no longer needed. Do not return it to the originator.

The findings in this report are not to be construed as an offical Department of the Army position unless so designated by other authorized documents.

TECHNICAL REPORT NO. 3

ANALYSIS OF STRUCTURES IN JOINTED ROCK

RESEARCH ON ROCK BOLT REINFORCEMENT AND INTEGRAL LINED TUNNELS

September, 1967

Sponsored by

OFFICE, CHIEF OF ENGINEERS
and
DEFENSE ATOMIC SUPPORT AGENCY

Under

Department of the Army, Military Construction and Investigational Programs, Sub-Projects I-4 and II-2

and

DASA Subtasks NWER 13.191 D.2 and NWER 13.191 E.3

Conducted for

OMAHA DISTRICT, CORPS OF ENGINEERS
Omaha, Nebraska 68102

Under

Contract DACA-45-67-C-0015

by

RICHARD E. GOODMAN, BERKELEY, CALIFORNIA

ABSTRACT

Two approaches to finite element analysis of the effects of rock joints and fractures on underground unlined, lined, or reinforced tunnel openings are considered. First, a three-dimensional ubiquitous joint analysis is described and applied to tunnel design. Although this approach allows an estimate of the weakening effect of closely spaced joint sets, it is based on the assumption that the existence of a joint does not alter the stress distribution significantly. Since this may not always be a satisfactory assumption and because it may sometimes be desirable to model the action of individual joints occurring in determined locations, a new rock joint representation is developed and a joint stiffness analysis applied to a series of basic problems. The different types of rock joints and their relative significance are discussed and a classification system based on shear strength of the joint, stiffness perpendicular to the joint and tangential stiffness of the joint is suggested.

Using a finite element axisymmetric program, states of stress in the rock due to single and multiple rock bolt installation are examined and iso-stress maps of the triaxial compression zones are shown. States of stress in the vicinity of the rock bolt anchor and bearing plate are investigated. The effectiveness of a single rock bolt installation to strengthen rock joints of various orientations is investigated.

In a very preliminary study, the theory of a layered orthographic shell was coded using a finite element plane strain representation. An evaluation of the load resisting capability of various tunnel linings incorporating different types of stiffeners was made. Further analytical work is recommended.

PREFACE

This investigation was authorized by the Chief of Engineers (ENGMC-EM) and was performed in FY 1967 under Contract No. DACA45-67-C-0015 between the Omaha District, Corps of Engineers and Dr. Richard E. Goodman, Berkeley, California.

O&M Army funds were used for the investigation to meet the objectives outlined in Sub-Project I-4, "Redistribution of Stress in Rock Bolt Systems" and Sub-Project II-2, "Investigation of Integral Tunnel Liners" of the OCE Missiles and Protective Structures Branch Long Range Program for Facilities Investigations and Studies, FY 1967-1971. Funds for monitoring the contract work were provided by the Defense Atomic Support Agency under Subtask NWER 13.191 D.2, "Strengthening of Rock Against Shock Effects" and 13.191 E.3, "Response of Lined Openings".

This report was prepared under the supervision of Dr. R. E. Goodman, Principal Investigator. Personnel contributing to the report were Dr. Robert L. Taylor, Dr. Tor Brekke, Dr. Hans Ewoldson, Gerald Goodreau, Micheal Cleary, Jan Roggeveen, and Fred Sage.

During the work period covered by this report, Colonel Harold J. St. Clair was District Engineer, succeeeded by Colonel William H. McKenzie III; Charles L. Hipp was Chief, Engineering Division; C. J. Distefano was technical monitor for the Omaha District under the general supervision of A. H. Bauman, Chief, Protective Structures Branch. N. G. Gulbranson and R. G. Dodson participated in the monitoring work.

TABLE OF CONTENTS

Table of Contents - continued

Table of Contents - continued

Table of Contents - continued

Table of Contents - continued

Table of Contents - continued

ANALYSIS OF STRUCTURES IN JOINTED ROCK

1. INTRODUCTION

This is a report of an investigation performed under Contract No. DACA 45-67-C-0015 between the Corps of Engineers Omaha District and Dr. Richard E. Goodman as contractor. It describes results of research on analysis techniques performed during the period October 6, 1966 to June 30, 1967. This work was not specifically tied to any project but is an outgrowth of previous analytical work on the Piledriver Project under Contract DA-25-066-ENG-14783 completed June 30, 1966. Further, in continuation of the work reported here, an effort will be made to match observed structural performance in the Piledriver test with measured material properties. Thus, many of the examples and illustrations have been developed with rock and joint parameters and loading conditions representative of the Piledriver test. Frequent reference is made to the final report of the previous contract (1).

In the previous contract the principal investigator studied the effect of geological factors on the behavior of several experimental tunnel sections of the Piledriver test. Particular attention was paid to the effect of closely spaced joint planes on the strength of a tunnel under static load. The strengthening effect of rock bolts and of composite steel - concrete liners were also considered.

---

1. Goodman, R. E., Geological Factors in Design of Blast Resistant Tunnels - Piledriver Project, U.S. Army Engineer District Omaha, Technical Report No. 2, Sept. 1966.

Because the previous contract was of relatively short duration and specific direction, a single course was pursued in the performance of the work. It is the objective of this report to probe the analysis possibilities more deeply to develop a viable technique for predicting or back calculating structural behavior in jointed rock.

The report is divided into three sections. Section 2 deals with the analysis of jointed rock, Section 3 is concerned with the action of rock bolt reinforcement, and Section 4 develops analytical tools for evaluation of steel liners.

2. ANALYSIS OF JOINTS AND FRACTURES

2.1 GENERAL

The importance of weakness surfaces on the mechanics of rock is self evident. The technology of prediction and description of joints and fractures has, until recently, exceeded the technology of analysis. In this section two approaches to analysis of the effect of joints and fractures will be considered. A three-dimensional ubiquitous joint analysis will be described and applied to tunnel design. Then a quite different joint stiffness analysis will be developed and applied to a series of basic problems. Finally, the question of joint classification will be discussed.

2.2 THE UBIQUITOUS JOINT ANALYSIS

(1) Two-Dimensional Analysis - Previous Work

In previous work on the Piledriver project, the importance of rock joints on the probable behavior of the test drifts was stated and a method was devised to make a behavior prediction. This method we have come to call the ubiquitous joint analysis. It involved the calculation of the area around a tunnel within which the traction across a joint of fixed orientation and given cohesion and friction is sufficient to induce sliding along or opening of the joint. The area of possible slip on joints was found to be vastly larger than the area of rock crushing calculated assuming continuous rock.

The ubiquitous joint analysis assumed (1) that the orientation of joints in a set can be measured with precision and (2) that a joint of a given set occurs everywhere. In fact the analysis may be termed one of anisotropic strength wherein failure is governed by two independent parameters -- stress orientation and stress intensity. An important result of the first study was the clear separation of the influence of (1) the orientation and (2) magnitude of the principal stresses.

A joint is stable which has traction in the compressive sense directed within the cone of static friction centered about its normal. Therefore, regions in a loaded rock body in which the joints are so oriented relative to the stress trajectories will never slip on the joints even if the intensity of stresses is large. As discussed in the previous report,* the cone of static friction centered about the normal to a joint has a vertex angle 2 φ_j, where φ_j is the joint angle of friction, if the principal stress ratio is 0. The cone containing the set of admissable traction directions across the joint has a smaller vertex angle if the principal stress ratio is negative (i.e. one stress tensile) going to 0 as the principal stress ratio goes to $-\infty$. As the principal stress ratio increases positively, the cone widens until it contains the whole joint at a principal stress ratio equal to $\text{ctn}^2\ (45 + \varphi_j/2)$.

According to the stress trajectories developed by a given loading, a bounded or partly bounded slip zone is defined. For very large applied pressures, or a very deep tunnel, the full zone of slip is developed for a given joint orientation and strength equation. At lesser pressures, or lesser depths, only a part of the slip zone is developed. The concept of a zone of slip is similar to Terzaghi's concept of arching in blocky ground. Beyond a certain depth corresponding to development of the full extent

---

*Cited on page 1.

of the "ground arch", the pressures on tunnel supports cease to increase. Similarly, beyond a given pressure, corresponding to full development of the slip zone, the mass of loosened rock ceases to augment.

A conclusion of the previous study was that the maximum extent of the slip zone is independent of joint cohesion, but depends simply on joint friction and, of course, on the ratio of stresses in the free field. The extent of the zone of slip for any pressure insufficient to fill out the maximum zone depends on the joint cohesion but can be expressed in dimensionless terms.

The result of the ubiquitous joint analysis was a diagram delimiting a zone about the tunnel in which joints of a given set would tend to slip. Whether these zones would be unstable depends in fact on whether any joints of the set actually occur in the zone of slip, i.e. on the actual joint spacing relative to the tunnel size. One can consider the calculated slip zone for a given joint as an influence diagram expressing the region around the tunnel in which the joint has an influence on stability. The application of the influence diagram demands close attention to the geological map which may indicate the actual spacings and surface conditions of each set of joints.

The stability of the slip zone also depends on the kinematic possibility of slip, i.e. on the existence of joints of other sets in a position to open. It is not generally theoretically sound to conclude that a zone of overlap of the influence diagrams of two existing sets of joints is a zone of slip on both sets simultaneously. This would only be strictly true if the sets were orthogonal. If the joints are not orthogonal, static equilibrium of the joint bounded block demands change in the resisting force mobilizing along each joint from the magnitude of the traction calculated assuming only one set to exist (1). However, as a method of application

---

1. Goodman, R. E. and Taylor, R. L., Proc. Eighth Symp. on Rock Mechanics, Sept. 1966 (in press).

it seems reasonable to direct close attention to any region of the tunnel showing overlap of the influence diagrams computed for two actually occurring joint sets. For in the zone of overlap kinematics and statics offer the possibility for movement of joint blocks.

A method of tunnel design can be developed from the ubiquitous joint concept. This will be discussed later.

(2) The Three-Dimensional Ubiquitous Joint

A major weakness of the analysis presented in the previous report is its limitation to two dimensions. Joint orientations were expressed in terms of their trace in the plane normal to the tunnel. There is no question that this simplification is artificial for the actual joint orientations are three-dimensional relative to the tunnel except for occasional fortuitous cases. The effect of the third dimension will now be considered.

The ubiquitous joint analysis consists of finding the normal and shear stress on the joint of given orientation at each point around the loaded area or tunnel and comparing these values to the maximum admissable values corresponding to a straight line Mohr envelope for the joint strength:

$$\tau = c_j + \sigma \tan \varphi_j \qquad (2\text{-}1)$$

In two dimensions, by substituting for σ and τ, an explicit formula was derived defining the major principal stress at the moment of slip, σ_{1_f}, on a joint oriented at ω relative to the maximum principal plane with principal stress ratio $\sigma_3/\sigma_1 = k$.

$$\sigma_{1_f} = \frac{2\, c_j / \tan \varphi_j}{\frac{\sin (|2\, \omega| - \varphi_j)}{\sin \varphi_j} (1 - k) - (1 + k)} \qquad (2\text{-}2)$$

At each point in a varying stress field, k is defined so the strength at each point can be determined. An advantage of this explicit strength equation is that the maximum dimensions of the zone of slip can be expressed entirely as a function of the principal stress ratio variation throughout the region.

In the case of three dimensions, expressions for σ and τ may be written in terms of the direction cosines of the normal to the joint plane and the stress components. Adopting x, y, and z axes in the σ_x, σ_y, and σ_z directions respectively, the normal stress is

$$\sigma = \ell^2 \sigma_x + m^2 \sigma_y + n^2 \sigma_z + 2\, m\, n\, \tau_{yz} + 2\, n\, \ell\, \tau_{zx} + 2\, \ell\, m\, \tau_{xy} \qquad (2\text{-}3)$$

The resultant traction across the plane is R given by

$$R^2 = (\ell\, \sigma_x + m\, \tau_{yx} + n\, \tau_{zx})^2 + (\ell\, \tau_{xy} + m\, \sigma_y + n\, \tau_{zy})^2 + (\ell\, \tau_{xz} + m\, \tau_{yz} + n\, \sigma_z)^2$$

The maximum shear τ is thus

$$\tau = \sqrt{R^2 - \sigma^2} \qquad (2\text{-}4)$$

The direction cosines for a given joint may be calculated from the bearing and dip of the joint relative to the axis of a tunnel. We will adopt the x, z plane as the plane of the tunnel with the x axis horizontal and the z axis vertical. The y axis is in the direction of the tunnel axis. Then

the direction cosines of a given joint are

$$\begin{aligned} \ell &= \cos\delta \sin\omega \\ m &= \cos\delta \cos\omega \\ n &= \sin\delta \end{aligned} \qquad (2\text{-}5)$$

where ω is the bearing of the normal to the plane relative to the tunnel axis and δ is the dip of the normal to the plane.

Unfortunately substitution of Equations 2-3 and 2-4 in Equation 2-1 does not yield a tractable equation which could be solved to express σ_{1_f} explicitly in terms of k for the three-dimensional case in the manner of Equation 2-2 for the two-dimensional case. Thus a different method of approach was followed to locate the boundary of the zone of slip for any given loading. The normal and shear stresses on the plane were calculated at each point of the region. The strength, S, of the plane at each point was calculated from the known normal stress. The boundary of the zone of slip was then drawn as the locus of points where the calculated strength equals the shear stress, τ.

There is a temptation to regard the ratio of S to τ as a "factor of safety" for each point. This is not useful, however, as S/τ of say 1.1 at a point in a body loaded to say 1,000 psi may remain a factor of safety of 1.1 even when the loading is increased to 10,000 psi. This behavior is due to the fact that joint strength depends on joint orientation as well as stress magnitude.

Despite this difficulty, the maximum extent of the zone of slip can be found easily. It is the boundary of the zone of slip at infinite applied pressure. In practise, to delimit the full zone of slip, a pressure of 100,000 psi was applied to the test tunnel at the desired free field principal stress ratio.

(3) Comparison of Two-Dimensional and Three-Dimensional Analysis

The two-dimensional ubiquitous joint may be considered a special case of the three-dimensional joint which lies parallel to the tunnel axis (y axis). To assess the importance of considering the third dimension, the magnitude of the slip zone will be compared for a two-dimensional joint of given slope in the tunnel cross section (x, z plane) and the family of three-dimensional joints having the same trace in the tunnel cross section (Fig. 2-1). This family can be generated by rotating about the xz trace; i.e. by finding the set of direction cosines of all planes whose intersection with the plane $y = 0$ is the straight line $z = Sx$. We require intersection of the plane

$$Ax + By + Cz = 0 \tag{2-5}$$

with the plane

$$y = 0 \tag{2-6}$$

obeying the constraint

$$z = Sx \tag{2-7}$$

Simultaneous solution of these equations yields the equation of the required planes as

$$Ax + By - \frac{A}{S} z = 0 \tag{2-8}$$

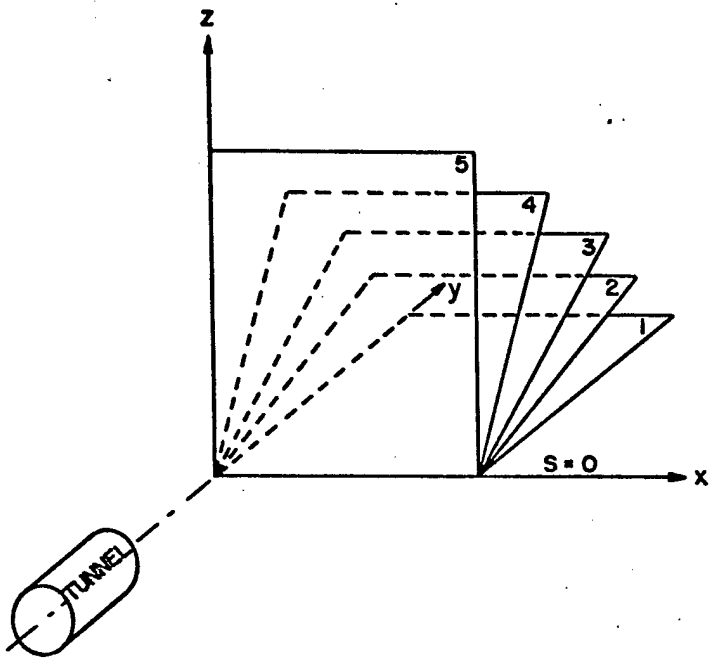

FIGURE 2-1a SEVERAL PLANES OF THE FAMILY APPEARING HORIZONTAL (S=0) IN THE TUNNEL CROSS SECTION (x z PLANE).

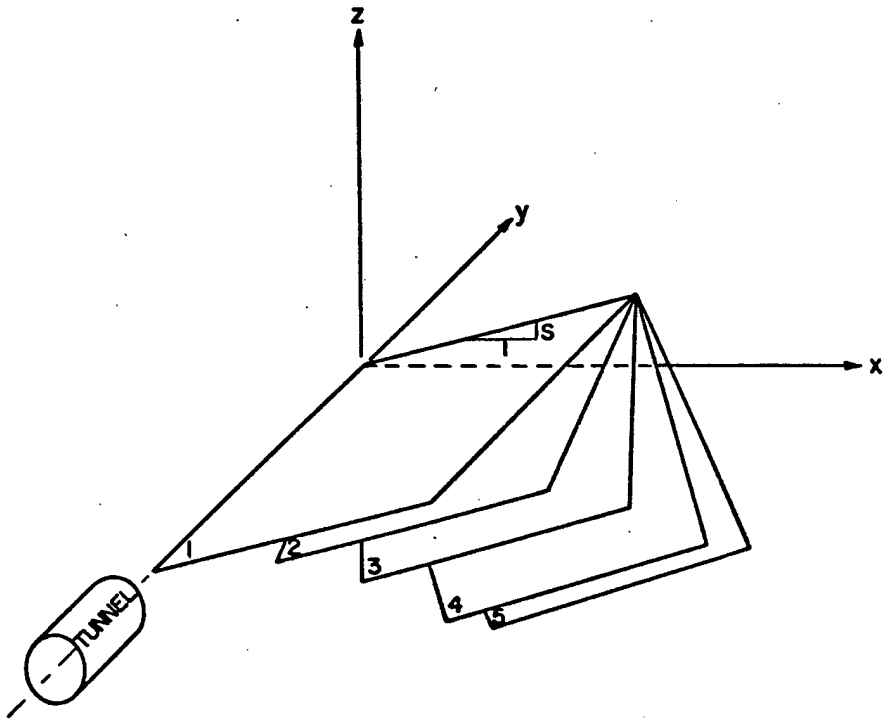

FIGURE 2-1b SEVERAL PLANES OF THE FAMILY APPEARING AS LINES WITH SLOPE S IN THE TUNNEL CROSS SECTION (x z PLANE).

The direction cosines of the normal to the family of planes therefore obey the law

$$\ell = S\,n \tag{2-9}$$

Since $\ell^2 + m^2 + n^2 = 1$

$$n = \sqrt{\frac{1 - m^2}{1 + s^2}} \tag{2-10}$$

Equations 2-9 and 2-10 define the members of the family of planes passing through a line of slope S in the tunnel cross section. To generate any member of the family, one may fix m at the desired value, and calculate ℓ and n. Table 2-1 presents values of ℓ and n corresponding to 10^o increments in values of $\beta = \cos^{-1} m$ for joints at 0^o, 30^o, 60^o, and 90^o as seen in the tunnel cross section. β is defined as the angle of the joint normal with the y axis (tunnel axis).

A joint considered in the two-dimensional analysis is, in reality, a three-dimensional joint with $\beta = 90^o$, as for example joint plane 1 in Figures 2.1a and 2.1b. To assess the effect of ignoring the third dimension, the slip zones on joints of a given trace in the tunnel cross section were calculated for β in 10^o increments from 90^o to 0^o, i.e. on all the joint planes of Table 2-1. The results are presented in Figures 2.2 to 2.9.

In these figures, the Kirsch solution to the plane problem of stresses about a tunnel was used. Since the conditions are those of plane strain, the longitudinal stress, σ_y, is at any point $(\nu)\ (\sigma_x + \sigma_z)$. In the case of a plane blast wave travelling across the tunnel in the x direction, confinement in the wave front leads to not only a z applied pressure but a y applied pressure as well, i.e. the wave exerts a longitudinal pressure on the tunnel. As a simplifying assumption, we have assumed that the longitudinal

TABLE 2-1. Direction Cosines for Families of Joints Having Given Inclinations in the Tunnel Cross Section

(Upward Normal Considered Positive, See Figure 2-13b)

Angle of joint with horizontal as seen in tunnel cross section	Direction cosines of normal to joint	β - angle of joint normal with tunnel axis									
		90°	80°	70°	60°	50°	40°	30°	20°	10°	0°
0°	ℓ	0.000	0.000	0.000	0.000	0.000	0.000	0.000	0.000	0.000	0.000
	m	0.000	0.174	0.342	0.500	0.643	0.766	0.866	0.940	0.985	1.000
	n	1.000	0.985	0.949	0.866	0.766	0.643	0.500	0.342	0.174	0.000
30°	ℓ	-0.500	-0.493	-0.470	-0.433	-0.383	-0.322	-0.250	-0.171	-0.087	0.000
	m	0.000	0.174	0.342	0.500	0.643	0.766	0.866	0.940	0.985	1.000
	n	0.866	0.853	0.814	0.750	0.663	0.557	0.433	0.296	0.150	0.000
60°	ℓ	-0.866	-0.853	-0.814	-0.750	-0.663	-0.557	-0.433	-0.296	-0.150	0.000
	m	0.000	0.174	0.342	0.500	0.643	0.766	0.866	0.940	0.985	1.000
	n	0.500	0.493	0.470	0.433	0.383	0.322	0.250	0.171	0.087	0.000
90°	ℓ	-1.000	-0.985	-0.940	-0.866	-0.766	-0.643	-0.500	-0.342	-0.174	0.000
	m	0.000	0.174	0.342	0.500	0.643	0.766	0.866	0.940	0.985	1.000
	n	0.000	0.000	0.000	0.000	0.000	0.000	0.000	0.000	0.000	0.000
-30°	ℓ	0.500	0.493	0.470	0.433	0.383	0.322	0.250	0.171	0.087	0.000
	m	0.000	0.174	0.342	0.500	0.643	0.766	0.866	0.940	0.985	1.000
	n	0.866	0.853	0.814	0.750	0.663	0.557	0.433	0.296	0.150	0.000
-60°	ℓ	0.866	0.853	0.814	0.750	0.663	0.556	0.433	0.296	0.150	0.000
	m	0.000	0.174	0.342	0.500	0.643	0.766	0.866	0.940	0.985	1.000
	n	0.500	0.493	0.470	0.433	0.383	0.322	0.250	0.171	0.087	0.000

applied pressure, p_y, is not concentrated around the tunnel. In Figures 2-6 to 2-9, the applied longitudinal pressure of p_y, as well as the quantity (ν) $(\sigma_x + \sigma_z)$ has been added to the stress system in calculating the ubiquitous joint slip zones. In a two dimensional analysis, of course, all joints parallel the tunnel axis so longitudinal stress need not be considered.

When no applied longitudinal pressure is considered, Figures 2-2 to 2-5 show that the effect of the third dimension is (1) to spread the influence of joints more evenly around the tunnel and (2) to reduce the magnitude of the slip zone particularly at low pressures. In no case does the influence of a joint increase when the joint is rotated away from parallelism with the tunnel axis. In all cases, the slip zone becomes insignificant when the angle of the joint normal with the tunnel axis is less than about 30°. (The angle of joint friction assumed in compiling these diagrams was 31°.) It can be concluded that a joint set which strikes nearly athwart the tunnel has little or no influence unless it dips at a flat angle.

The 90° joint has its greatest influence at about 20° of the wall. A 60° joint has two influence zones, a larger one at -40° and a smaller zone developing at springline at the higher pressures. The 30° joint is important at $+60^{\circ}$ and -60°. The 0° joint is important at $+40^{\circ}$ and -40°. In the case of a vertical blast or gravity acceleration, the coordinate axes should be rotated through 90°. Thus a 0° joint is a horizontal joint in the horizontal blast problem but a vertical joint in the gravity or vertical blast problem.

Failure to include an applied longitudinal pressure in the blast problem leads to the following conclusions, as evidenced by Figures 2-6 to 2-9. The joint striking parallel to the tunnel axis is, of course,

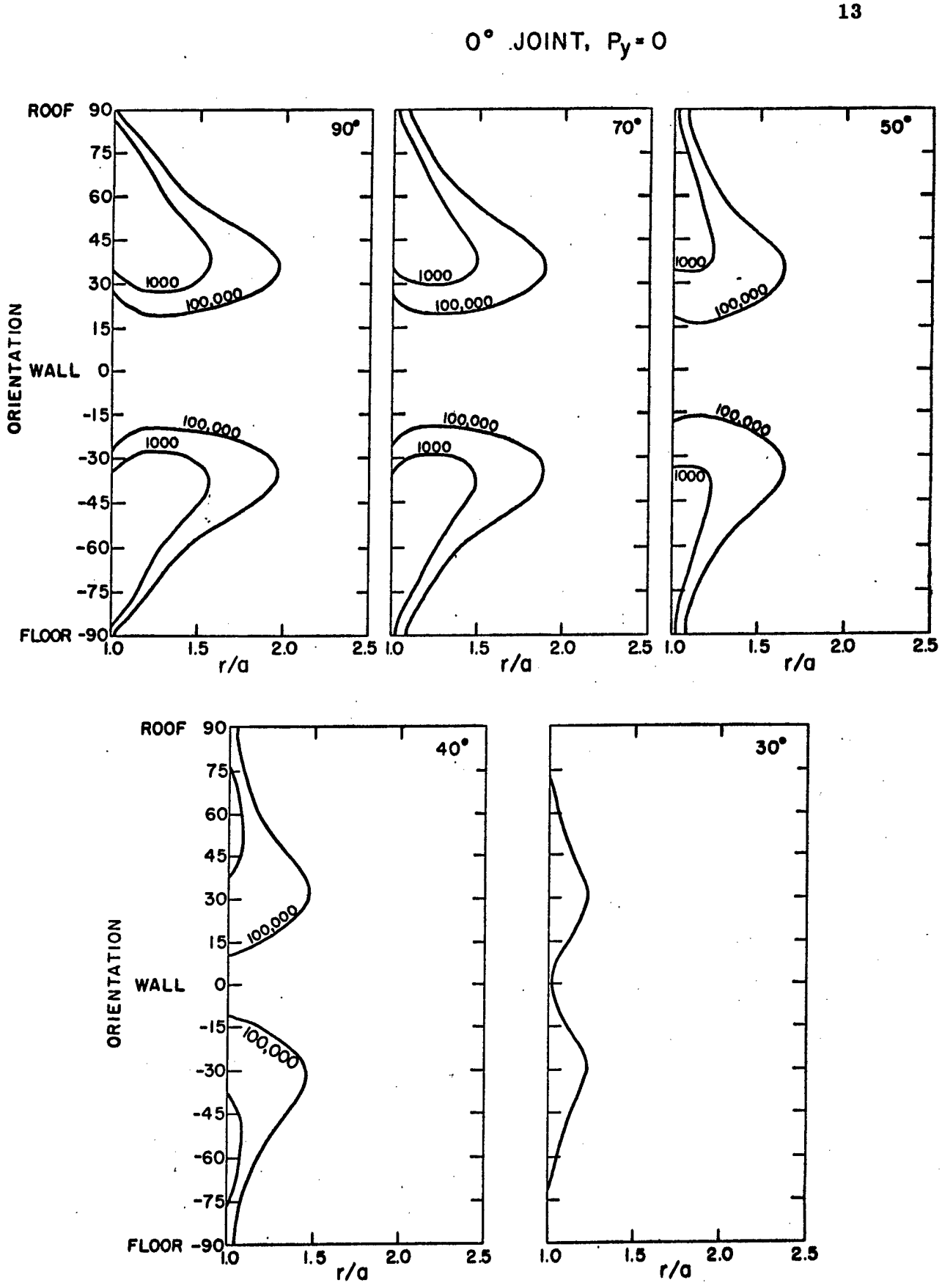

Fig. 2-2. Joint Influence Diagrams

Horizontal applied pressure, $p_2/p_1 = 0.43$.

Contour values are to be multiplied by $\frac{c}{100}$, where c is the joint cohesion in psi.

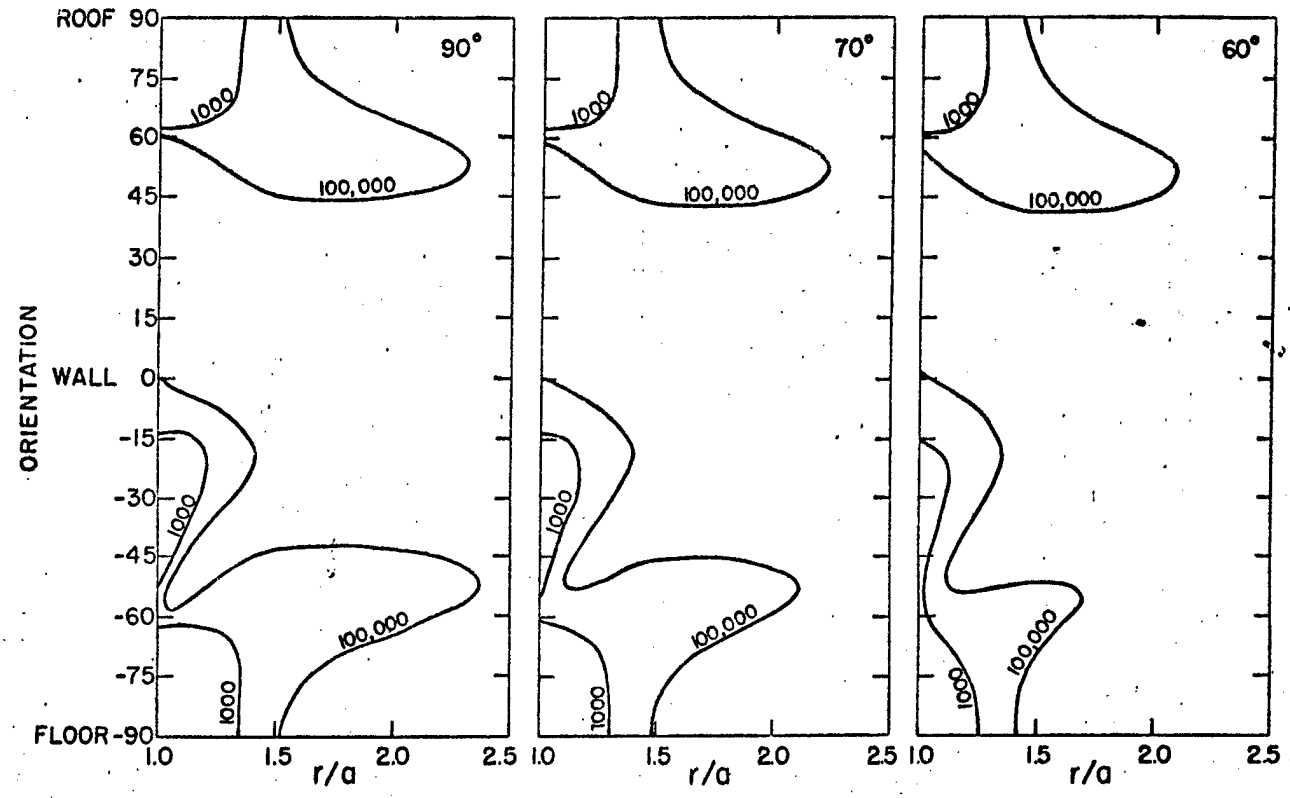

Contour values are to be multiplied by $\frac{c}{100}$, where c is the joint cohesion in psi.

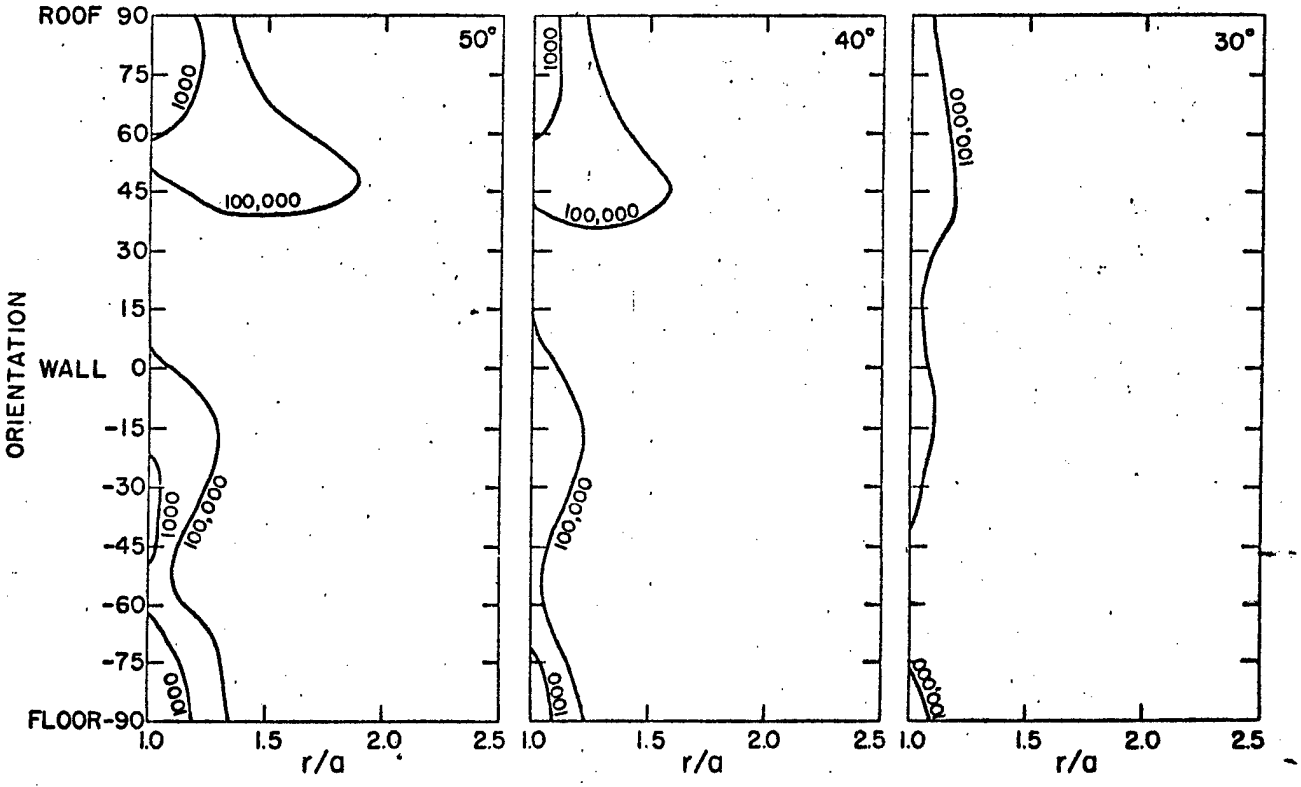

Fig. 2-3. Joint Influence Diagrams
Horizontal applied pressure, $p_2/p_1 = 0.43$.

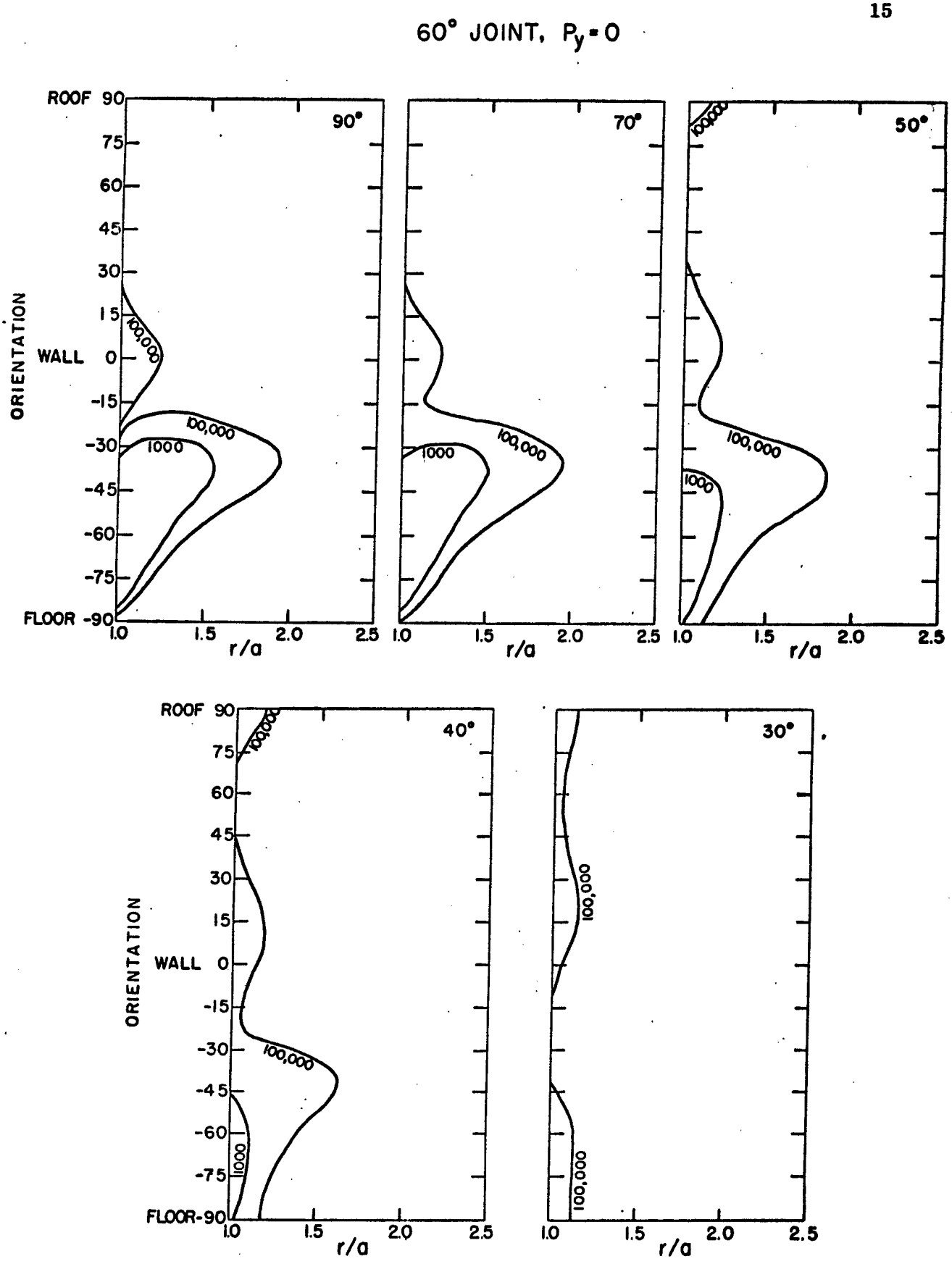

Fig. 2-4. Joint Influence Diagrams

Horizontal applied pressure, $p_2/p_1 = 0.43$.

Contour values are to be multiplied by $\frac{c}{100}$, where c is the joint cohesion in psi.

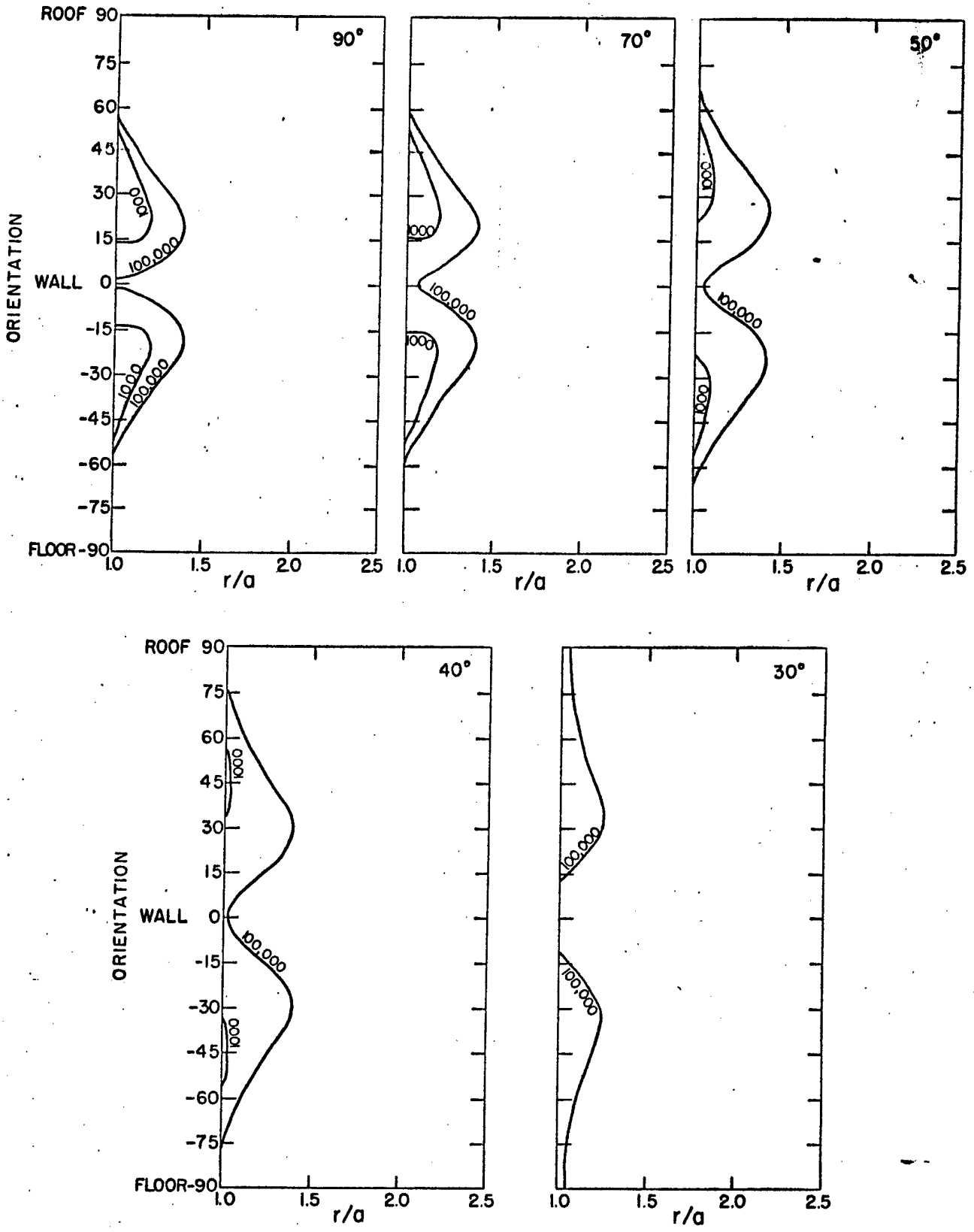

Fig. 2-5. Joint Influence Diagrams

Horizontal applied pressure, $p_2/p_1 = 0.43$.

Contour values are to be multiplied by $\frac{c}{100}$, where c is the joint cohesion in psi.

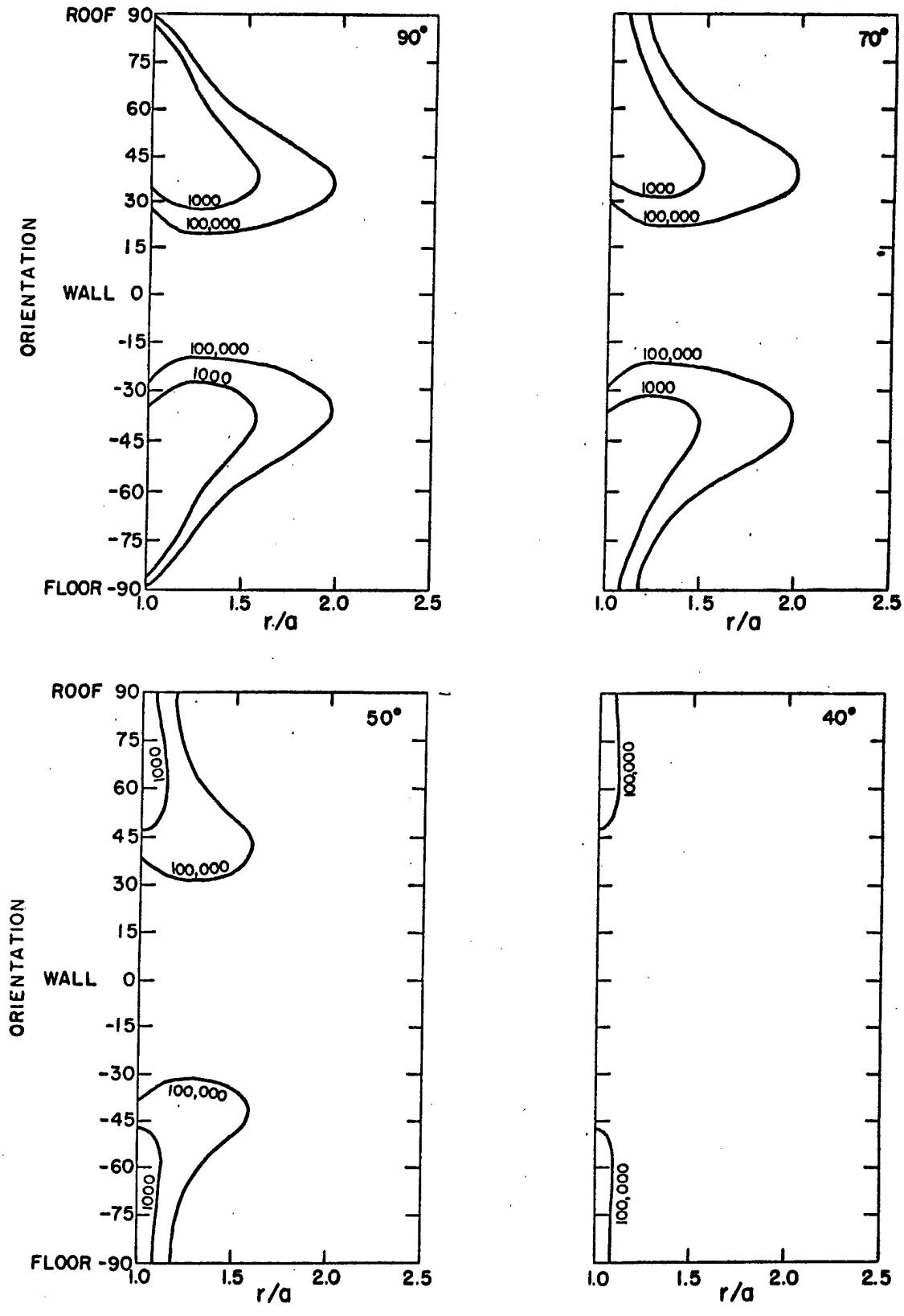

Fig. 2-6. Joint Influence Diagrams

Horizontal applied pressure, $p_2/p_1 = 0.43$.

Contour values are to be multiplied by $\frac{c}{100}$, where c is the joint cohesion in psi.

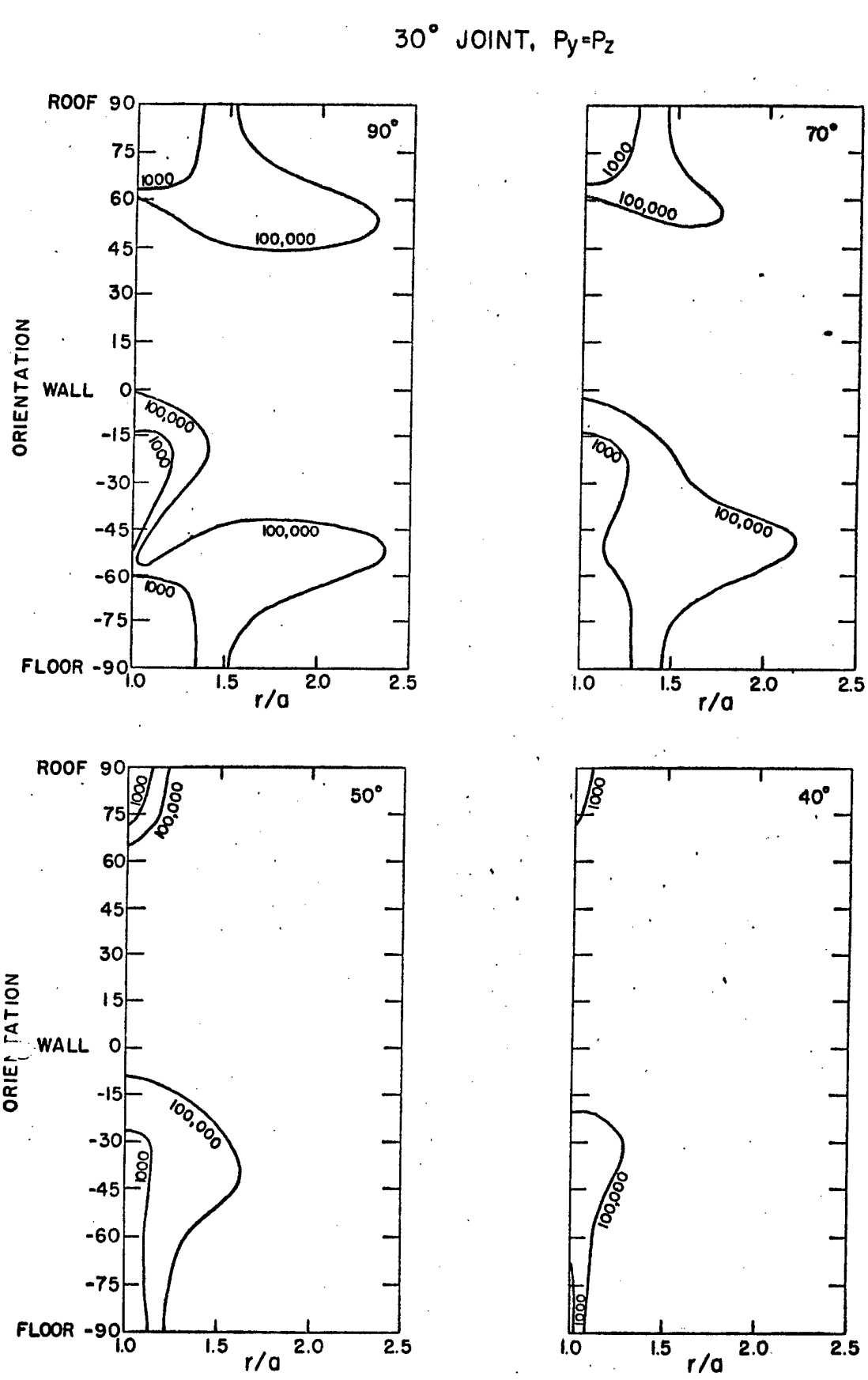

Fig. 2-7. Joint Influence Diagrams
Horizontal applied pressure, $p_2/p_1 = 0.43$.

Contour values are to be multiplied by $\frac{c}{100}$, where c is the joint cohesion in psi.

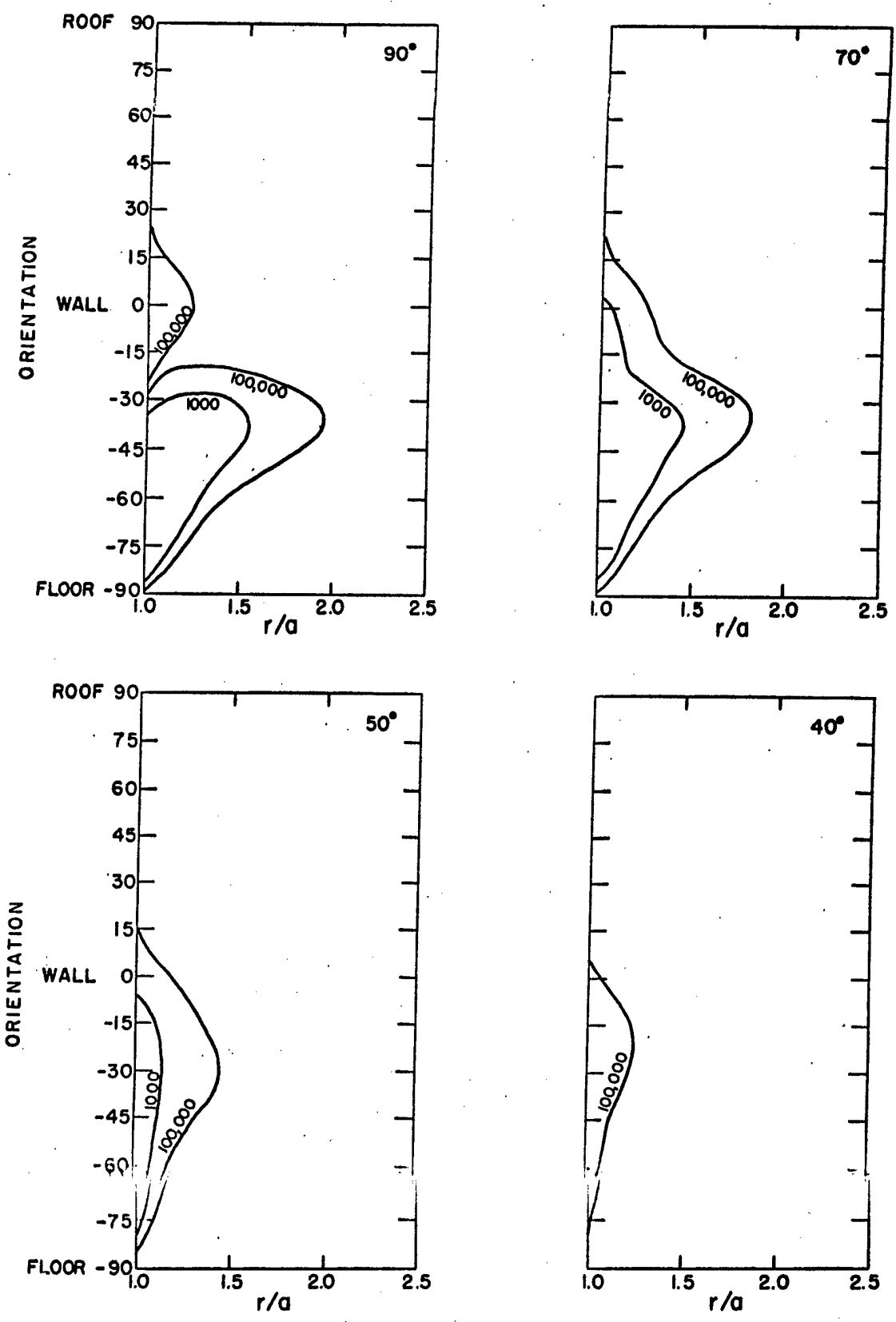

Fig. 2-8. Joint Influence Diagrams

Horizontal applied pressure, $p_2/p_1 = 0.43$.

Contour values are to be multiplied by $\frac{c}{100}$, where c is the joint cohesion in psi.

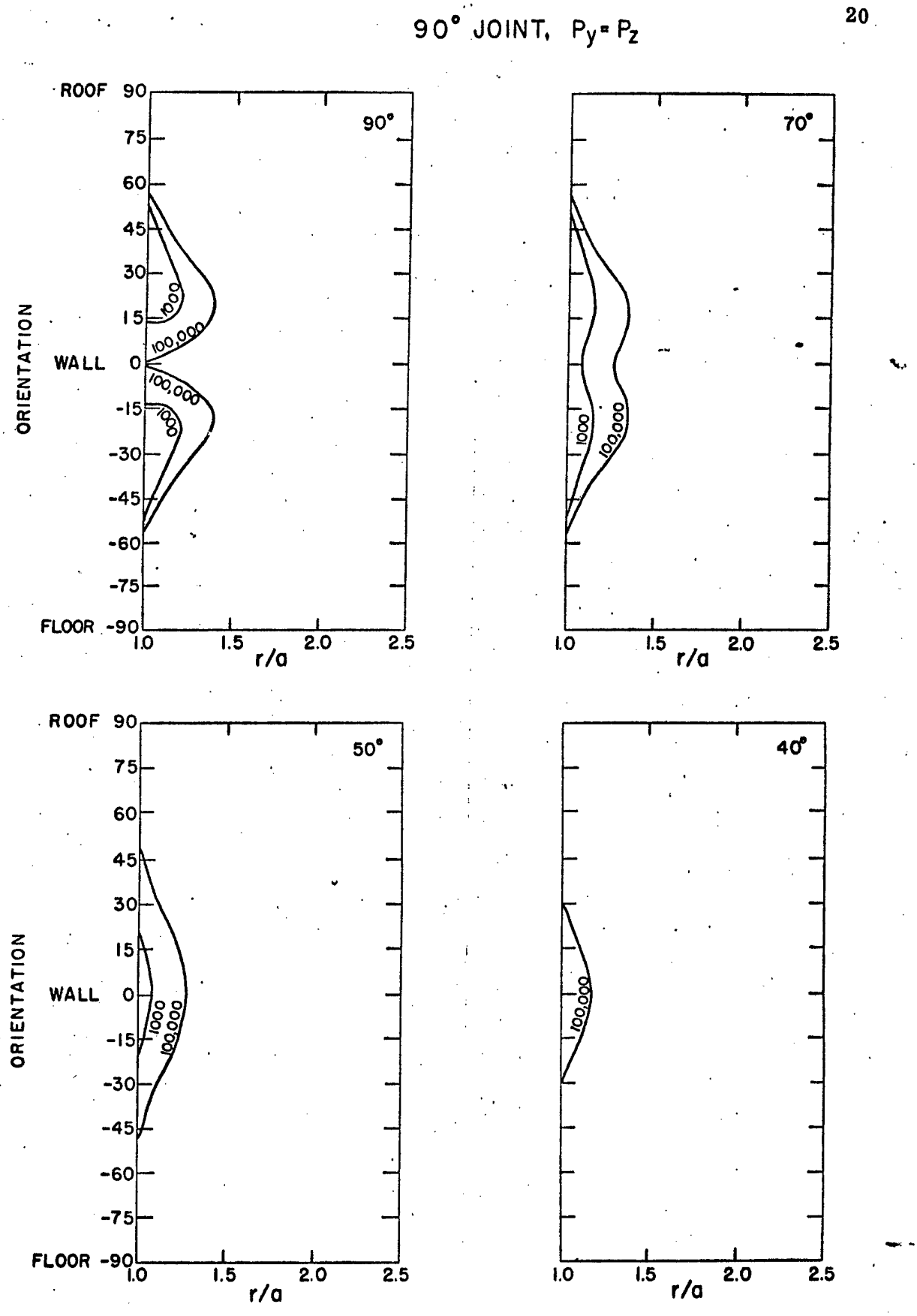

Fig. 2-9. Joint Influence Diagrams

Horizontal applied pressure, $p_2/p_1 = 0.43$.

Contour values are to be multiplied by $\frac{c}{100}$, where c is the joint cohesion in psi.

affected in no way by the longitudinal pressure. All other joint sets are strengthened by the longitudinal applied pressure, i.e. their influence diagrams are considerably reduced in size. Further, joints cease to have any weakening effect if their angle with the tunnel axis is less than 40^{o} as opposed to 30^{o} in the absence of applied longitudinal pressure. The 0^{o} and 30^{o} joints have their influence regions shifted away from spring line toward the roof and floor. The 60^{o} joint has its slip zone spread to the side wall below the springline, while the 90^{o} joint influences the side wall.

Thus, failure to consider the third dimension is conservative. This same result has also been found in analyzing the influence of rock joint sets on slope stability.

(4) Enlargement of the Slip Zone - Effect of Faults

It is tacitly assumed, in the examples of the previous section, that the weakness surfaces of the rock do not change the stress distribution around the tunnel. This is believed to be a reasonable assumption if: (1) the joints are but incipient weakness elements revealing themselves only at the point of failure; (2) they retain residual strength after slipping; and (3) the ratio of minor to major applied pressures is not small. In the previous study, the effect of stress redistribution due to slip on joints was calculated and the migration of the slip zones during the buildup of stress was plotted for a number of cases. It was found that if the deformability of the slip zone after failure was large, or if the shear stress in the wave front was large, the slip zone augmented considerably.

Should a major weakness zone come within the region of influence of a tunnel, it remains to consider whether or not the alteration of the stress distribution about the tunnel owing to the existence of the fault could significantly alter the zone of slip.

Calculation of the effect of a fault on the stresses around a tunnel can be performed by finite element analysis. Representation of the fault in the analysis must be discussed. In the next section a joint element of a linkage type is derived which can be used for this purpose, particularly if the fault is very thin. If the fault has an appreciable thickness of soft crushed rock or gouge, it may be represented as a line of elastic continuum elements which are assigned a lower elastic modulus. This was the procedure followed in this section.

As even a thick fault zone is still tabular in shape, to model a fault zone with elastic continuum elements, it is desirable to know the limiting length to width ratio (aspect ratio) which can be used without introducing error. A series of small finite element meshes were made for this purpose incorporating a soft fault seam. The number of rows and the aspect ratio of the elements comprising the fault were varied systematically. It was found that no significant loss of precision occurred as long as the aspect ratio was less than about three times the number of rows of elements comprising the fault. To model a fault, two rows of elements six times as long as wide are about as precise as one row of elements three times as long as wide.

Figure 2-10a presents contours of maximum shear stress developed around a tunnel with applied pressure, p horizontally and 0.43 p vertically. The contour values are expressed as multiples of p. Figures 2-10b,c,d,and e present maximum shear stress contours for four cases in which a thick horizontal fault occurs at varying positions as shown. The fault is 100 times as deformable as the rock.

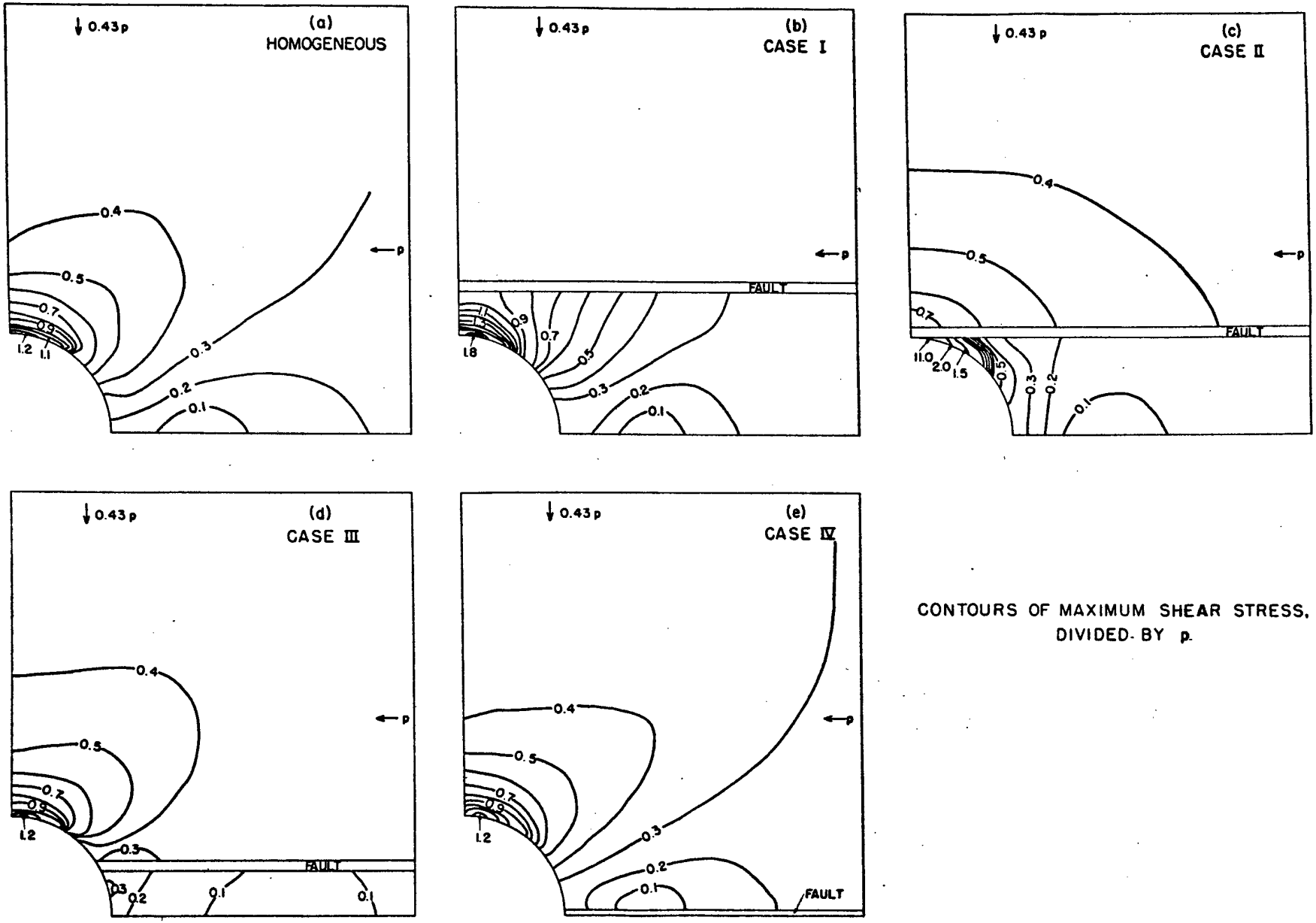

CONTOURS OF MAXIMUM SHEAR STRESS, DIVIDED BY p.

Fig. 2-10. Maximum shear stress around a circular tunnel with and without a fault zone.

In the homogeneous case, the maximum shear stress occurs at the crown and is about 1.25 p (see Fig. 2-10a). In Case I where a horizontal fault is centered a/2 above the top of the tunnel (see Fig. 2-10b), a magnification of shear stress to about 1.8 p occurs and the center of maximum shear is shifted by the fault about 10^{o} from the crown. A similar but more drastic result is found when the fault occurs just above the crown (see Fig. 2-10c) -- the wedge of rock between the tunnel and the fault is under intolerable shear stresses exceeding 2 p. When the fault intersects the tunnel, as in Figures 2-10d and e, no appreciable shear stress concentration results.

The effect of these stress changes on the slip zones of a 30^{o} joint is shown in Figures 2-11 to 2-16. The shear stress concentration above the crown when the fault is above the tunnel leads to an accentuation of the slip zone development in this region and the fault neatly truncates the slip zone. The effect of the fault is optimum when it occurs just above the tunnel. It is as if the occurrence of the fault above the tunnel focuses the applied pressure on the wall rock. In other than the optimum positions of Case I and Case II, the fault changes the ubiquitous joint slip zone only in detail.

(5) Application to Design of Tunnels

The concept of a joint slip zone offers an approach for estimating tunnel support forces required under a given acceleration. With respect to blast resistant design, assume that the zone of slip is developed by the passage of the stress wave and the later accelerations hurl the loosened mass toward the opening in the direction of the advancing wave front. With respect to selection of tunnel supports, assume development of the slip zone by stress concentrations during excavation and its subsequent acceleration downward by gravity. In each case if the assumption is reasonable, an approximation of the net rock load to be supported is the

FIGURE 2-11
EFFECT OF FAULT ON SLIP ZONE
30° JOINTS, $\beta = 90°$
$E_{FAULT} = E_{ROCK}/100$

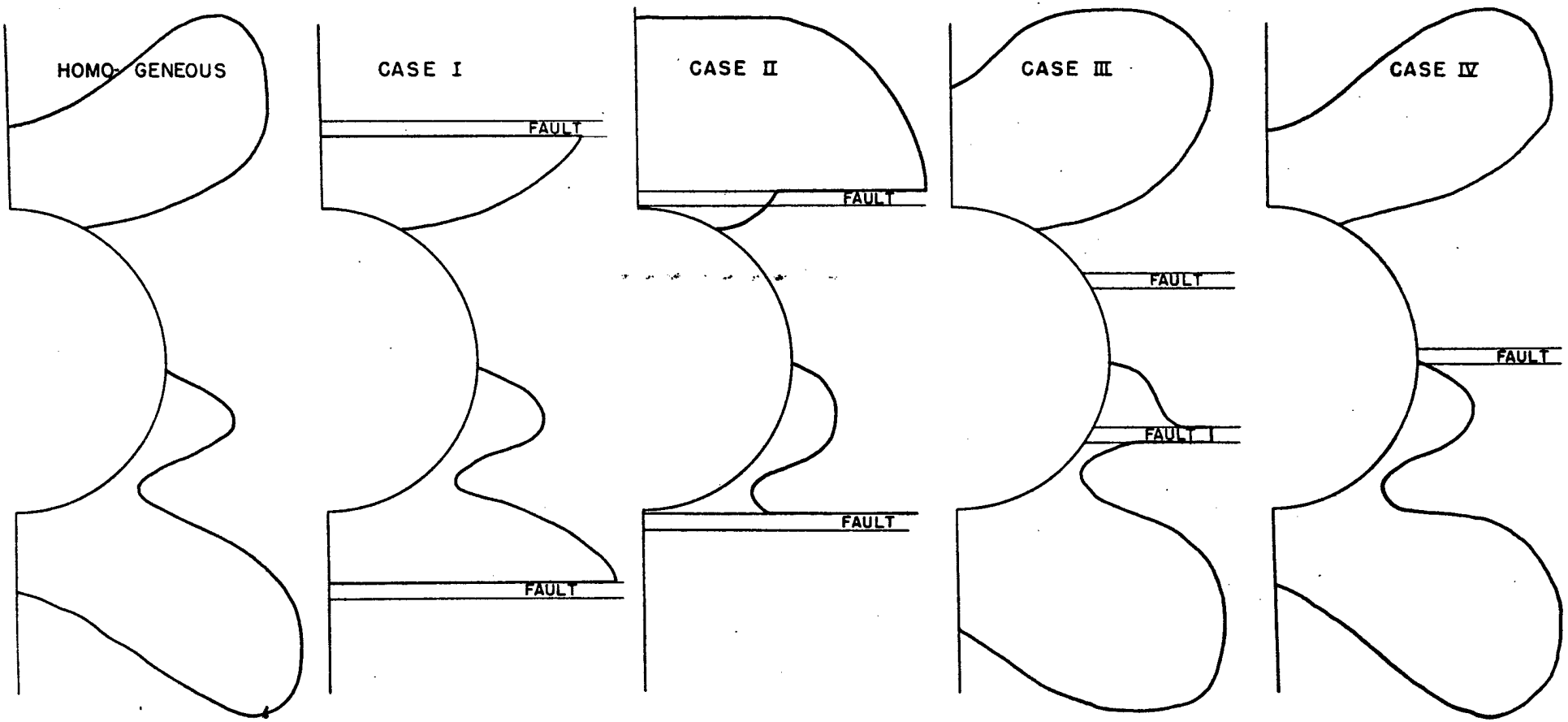

FIGURE 2-12
EFFECT OF FAULT ON SLIP ZONE
30° JOINTS, $\beta = 70°$
$E_{FAULT} = E_{ROCK}/100$

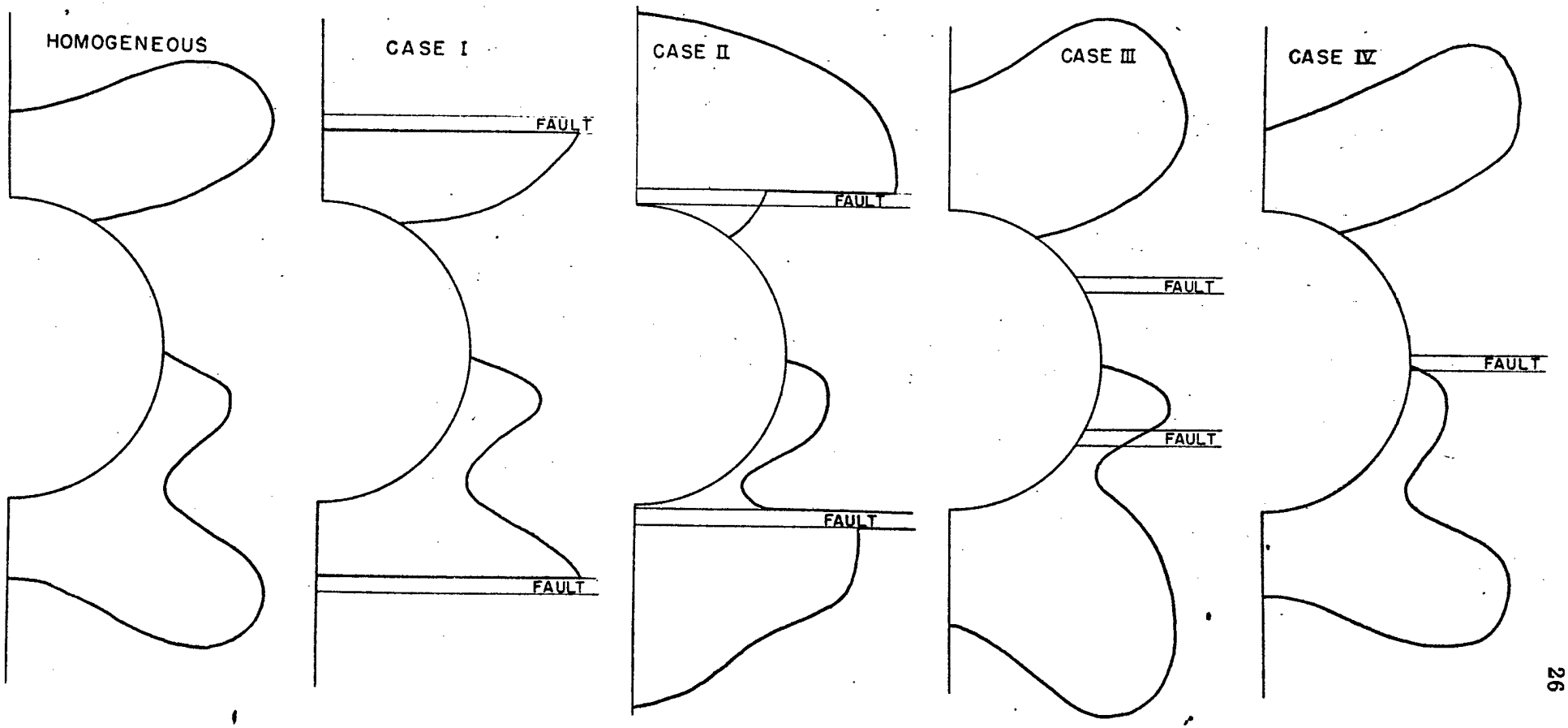

FIGURE 2-13
EFFECT OF FAULT ON SLIP ZONE
30° JOINTS, $\beta = 60°$
$E_{FAULT} = E_{ROCK}/100$

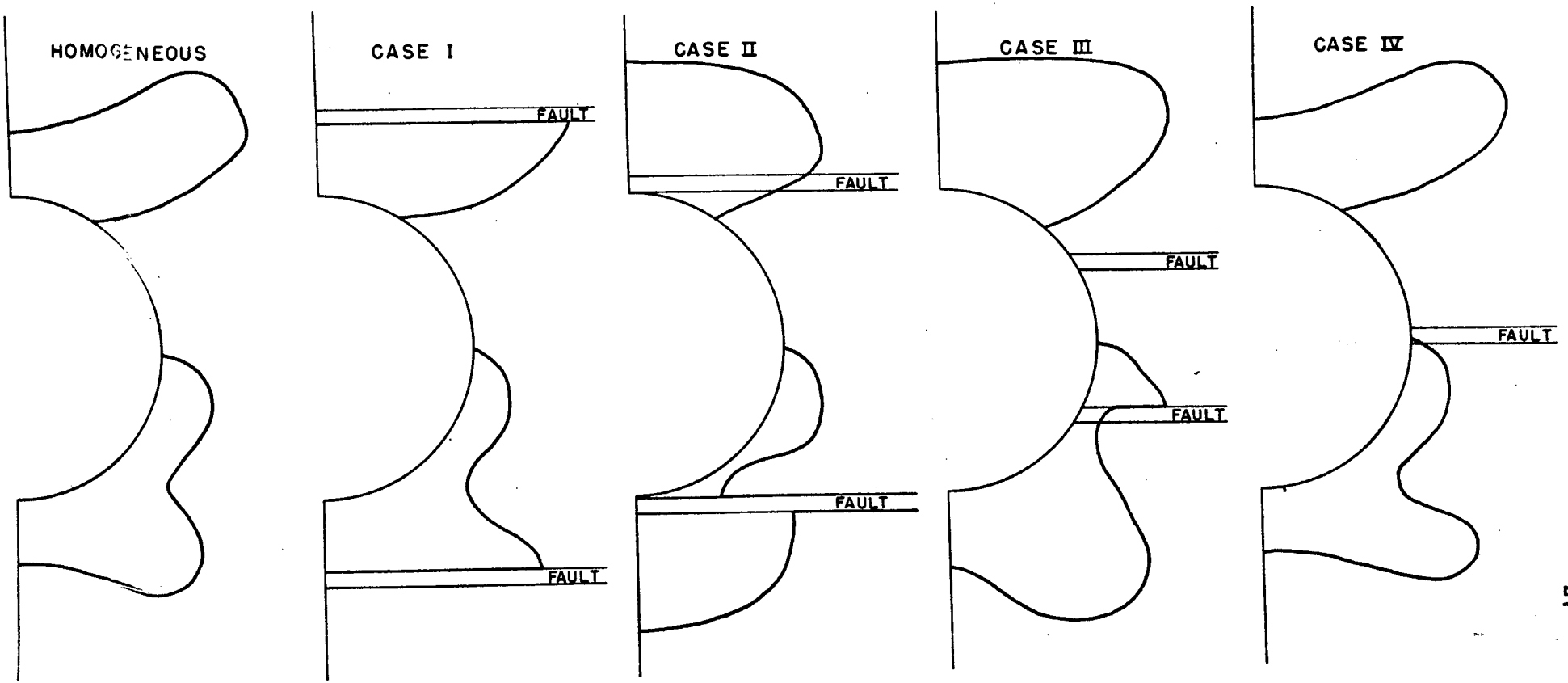

FIGURE 2-14
EFFECT OF FAULT ON SLIP ZONE
30° JOINTS, $\beta = 50°$
$E_{FAULT} = E_{ROCK}/100$

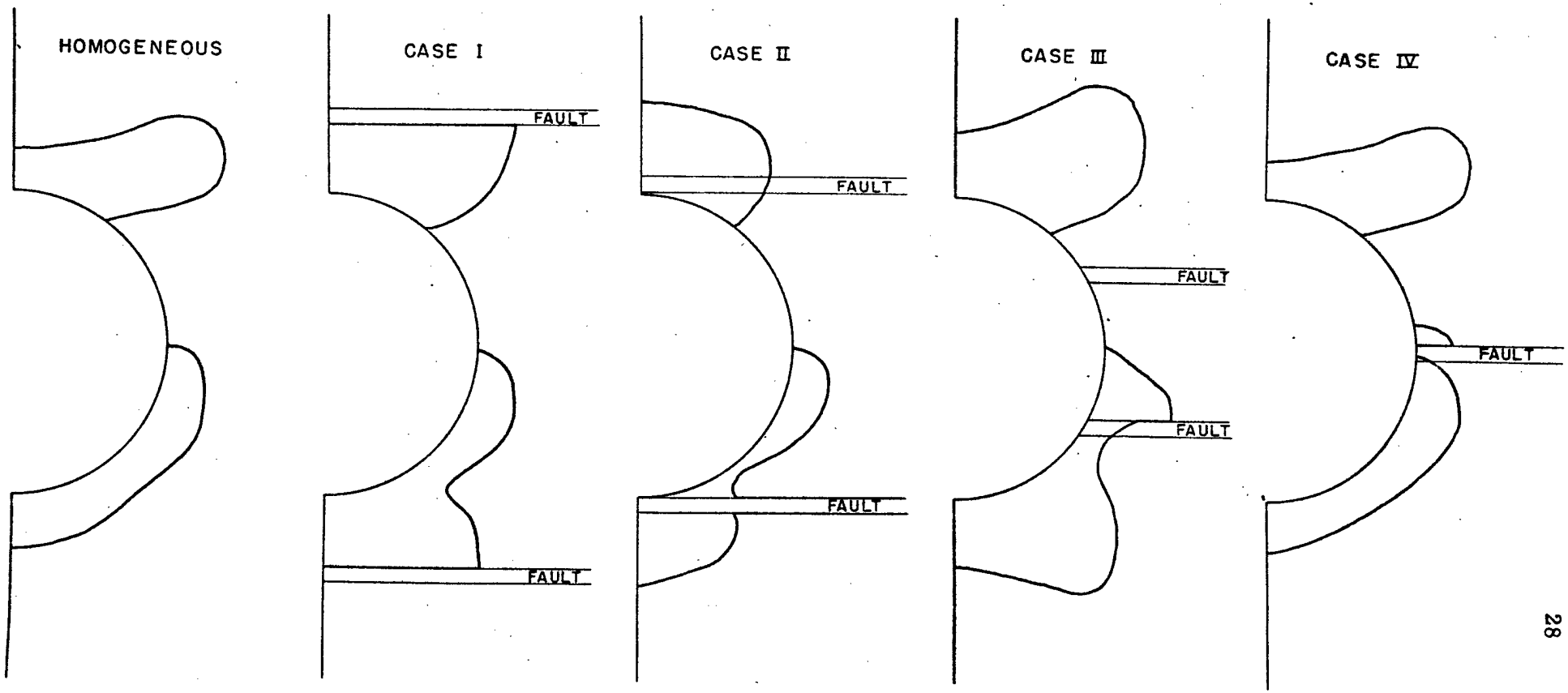

FIGURE 2-15
EFFECT OF FAULT ON SLIP ZONE
30° JOINTS, $\beta = 40°$
$E_{FAULT} = E_{ROCK}/100$

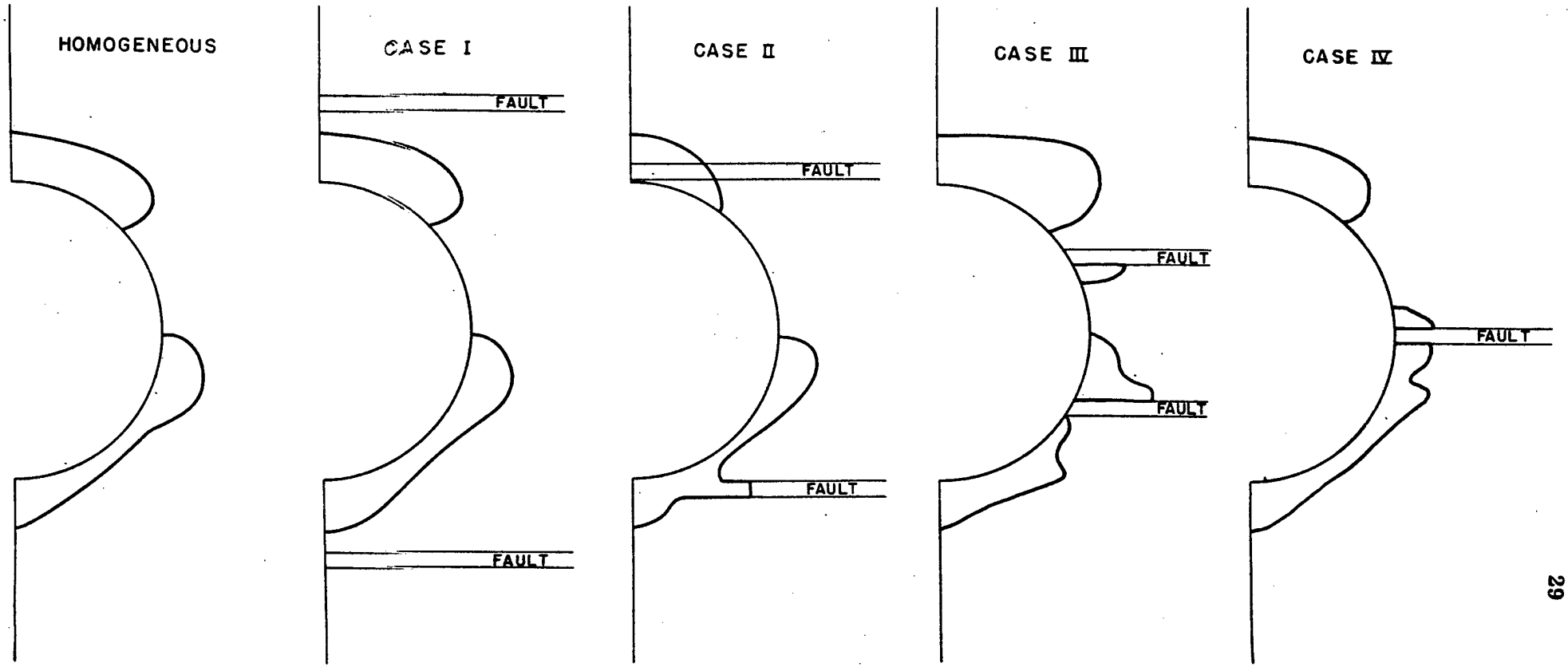

FIGURE 2-16
EFFECT OF FAULT ON SLIP ZONE
30° JOINTS, $\beta = 30°$
$E_{FAULT} = E_{ROCK}/100$

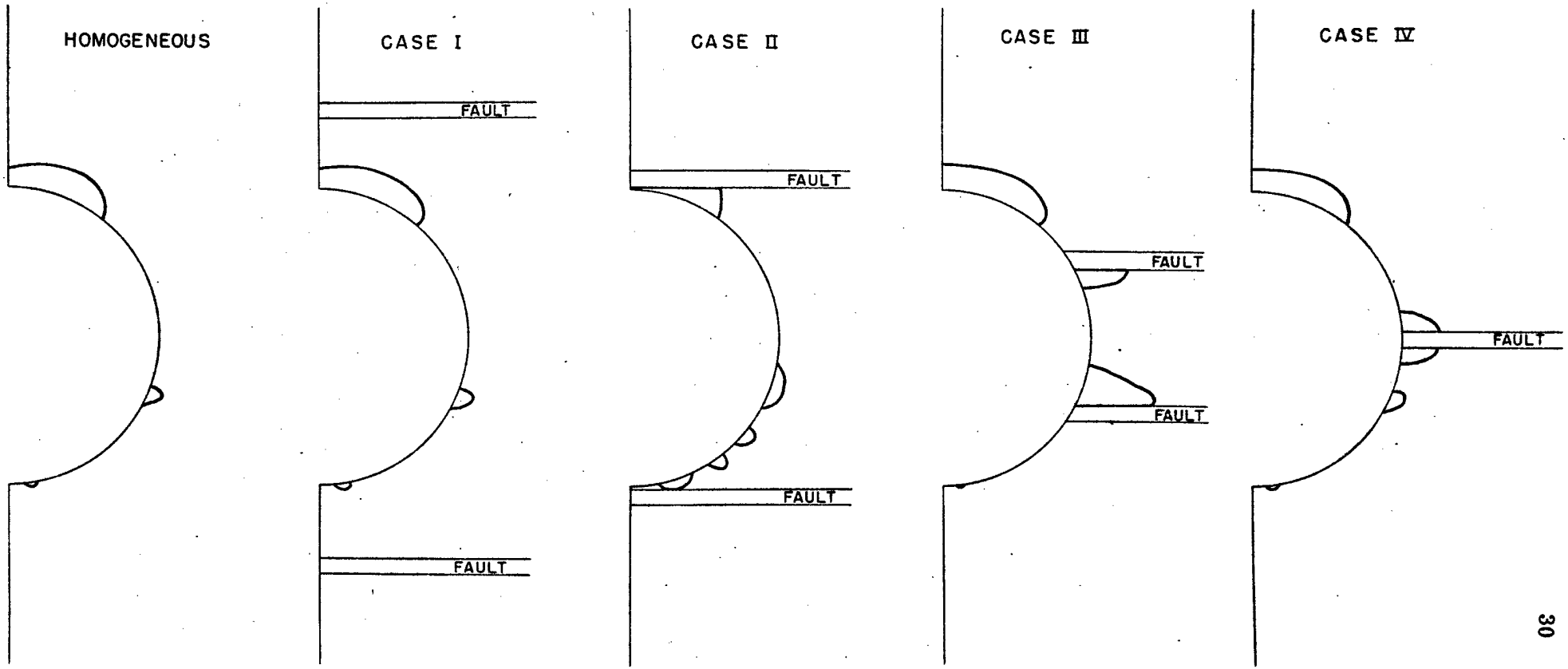

integral over the tunnel wall area of the acceleration times the mass of rock in the slip zone behind each unit of wall. The steel sets or steel or concrete liner or rock bolts must then be sufficiently strong to resist the net rock load. Figure 2-17 illustrates the essential features of the idea. In this figure, the concrete must withstand

$$\alpha \sum_{i=1}^{7} m_i$$

where α is the blast acceleration. The load is distributed according to the variation of slip zone depth. The sound rock between m_0 and the lining in the direction of the blast must support $\alpha\, m_0$ or the slip zone will enlarge upward.

Figures 2-2 to 2-9 give the dimensions of the slip zone around circular tunnels for joints of various orientation for an angle of friction of 31^o and a free field stress ratio of 0.43. These figures can be used for design according to the above concept. To calculate the mass and the load variation along the wall of the tunnel, the length of slip zone behind each point of the wall must be known, measured in the blast propagation direction. In these figures, a transformation has been made which mapped the circular tunnel wall onto a straight line, i.e. the slip zone has been plotted on a Cartesian frame whose y and x axes are respectively θ and r/z.

Since these figures were developed for the condition of maximum applied pressure horizontally, the direction of the rock load is horizontal, and we need to know the set of curves in the figures describing true horizontal lines. (In the case of a tunnel under gravity loads, the maximum applied pressure would most likely be vertical so the following discussion would apply simply by turning the figures through 90^o) With reference to Figure 2-18, a horizontal line crossing the tunnel wall, r/a = 1, at $\theta = \theta_1$ transforms to a curved line given by

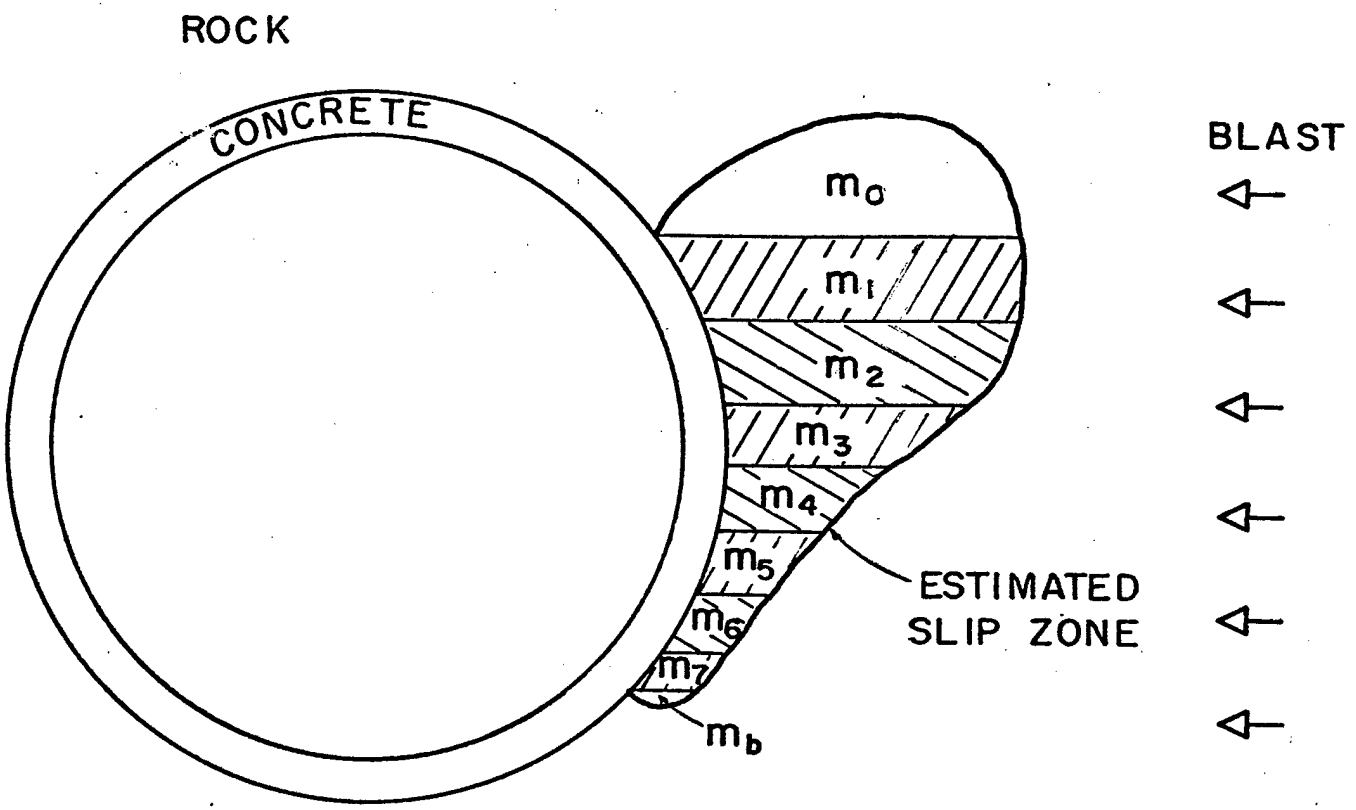

Fig. 2-17. The net force to be resisted by the concrete lining equals $\alpha \sum_{i=1}^{7} m_i$ where α is the blast acceleration.

$$\sin \theta = \frac{\sin \theta_1}{r/a} \qquad (2\text{-}11)$$

The rock load behind any point of a lining is proportional to the depth, d, of the failed zone behind the lining. A point at horizontal depth, d, behind a point of the tunnel wall at $\theta = \theta_1$ has coordinates r and θ given by

$$\frac{d}{a} = \left(\frac{r}{a} \cos \theta - \cos \theta_1\right) \qquad (2\text{-}12)$$

Equations 2-11 and 2-12 were used to construct the graphical integrator of Figure 2-19. This figure may be overlain on the slip zone diagrams of Figures 2-2 to 2-9 to define the net rock load and the load distribution. An illustrative example follows.

Example 1 - Rock Load in a Tunnel Due to a Blast

Three sets of weakness planes were logged in a hypothetical tunnel section as shown in Figure 2-20a. Joint Set 1 strikes 50^o with respect to the tunnel axis and dips 42^o; it is spaced at about 5 foot increments. Joint Set 2, spaced every 2 feet, strikes 70^o with the tunnel and dips 65^o. A horizontal sheared zone, consisting of numerous closely spaced horizontal sheared surfaces will cross the tunnel 30^o - 45^o below the springline. The tunnel is circular, 20 feet in diameter. It is to be subjected to a blast with a horizontally travelling plane wave. The peak pressure is 10,000 psi and the peak acceleration 50 g. The joint sets are believed to have considerable cohesion, ca. 1,000 psi, whereas the sheared zone has only 100 psi cohesion. The rock weighs 165 pcf.

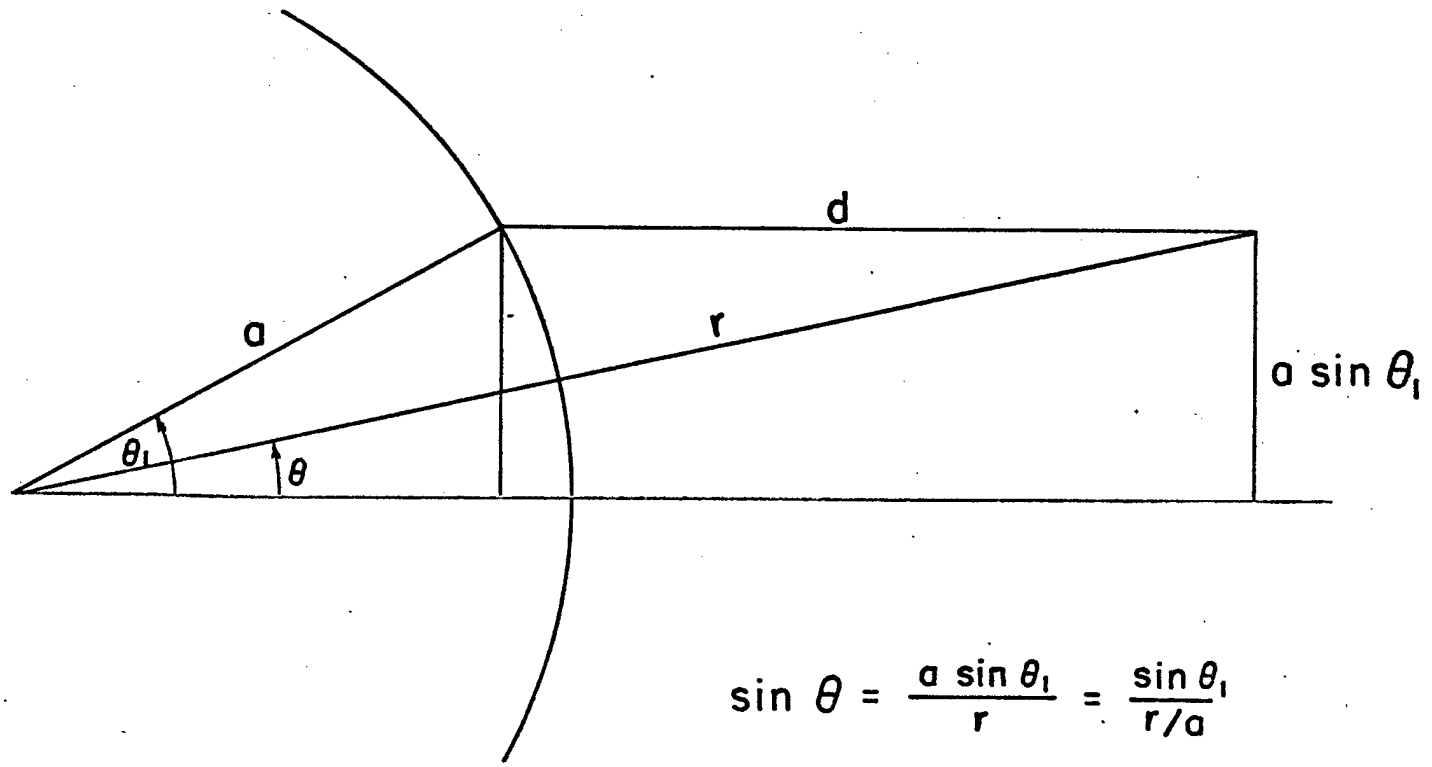

$$\sin\theta = \frac{a \sin\theta_1}{r} = \frac{\sin\theta_1}{r/a}$$

$$d = r\cos\theta - a\cos\theta_1$$

FIGURE 2-18. THE TRANSFORMATION OF HORIZONTAL LINES INTO THE COORDINATE SPACE OF FIGURES 2-2 TO 2-9.

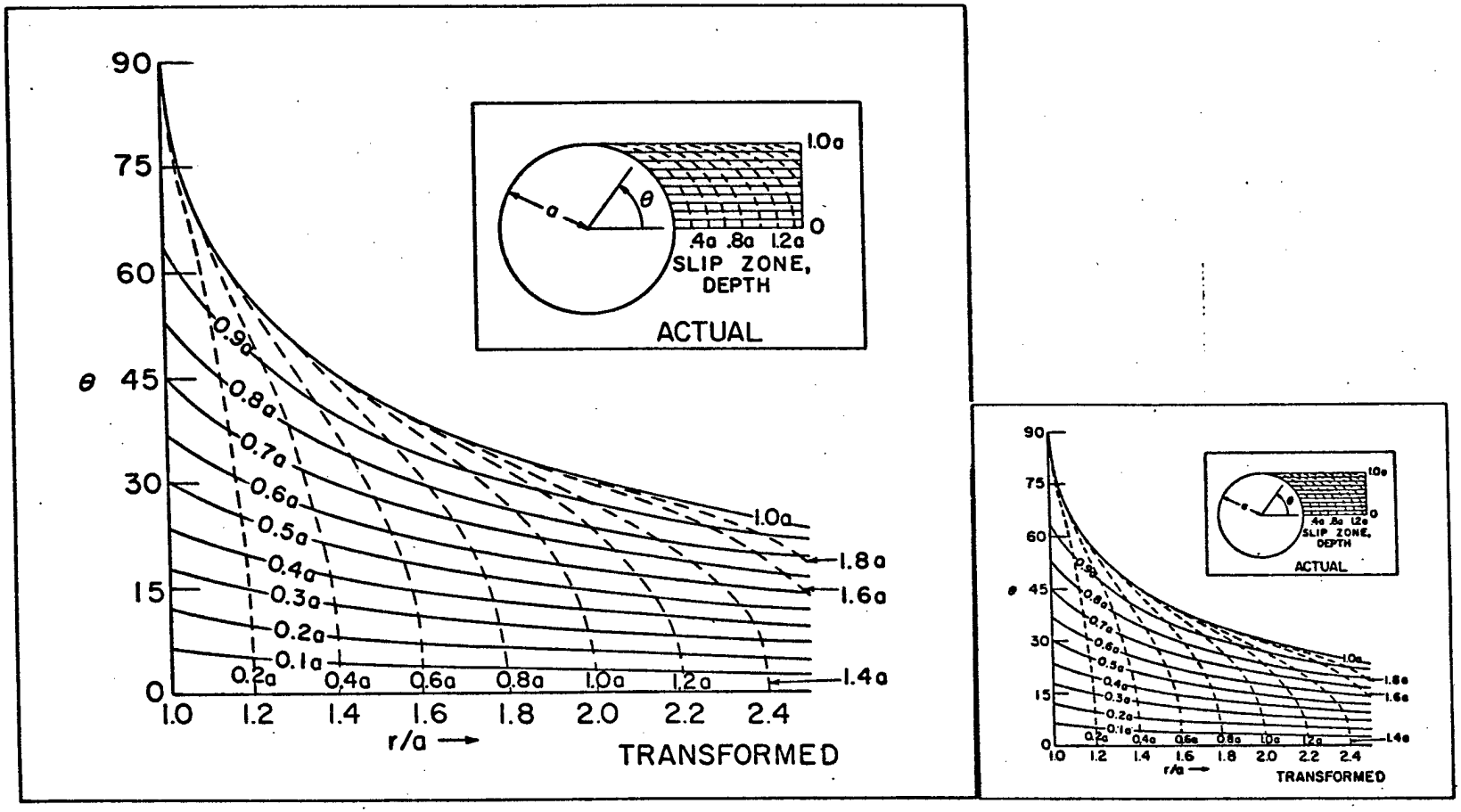

Fig. 2-19. Chart for integrating slip zones plotted with θ and r/a as ordinate and abiscassa respectively. (Figure repeated on the right to same scale as Figures 2-2 to 2-9.)

Table 2-2 summarizes the geometric and strength data for the weakness planes. To make use of the ubiquitous joint influence diagrams (Figs. 2-2 to 2-9), the inclination, θ, of each joint in the tunnel cross section and the angle of the joint normal with the tunnel axis, β, will be calculated as follows (Fig. 2-21):

$$\beta = \cos^{-1} (\sin D \sin \sigma) \qquad (2\text{-}11a)$$

$$\theta = \tan^{-1} (\tan D \cos \sigma) \qquad (2\text{-}11b)$$

where D is the dip of the joint down from horizontal and positive if the y component is positive, and σ is the strike of the joint relative to the tunnel axis and positive clockwise.

θ and β for the three weakness plane sets calculated by Equation 2-11 are given in the last two columns of Table 2-2. It is apparent immediately that Joint Set 2 has no weakening effect on the tunnel because β is less than 40° (31.5°). In the region of occurrence of the sheared zone, defined between horizontal lines piercing the tunnel at $\theta = -30^{\circ}$ and -45°, the overlapping of the slip zones for Joint Set 1 and the sheared zone are as drawn in Figure 2-22. This figure was obtained as follows:

(a) Since the joint cohesion is 10 x 100 psi, its slip zone for 1,000 psi is required. Trace the portion of the slip zone between $\theta_1 = -30^{\circ}$ and -45° for Joint Set 1 from Figure 2-7 (30° joint at $\beta = 60^{\circ}$ with $p_y = p_z$).

(b) Since the sheared zone has cohesion 100 psi, its slip zone for 10,000 psi is required. Trace the portion of the slip zone between $\theta_1 = -30^{\circ}$ and -45° for the sheared zone from Figure 2-6 (horizontal joints at $\beta = 90^{\circ}$ with $p_y = p_z$).

(c) Trace the region common between (a) and (b).

TABLE 2-2. Weakness Planes in the Rock at the Hypothetical Tunnel for Calculation of Rock Load Due to Blast

Weakness Type	(φ)	(c) psi	Strike Relative to Tunnel Axis (σ)	Dip of Plane (D)	Inclination of Trace in Tunnel Cross Section (θ)	Angle of Normal with Tunnel Axis (β)
Joint Set 1 5' spacing	31°	1000	+ 50°	+ 42°	+ 30.0°	59.0°
Joint Set 2 2 ' spacing	31°	1000	+ 70°	+ 65°	+ 36.2°	31.5°
Shear Zone, occurs in rock from 30° - 45° below springline	31°	100	--	0°	0°	90.0°

TABLE 2-3. Weakness Planes in the Rock at Second Hypothetical Tunnel for Calculation of Rock Loads on Tunnel Supports

Joint Set	φ	c	σ	D	θ	90 - θ	β
1	31°	0	50	30	20	70	20
2	31°	0	0	30	30	60	90
3	31°	0	50	-40	-28	-62	-61

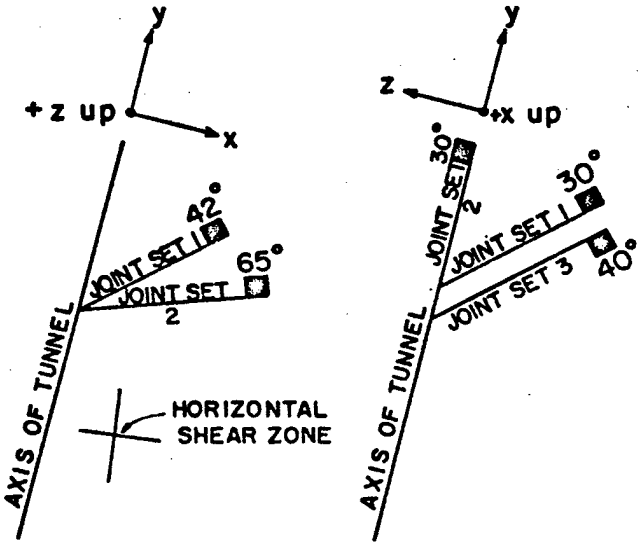

a. EXAMPLE 1. b. EXAMPLE 2.

FIGURE 2-20 GEOLOGY OF ILLUSTRATIVE EXAMPLES.

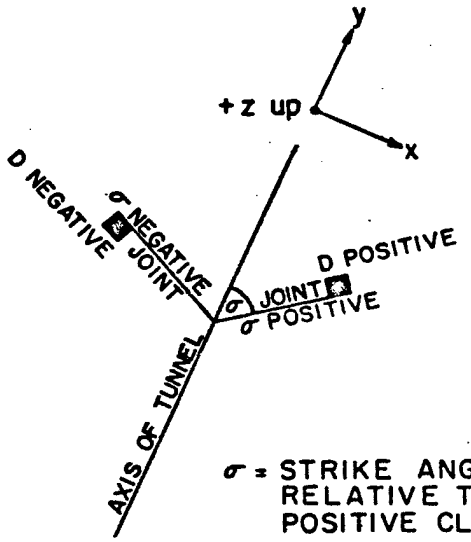

σ = STRIKE ANGLE RELATIVE TO TUNNEL POSITIVE CLOCKWISE

D = DIP ANGLE, DOWN FROM HORIZONTAL POSITIVE IF y COMPONENT IS POSITIVE.

FIGURE 2-21 TERMINOLOGY AND SIGN CONVENTION.

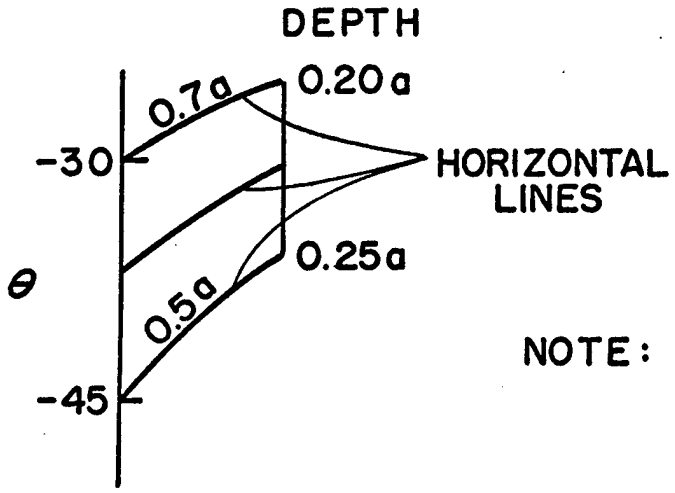

FIGURE 2-22 ROCK LOAD IN EXAMPLE 1.

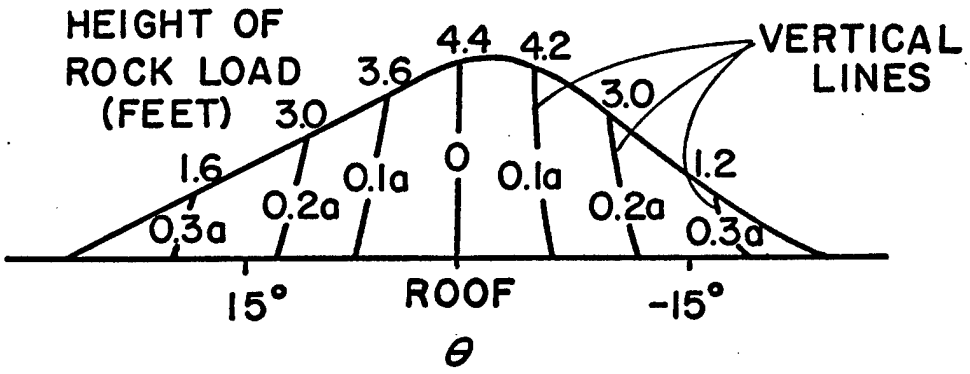

FIGURE 2-23 ROCK LOAD IN EXAMPLE 2.

(d) Note that the regions in question are bounded by horizontal lines which transform to the solid lines .5a and .7a in Figure 2-19. (Since θ_1 is negative, Figure 2-19 should be turned over.)

Integrating Figure 2-22, the net force per foot to be resisted by the lining is

$$F = \gamma A \frac{\alpha}{g} = (165 \text{ pcf}) (0.045 \times 100 \text{ ft}^2) (\frac{50 \not{g}}{\not{g}})$$

$$= 37,100 \text{ pounds / foot}$$

This force is distributed fairly evenly over a two foot section of the wall below the springline. It could be sustained by rock bolts, providing they are sufficiently long that the anchor lies behind the slip zone.

Example 2 - Rock Load on Tunnel Supports

Table 2-3 lists data on the three closely spaced joint sets mapped at the site of a circular tunnel 40 feet in diameter (see Fig. 2-20b). The tunnel is 1,000 feet deep. Joint Set 1 with $\beta = 20^o$ does not tend to slip. The common region of slip of Joint Sets 2 and 3 will be determined so that the rock load on tunnel supports due to gravity can be calculated.

In this case, the major applied pressure, the x axis, is vertical. The y axis remains the tunnel axis but x and z are rotated through 90^o so that $90^o - \theta$, rather than θ, is required for entering the slip zone charts. The cohesion is 10 psi. This means that the slip zone will develop outward to the 10,000 psi contour; thus virtually the entire zone of slip is developed. Stated another way, the full height of the ground arch develops.

Figure 2-23 shows the slip zone common to Joints 2 and 3. The slip zone for the $- 60^o$ joint (Joint 3) is obtained by turning Figure 2-4 upside down. The slip zone for Joint 2 was obtained by using Figure 2-4

as presented. Figure 2-19, turned 90°, was used to measure the height of the slip zone at each point.

The net rock load per foot of tunnel length is

$$F = \gamma A \frac{\alpha}{g}$$

$$= (165 \text{ pcf}) (42 \text{ ft}^2/\text{ft}) (1)$$

$$= 6{,}900 \text{ pounds/foot}$$

The load is distributed as shown in Figure 2-23.

2.3 JOINT STIFFNESS ANALYSIS

(1) General

The method of the preceding section allows an estimate of the weakening effect of closely spaced joint sets. It is predicted on the assumption that the existence of a joint does not alter the stress distribution significantly. This may not always be a satisfactory assumption. Further, it may sometimes prove desirable to model the action of individual joints occurring in determined locations, and the ubiquitous joint analysis does not offer this capability. Thus, in this section, a new joint representation is presented.

(2) The Prototype Joint

A meaningful representation for joints in finite element analysis must closely model the actual prototype characteristics. There are many types of joints, and detailed quantitative data on the mechanical behavior of all types have not yet been obtained. However, the following list of characteristics can serve as a beginning:

(a) Joints are tabular. In any two-dimensional representation they more closely resemble an irregular line than a zone of some appreciable thickness.

(b) They have essentially no resistance to a net tension force directed in the normal.

(c) They offer high resistance to compression in the direction of the normal but may deform somewhat under normal pressure, particularly if there are crushable asperities, contiguous altered rock, apertures, or compressible filling material.

(d) At low normal pressures, shearing stresses along a joint produce a tendency for one block to ride up onto the asperities of the other. At high normal pressures, shear failure along joints involves shearing through the asperities.

(e) As a first approximation, the shear strength may be represented by a linear Mohr envelope, though a bilinear Mohr envelope would be better. Shearing may be accompanied by dilation, particularly at low normal pressures.

(f) Small shear displacements probably occur as shear stress builds up below the yield shear stress.

The plane strain continuum element, whose derivation is written fully in the Piledriver report, cannot satisfactorily model this prototype behavior. It is not a line element and in fact, high eccentricity leads to inaccuracy in stress determination as discussed in Section 2.2 -(4). Instead, the stiffness of a special joint element will be derived. First, it will be useful to trace the main steps of the derivation of the constant strain triangle stiffness as the joint element will be designed to be compatible with continuum elements and will be added with them into the structural stiffness matrix (1).

(3) Continuum Element Stiffness Derivation

The finite element analysis consists of replacing a complex structure by an assemblage of small elements. It may be derived in terms of energy, in which case the finite element approximation may be stated as a decomposition of the total potential energy of a body into the sum of potential energies of all component bodies. After calculation of the element stiffness, the structural stiffness matrix is formed at each nodal point in turn by adding stiffnesses of all elements containing the given nodal point.

---

*A fuller derivation and complete description of all matrix quantities will be found in the previous report, cited on Page 1.

1. The idea of adding linkage element stiffness to the total structural stiffness was developed by Ngo and Scordellis, Jour. Amer. Concrete Inst., v. 64, n. 3, March 1967.

To trace the steps in formulating the element stiffness matrix, the problem will be simplified by considering a one element mesh with area A as shown in Figure 2-24. A boundary pressure, P, exists along the side of length, L. The element is one unit thick.

The potential energy of the element, in the absence of body forces is:

$$\phi = \int_{vol} \frac{1}{2} \varepsilon_i \sigma_i \, dv - \int_{area} w_i P_i \, dA \qquad (2\text{-}10)$$

where w_i is the tensor of displacement throughout the element. In matrix notation

$$\phi = \int_{vol} \frac{1}{2} (\varepsilon)^t (\sigma) \, dv - \int_{area} (w)^t (P) \, dA \qquad (2\text{-}11)$$

As fully described in the previous report, the displacements (w) may be expressed in terms of the displacements (u) at the corners (nodal points) by a linear interpolation formula

$$(w) = (\varphi) (\varphi_0)^{-1} (u) \qquad (2\text{-}12)$$

and the strains (ε) may also be written as a function of (u)

$$(\varepsilon) = (\varphi') (\varphi_0)^{-1} (u) \qquad (2\text{-}13)$$

The stresses (σ) are related to strain (ε) through the stress - strain matrix (H)

$$(\sigma) = (H) (\varepsilon) = (H) (\varphi') (\varphi_0)^{-1} (u) \qquad (2\text{-}14)$$

Substituting Equations 2-12, 2-13, and 2-14 in the potential energy statement 2-11, we obtain

$$\phi = \int_{vol} \frac{1}{2} (u)^t (\varphi_0)^{-1^t} (\varphi')^t (H) (\varphi') (\varphi_0)^{-1} (u) \, dv$$

$$- \int_{area} (u)^t (\varphi_0)^{-1^t} (\varphi)^t (P) \, dA \qquad (2\text{-}15)$$

In the case of plane strain, none of the quantities in the integrands of Equation 2-15 vary throughout the region, so for a structure of unit thickness, the integration yields:

$$\phi = \frac{1}{2} A (u)^t \left[(\varphi_0)^{-1^t} (\varphi')^t (H) (\varphi') (\varphi_0)^{-1} \right] (u)$$

$$- L (u)^t (\varphi_0)^{-1^t} (\varphi)^t (P) \qquad (2\text{-}16)$$

The potential energy is minimized by differentiation with respect to the displacement at each nodal point in turn, and equating to 0

$$\sum_{n=1}^{N} \frac{\partial \phi}{\partial u_n} = 0$$

This yields

$$A \left[(\varphi_0)^{-1^t} (\varphi')^t (H) (\varphi') (\varphi_0)^{-1} \right] (u) = L (\varphi_0)^{-1^t} (\varphi)^t (P) \qquad (2\text{-}17)$$

or

$$A \; K \; u = F \qquad (2\text{-}18)$$

Thus the element stiffness per unit area is the term in parenthesis in Equation 2-17. It is also contained in the parenthesis of 2-16.

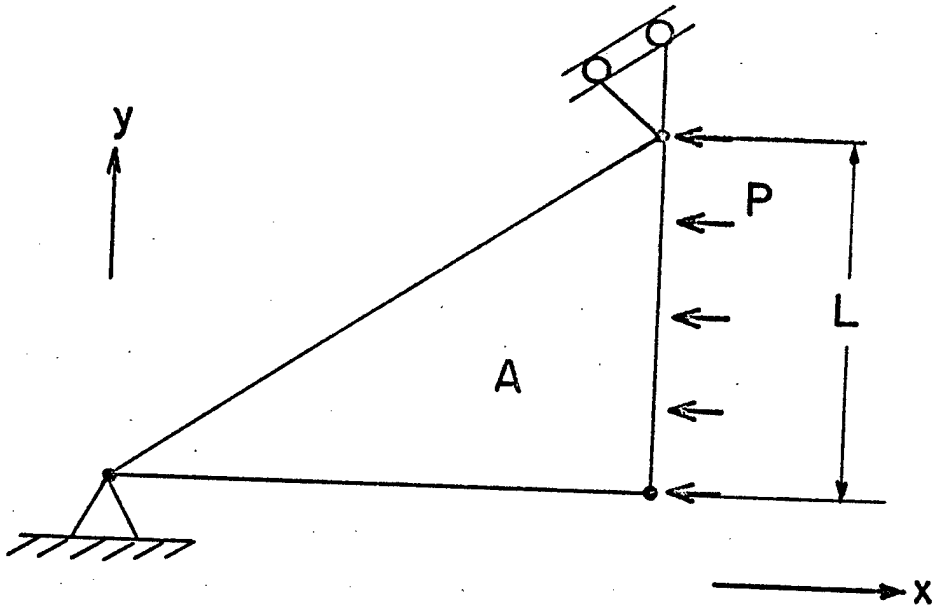

FIGURE 2-24 STRUCTURE CONSISTING OF TRIANGULAR CONTINUUM ELEMENT.

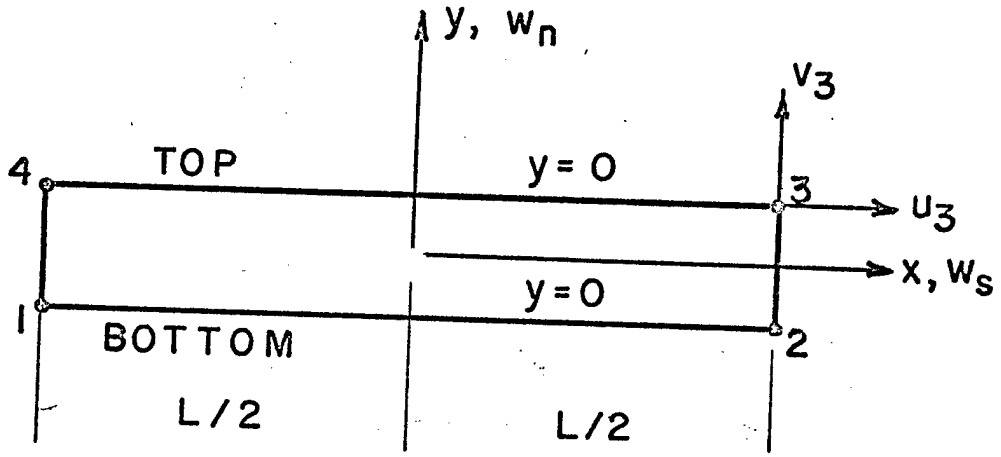

FIGURE 2-25 JOINT ELEMENT-WIDTH = 0; LOCAL COORDINATE SYSTEM

(4) Joint Element Stiffness

In analogous fashion, beginning from an energy equation and minimizing with respect to nodal point displacements, we will derive the element stiffness for the four nodal point element of Figure 2-25. This element has length, L, but zero width as the nodal point pairs (1,4) and (2,3) have identical coordinates. It is shown in a local coordinate system with the x axis along the length. The origin is at the center.

The stored energy, ϕ, in such an element is due to the applied forces per unit length acting through the displacements and must be summed through the element. Thus

$$\phi = \frac{1}{2} \int_{-L/2}^{L/2} w_i P_i \, dx \qquad (2\text{-}19)$$

In matrix notation

$$\phi = \frac{1}{2} \int_{-L/2}^{L/2} (w)^t (P) \, dx \qquad (2\text{-}20)$$

where

$$(w) = \begin{pmatrix} w_s^{top} - w_s^{bottom} \\ w_n^{top} - w_n^{bottom} \end{pmatrix} \qquad (2\text{-}20a)$$

= the relative displacement vector

and

$$(P) = \begin{pmatrix} P_s \\ P_n \end{pmatrix} = \text{the vector of force per unit length} \qquad (2\text{-}20b)$$

The vector (P) may be expressed in terms of a product of unit joint stiffness and displacement

$$(P) = (k)\ (w) \tag{2-21}$$

where (k) is a diagonal matrix expressing the joint stiffness per unit length in the normal and tangential directions.

$$(k) = \begin{bmatrix} k_s & 0 \\ 0 & k_n \end{bmatrix} \tag{2-21a}$$

To clarify the meaning of unit joint stiffness, consider a direct shear test on a rock joint of length, L, and unit width. At first, a normal force is applied and the specimen shortens as the asperities in the joint deform. The specimen also shortens elastically in the solid blocks above and below the joint. Subtracting the elastic deformation from the total shortening, we obtain the joint normal deformation, w_n, which we may plot against the applied force per unit length, F_n/L. Figure 2-26, curve 1, shows hypothetical data from such an experiment. Similarly, as we apply tangential force, we plot the tangential deformation w_s against the shearing force per unit length as in Figure 2-26, curve 2. In the pre-peak region, the slopes of the two curves give the unit normal and unit tangential stiffness for the joint respectively.

Substituting Equation 2-21 in 2-20

$$\phi = \frac{1}{2} \int_{-L/2}^{L/2} (w)^t\ (k)\ (w)\ d\,x \tag{2-22}$$

The displacements (w) may be expressed in terms of the nodal point displacements (u) through a linear interpolation formula. Let u_i and v_i be displacements in the tangential and normal directions respectively at nodal point i along the bottom of the joint element

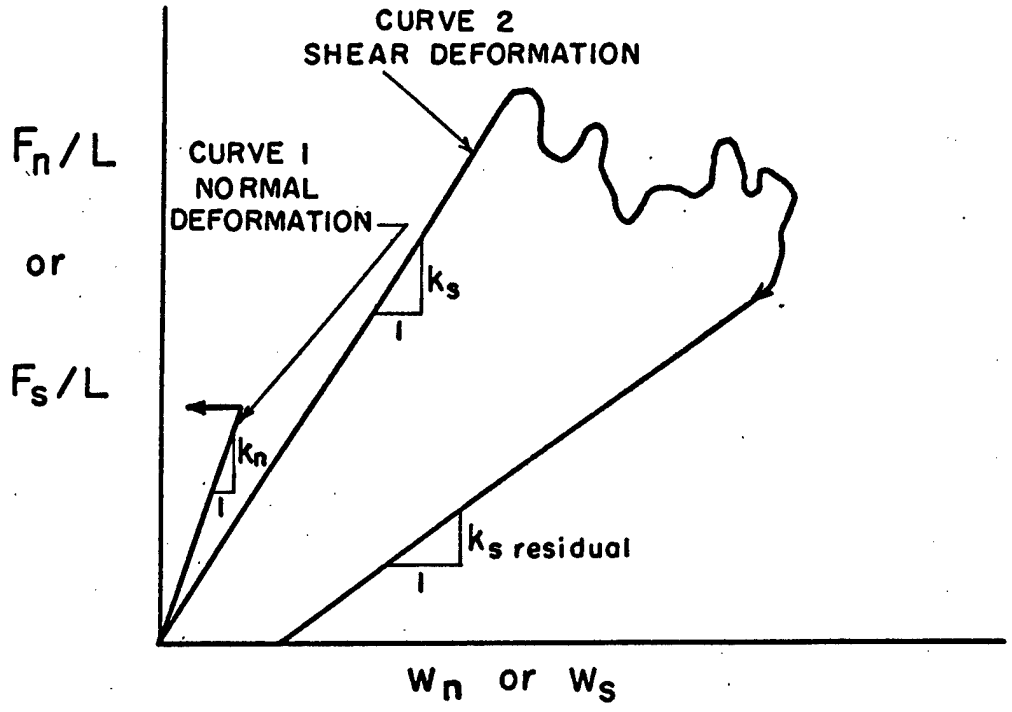

Fig. 2-26. Data from a hypothetical direct shear test on a rock joint.

Specimen Length = L
Specimen Width = 1

$$\begin{bmatrix} w_s^{\text{bottom}} \\ w_n^{\text{bottom}} \end{bmatrix} = \frac{1}{2} \begin{bmatrix} 1 - \frac{2x}{L} & 0 & 1 + \frac{2x}{L} & 0 \\ 0 & 1 - \frac{2x}{L} & 0 & 1 + \frac{2x}{L} \end{bmatrix} \begin{bmatrix} u_1 \\ v_1 \\ u_2 \\ v_2 \end{bmatrix} \quad (2\text{-}23)$$

and along the top of the joint element

$$\begin{bmatrix} w_s^{\text{top}} \\ w_n^{\text{top}} \end{bmatrix} = \frac{1}{2} \begin{bmatrix} 1 + \frac{2x}{L} & 0 & 1 - \frac{2x}{L} & 0 \\ 0 & 1 + \frac{2x}{L} & 0 & 1 - \frac{2x}{L} \end{bmatrix} \begin{bmatrix} u_3 \\ v_3 \\ u_4 \\ v_4 \end{bmatrix} \quad (2\text{-}24)$$

Thus the relative displacement in the joint element is

$$(w) = \begin{bmatrix} w_s^{\text{top}} - w_s^{\text{bottom}} \\ w_n^{\text{top}} - w_n^{\text{bottom}} \end{bmatrix} = \frac{1}{2} \begin{bmatrix} -A & 0 & -B & 0 & B & 0 & A & 0 \\ 0 & -A & 0 & -B & 0 & B & 0 & A \end{bmatrix} \begin{bmatrix} u_1 \\ v_1 \\ u_2 \\ v_2 \\ u_3 \\ v_3 \\ u_4 \\ v_4 \end{bmatrix} \quad (2\text{-}25)$$

where

$$A = 1 - \frac{2x}{L} \qquad B = 1 + \frac{2x}{L}$$

Symbolically,

$$(w) = \frac{1}{2} (D) (u) \quad (2\text{-}25a)$$

where (D) and (u) are defined by Equation 2-25.

Substituting Equation 2-25a in 2-22 yields

$$\phi = \frac{1}{2} \int_{-L/2}^{L/2} \frac{1}{4} (u)^t (D)^t (k) (D) (u) \, dx \qquad (2\text{-}26)$$

Performing the multiplication indicated by Equation 2-26

$$(D)^t (k) (D) = \begin{bmatrix} -A & 0 \\ 0 & -A \\ -B & 0 \\ 0 & -B \\ B & 0 \\ 0 & B \\ A & 0 \\ 0 & A \end{bmatrix} \begin{bmatrix} k_s & 0 \\ 0 & k_n \end{bmatrix} \begin{bmatrix} -A & 0 & -B & 0 & B & 0 & A & 0 \\ 0 & -A & 0 & -B & 0 & B & 0 & A \end{bmatrix}$$

$$(D)^t (k) (D) = \begin{bmatrix} k_s A^2 & 0 & ABk_s & 0 & -ABk_s & 0 & -A^2k_s & 0 \\ 0 & A^2k_n & 0 & ABk_n & 0 & -ABk_n & 0 & -A^2k_n \\ ABk_s & 0 & B^2k_s & 0 & -B^2k_s & 0 & -ABk_s & 0 \\ 0 & ABk_n & 0 & B^2k_n & 0 & -B^2k_n & 0 & -ABk_n \\ -ABk_s & 0 & -B^2k_s & 0 & B^2k_s & 0 & BAk_s & 0 \\ 0 & -ABk_n & 0 & -B^2k_n & 0 & B^2k_n & 0 & BAk_n \\ -A^2k_s & 0 & -ABk_s & 0 & ABk_s & 0 & A^2k_s & 0 \\ 0 & -A^2k_s & 0 & -ABk_s & 0 & ABk_s & 0 & A^2k_s \end{bmatrix} \qquad (2\text{-}27)$$

In Equation 2-26 the only terms that vary along the length are the three products of $1 - \frac{2x}{L}$ and $1 + \frac{2x}{L}$, i.e. A^2, AB, and B^2. There are thus three integrals to be evaluated as follows.

$$\int_{-L/2}^{L/2} \left(1 - \frac{2x}{L}\right)^2 \, dx = \frac{4}{3} L \tag{2-27a}$$

$$\int_{-L/2}^{L/2} \left(1 + \frac{2x}{L}\right)^2 \, dx = \frac{4}{3} L \tag{2-27b}$$

and

$$\int_{-L/2}^{L/2} \left(1 - \frac{4x^2}{L^2}\right) \, dx = \frac{2}{3} L \tag{2-27c}$$

Using the results of Equation 2-27, the expansion of 2-26 is

$$\phi = \frac{1}{2} L \, (u)^t \, (K) \, (u) \tag{2-28}$$

in which

$$K = \frac{1}{6} \begin{bmatrix} 2k_s & 0 & 1k_s & 0 & -1k_s & 0 & -2k_s & 0 \\ 0 & 2k_n & 0 & 1k_n & 0 & -1k_n & 0 & -2k_n \\ 1k_s & 0 & 2k_s & 0 & -2k_s & 0 & -1k_s & 0 \\ 0 & 1k_n & 0 & 2k_n & 0 & -2k_n & 0 & -1k_n \\ -1k_s & 0 & -2k_s & 0 & 2k_s & 0 & 1k_s & 0 \\ 0 & -1k_n & 0 & -2k_n & 0 & 2k_n & 0 & 1k_n \\ -2k_s & 0 & -1k_s & 0 & 1k_s & 0 & 2k_s & 0 \\ 0 & -2k_n & 0 & -1k_n & 0 & 1k_n & 0 & 2k_n \end{bmatrix} \tag{2-29}$$

By analogy to Equation 2-16, K is the joint element stiffness, per unit length. The factor $\frac{1}{2}$ in Equation 2-28 will disappear in taking the variation of ϕ as in Equation 2-17.

The last step in the joint stiffness derivation is to place the element in a coordinate system for the entire structure. Adopting a global coordinate system X, Y as drawn in Figure 2-27,

$$\begin{bmatrix} x \\ y \end{bmatrix} = \begin{bmatrix} \cos & \sin \\ -\sin & \cos \end{bmatrix} \begin{bmatrix} X \\ Y \end{bmatrix}$$

where x and y are local coordinates in the tangential and normal directions respectively.

(5) Computer Code

The joint element stiffness matrix is constructed for each joint element in a subroutine called "joint stiff". The structural stiffness matrix for the entire system of blocks and joints is then assembled by adding the appropriate terms of elements contributing stiffness, be they joints or continuum elements, at each nodal point in turn as described fully in the previous report. After solution of the stiffness equations, the joint stresses are calculated from the known displacements in a subroutine called "joint stress". If the joint normal stress is tensile in any element, both k_s and k_n are set equal to zero for the element and the problem is repeated. Also, the joint cohesion, joint friction, and residual tangential stiffness (see Fig. 2-26) are read in as data and the shear strength is calculated for the indicated normal pressure on each joint. If the joint shear stress exceeds the shear strength, then k_s is set equal to $k_{s_{residual}}$ and the problem is repeated.

Any problem can be restarted where it was left off previously so that the number of cycles can be increased gradually till a stable state is found.

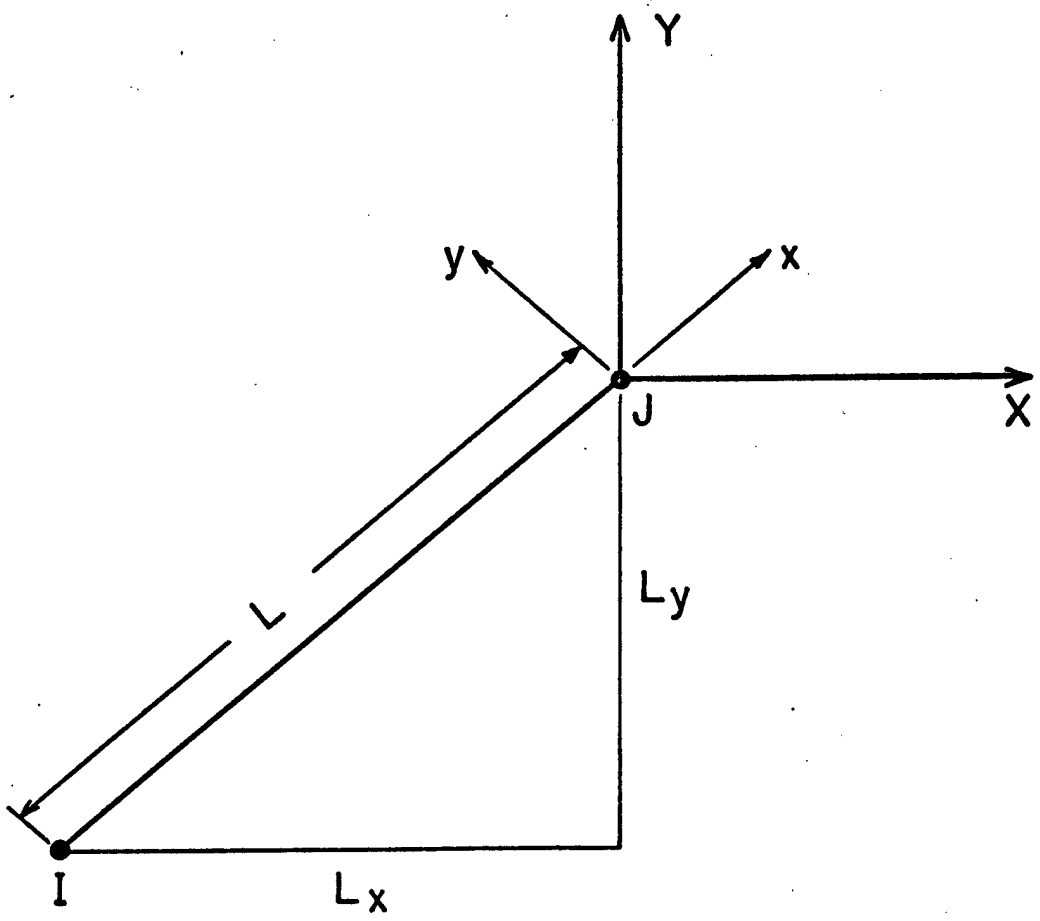

Fig. 2-27. Definition of local coordinate system (x,y) for joint elements in terms of global system X,Y.

(6) Application to Several Basic Problems

To gain experience with the method and to assess its capabilities, several problems increasing in complexity were run. These include (a) Patton's problem -- sliding of a joint with a tooth; (b) behavior at joint intersections; and (c) Trollope's problem -- arching of staggered blocks over a trapezoidal tunnel.

(a) Patton's Problem - Dr. Franklin Patton (1) investigated the shear strength of a joint surface containing a tooth. At low normal pressures, he found that failure occurs when one block rides up on the tooth causing opening of the flat regions of the joint. At high normal pressures, the energy required for one block to move up the asperities of the other was greater than the energy required to shear through the tooth. While the shear strength of the joint must be considered purely frictional when one block slides over the asperities of the other, a cohesional contribution is added when the failure is ascribed to shearing of the asperities. The cohesion is a wall rock property as will the frictional contribution be in part when asperities are sheared.

Figure 2-28a shows a finite element model of the problem. It contains 16 continuum elements and 4 joint elements (heavy lines). The bottom block was restrained and the top block was pulled sideways by applying nodal point forces and boundary conditions as shown. After three cycles, the displacements converged to the solution shown in Figure 2-28b. Only the stoss side of the tooth remained in contact, the other joints opening to the indicated apertures. Shear stress was high in the tooth.

---

1. Patton, F., Multiple Modes of Shear Failure in Rock and Related Materials, Ph.D. thesis, Geology, Univ. of Illinois, 1966. (See also Horn and Deere, Geotechnique, v. XII, p. 319-335, 1962.)

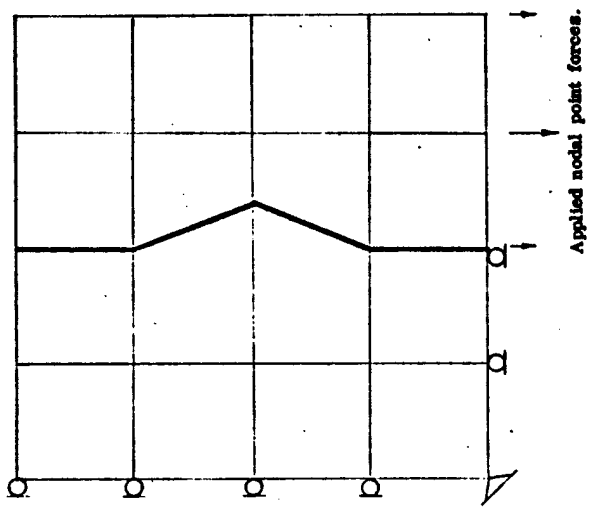

Fig. 2-28a. Patton's Problem Model

Joint is drawn with heavy line.

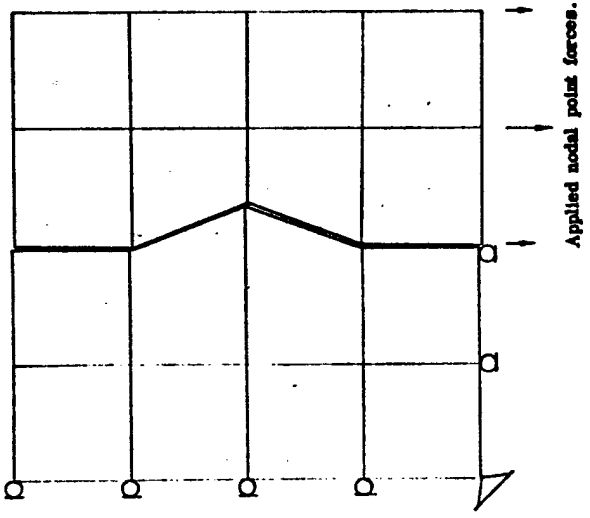

Fig. 2-28b. Patton's Problem

Third approximation. Three of the four joint elements have failed. The top block is moving on the joint element that is inclined in the direction of the thrust.

(b) Behavior at Joint Intersections - A basic attribute of a blocky rock system is the freedom of blocks to shift and rotate forming natural arches and beams. To reproduce this behavior in a complex structure, an analysis technique must be able to simulate block movements in a simple intersection. Figure 2-29a shows a mesh used to simulate the intersection of a through going and a staggered joint set. There are three elastic blocks, each composed of 16 elements. The two joints are developed by 8 joint elements. The details at the intersection are shown in Figure 2-30. Three nodal points with identical coordinates are used at the intersection.

Two problems were run. In Problem 1, the bottom was placed on rollers in the outer corners (A in Figure 2-29a). This creates an unstable situation in which the top block tends to drop down with rotations about the Points A. In Problem 2, the hinges were moved inward to B (Fig. 2-29a) creating the tendency for the opposite sense of rotation.

Figure 2-31 shows the details of displacements in Problem 1 along the joints and in the 14 contiguous elements of the blocks. In Figure 2-31a, after one cycle, failure has initiated along the bottom with partial opening of the vertical joint. After three cycles, as shown in Figure 2-31b, crack opening has propagated upward in the vertical joint and has begun in the center of the horizontal joint while the stresses in the block corners are so high as to induce localized crushing or plastic hinging as inferred by the shaded zones. In the fourth cycle, total collapse was indicated.

Figure 2-32 shows the results for Problem 2, with hinges at B. As shown in 2-32a, after one cycle, the vertical joint had opened at the top. After three cycles the joint opening had propagated farther (Fig. 2-32b) but the shear strength in the horizontal joint had stabilized the system. Even though three joint elements had failed, the system reached stable equilibrium.

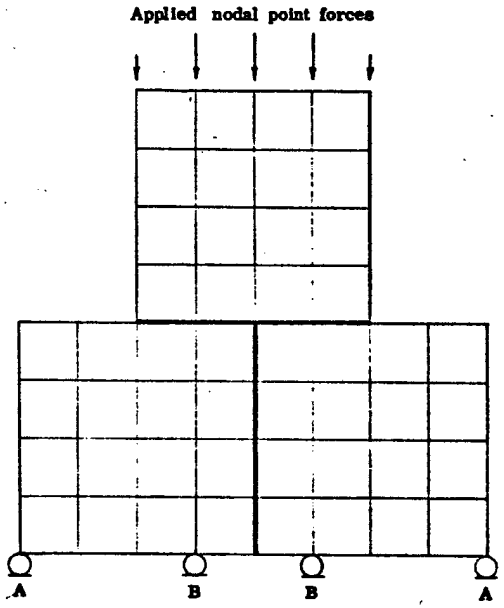

Fig. 2-29a. Intersection of Joints - Model

Joints are drawn with heavy lines. Rollers are applied at A only in Problem 1 and at B only in Problem 2.

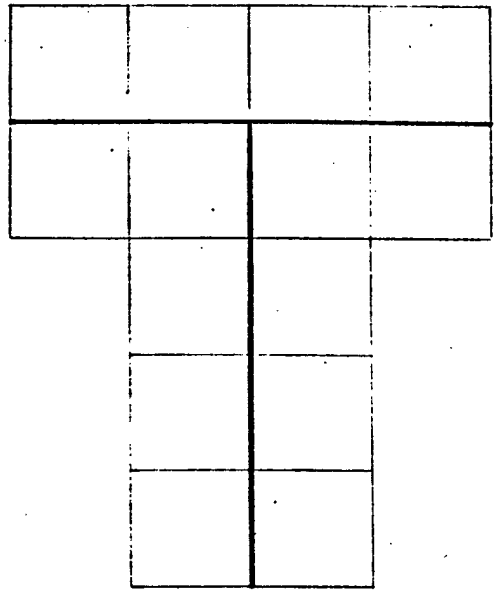

Fig. 2-29b. Intersection of Joints - Problems 1 and 2

The initial situation of the eight joint elements and of the adjacent block elements.

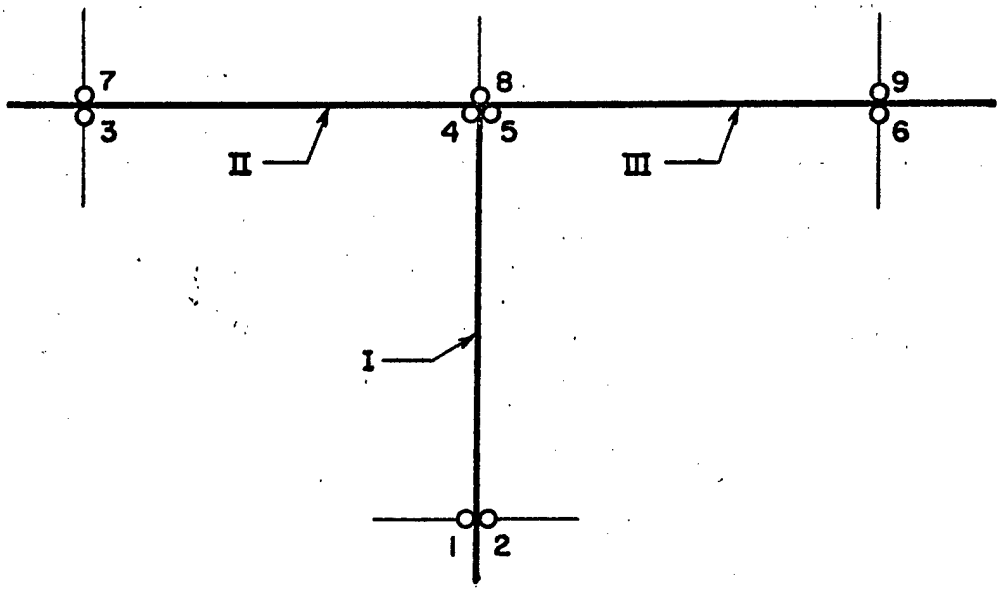

FIGURE 2-30.

INTERSECTION OF JOINTS. DETAIL.

Initially, the coordinates are the same for nodal points 1 and 2, for nodal points 4, 5 and 8 etc.

Element I is defined by nodal points 2 - 5 - 4 - 1.
Element II is defined by nodal points 3 - 4 - 8 - 7.
Element III is defined by nodal points 5 - 6 - 9 - 8.

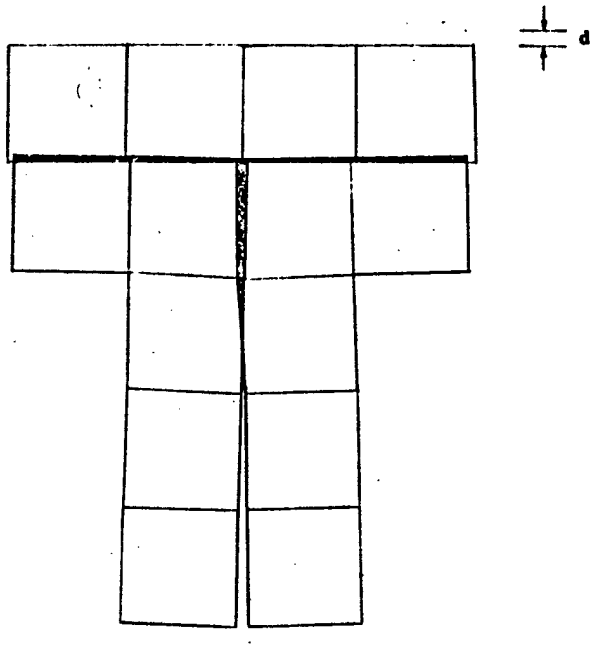

Fig. 2-31a. Intersection of Joints - Problem 1

First approximation. Failure is initiated in the lower part of the vertical joint.

The apparent mutual penetration of block elements (shaded) indicates areas of compression normal to joint elements.

d is the downward movement of nodal points in the top line.

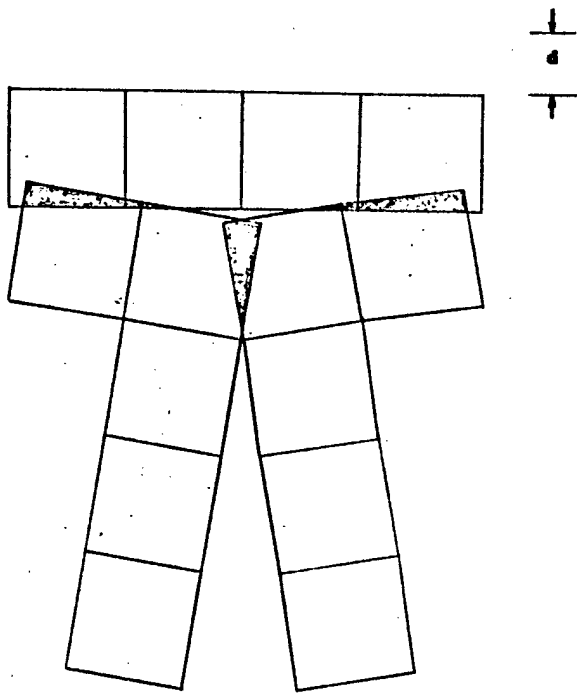

Fig. 2-31b. Intersection of Joints - Problem 1

Third approximation. The bottom blocks are rotating as initial failure is taking place even in the horizontal joint elements adjacent to the intersection with the vertical joint.

The following approximation showed total collapse.

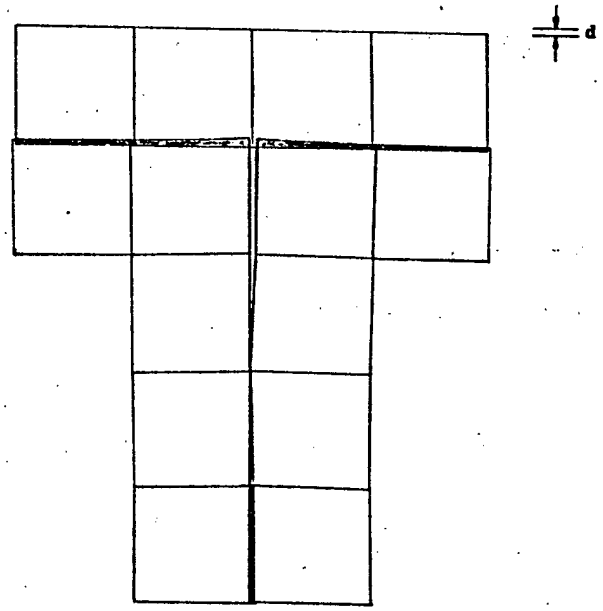

Fig. 2-32a. Intersection of Joints - Problem 2

First approximation. High tensile stresses have been developed normal to the top elements of the vertical joint. However, failure does not occur in these elements until the following approximation.

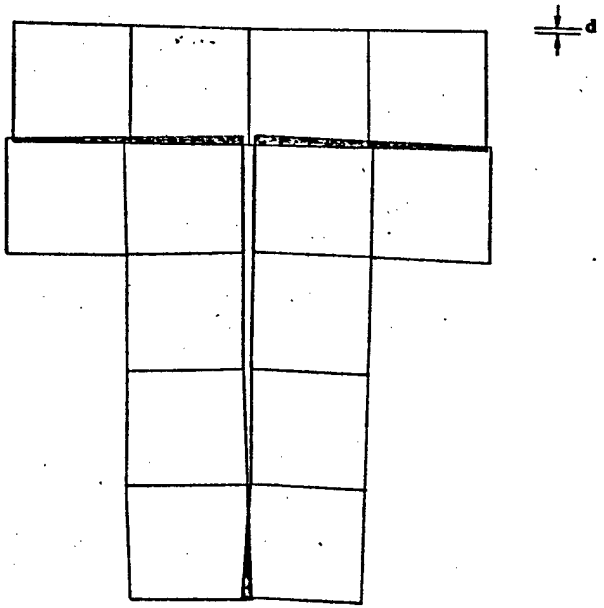

Fig. 2-32b. Intersection of Joints - Problem 2

Third approximation. The upper three elements in the vertical joint have failed. The other joint elements are in compression.

Further approximations do not change the displacements or the stresses. Thus, the model is now stable even though three joint elements have failed.

(c) Trollope's Problem - A tunnel in a system of staggered blocks. Trollope (1) has studied the behavior of trapezoidal tunnels formed by removing blocks in a construction type sequence from a regular stacking of 5/8" smooth plastic cubes. In Figure 2-33, reproduced from the cited work, two regions are apparent -- a triangular "suspended" zone above the opening and a stable zone outside. Trollope stated that "...for a given trapezoidal opening, the 'roof' can easily be fretted away until a very stable triangular opening is established". The simple horizontal row of blocks is a fundamental unit; it tends to fail by shear along vertical joints and by bending as observed in the previous example (see Fig. 2-32). During pure bending, joint elements in tensile zones will initially fail in tension rather than in shear.

Figure 2-34 is a finite element mesh to model the essential features of Trollope's block jointed model. To meet band width restrictions so that a direct solution method could be used in the computer available (IBM 7094), blocks well outside the expected suspended zone were omitted and a condition of no horizontal displacement was set at the side margins as shown. The model has been tested with two different sets of values for the joint parameters as listed in Table 2-4.

TABLE 2-4

Joint Parameters	Case I*	Case II*
k_n	Moderate	High
k_s	Moderate	Moderate
$k_{s_{residual}}$	0	$2/3\ k_s$
Cohesion	0	Moderate
Friction Angle	Moderate	Moderate

1. Trollope, D. H., Felsmechanik und Ingenieurgeologie, v. IV/3, 1966.

*Not to be mistaken with the cases discussed in Trollope's paper (1).

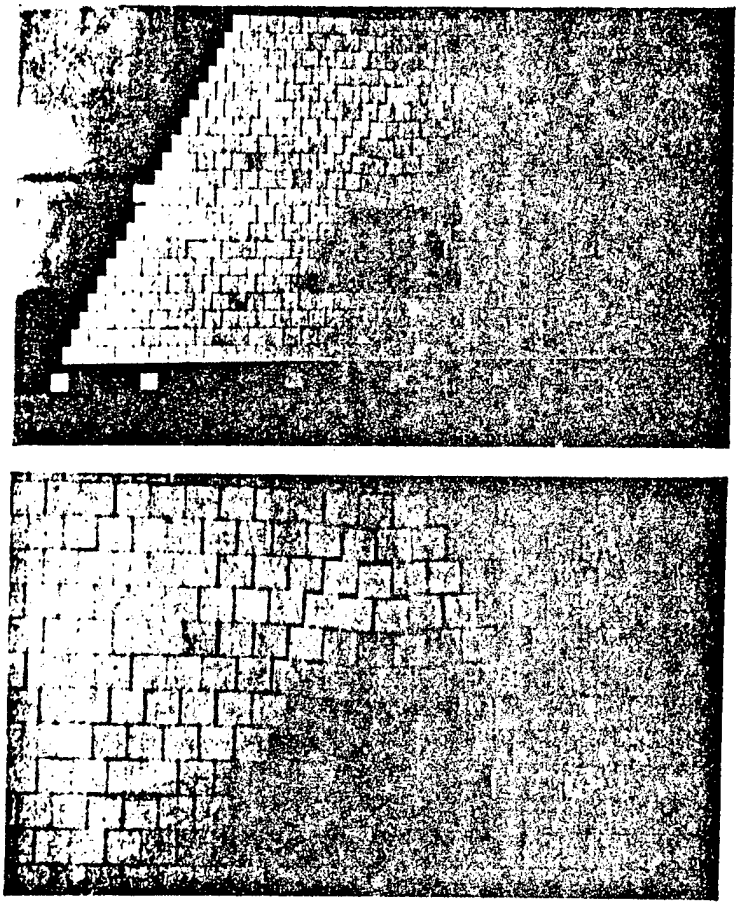

Fig. 2-33. Block-jointed model (after Trollope[1])

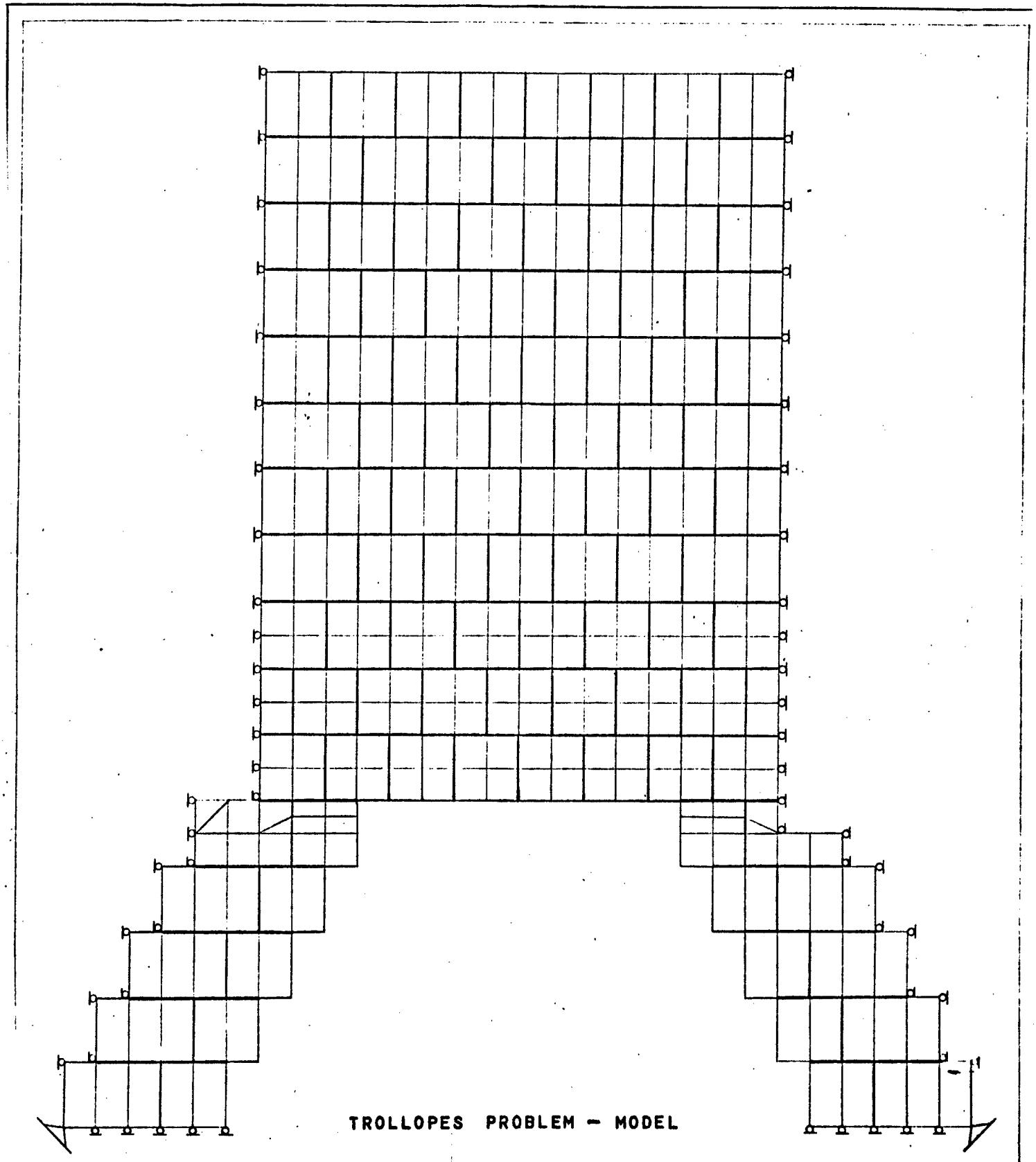

Fig. 2-34.

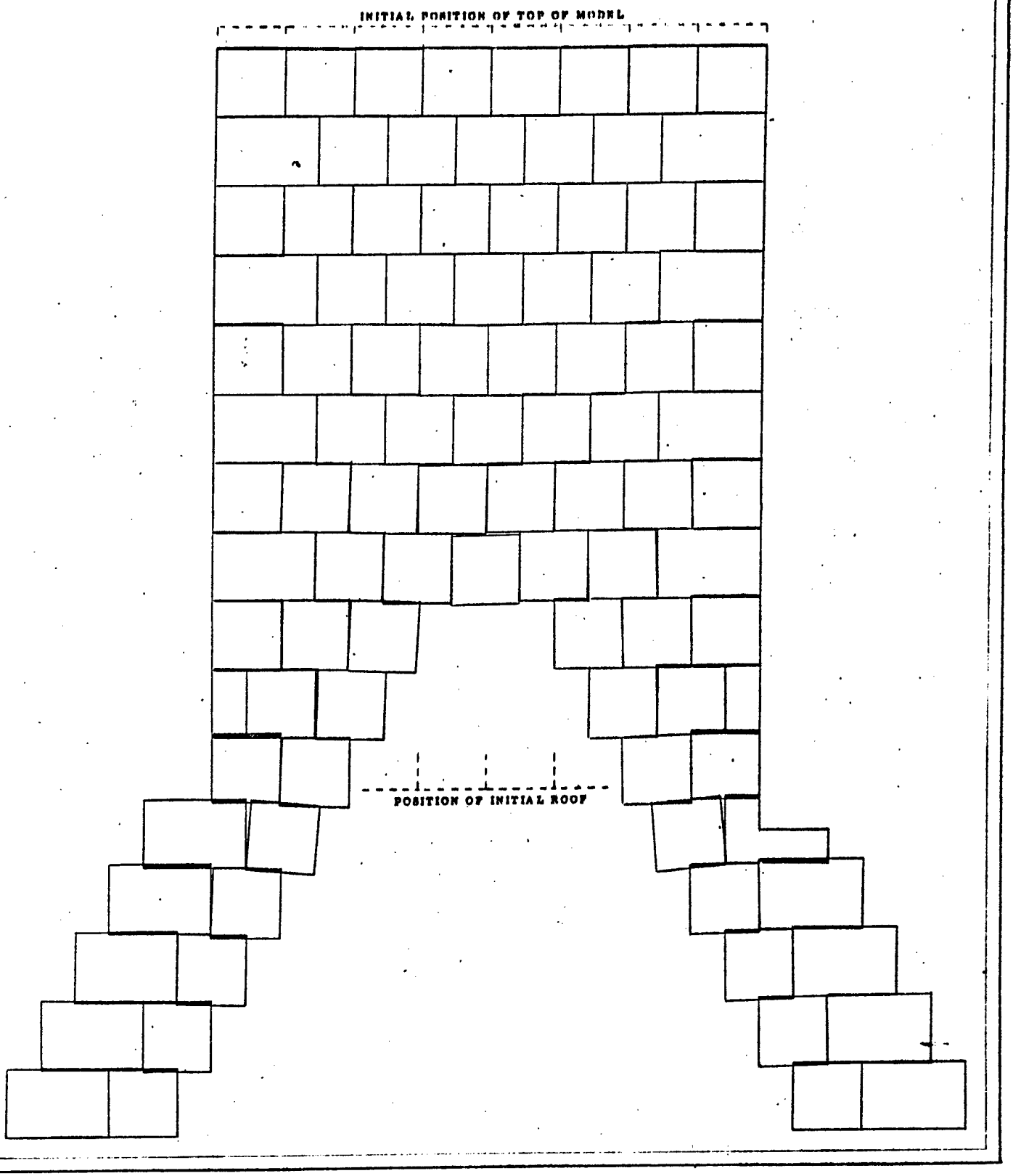

Fig. 2-35. Trollope's Problem - Case I. Collapse of Initial Roof

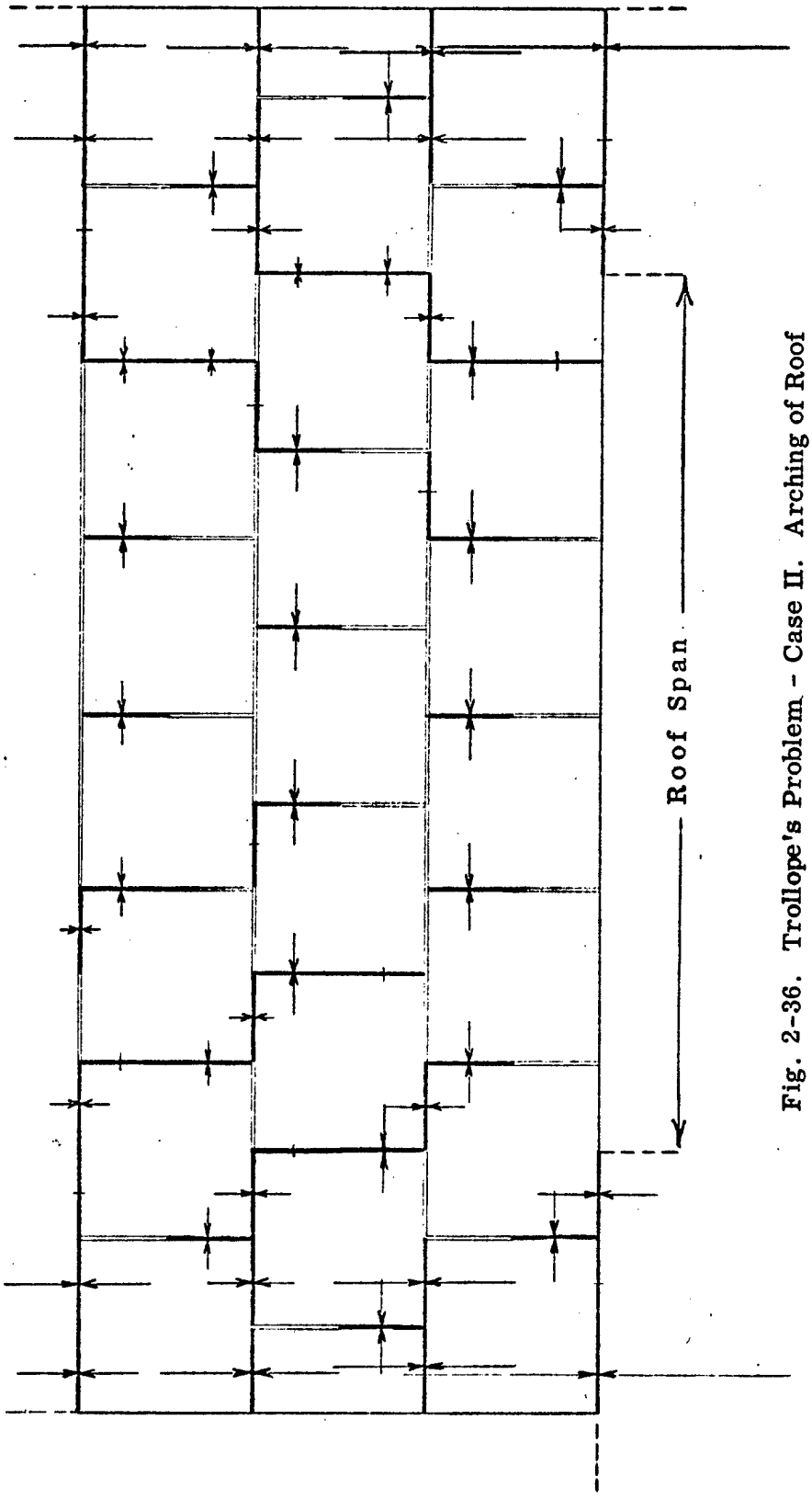

Fig. 2-36. Trollope's Problem - Case II. Arching of Roof

Heavy Line: Joint element in compression.
Double Line: Joint element which has opened in response to tension.
Arrows: Indicate relative values of compressive forces across joint elements.

In Case I, the initial roof is unstable as shown in Figure 2-35. Blocks in the roof have slipped out and rotation of blocks adjacent to the opening is easily recognized in the figure (the displacements are drawn to scale). The data used are from the third approximation. It is seen from the figure that equilibrium has not yet been achieved. For example, the central block in the roof formed is in the process of slipping. Subsequently, however, the roof formed should be stable.

To illustrate the behavior of the model in Case II, only the three lower block rows of the roof are shown in Figure 2-36. With the joint parameters mentioned, the initial roof is stable. Joint elements are shown as double lines when they have failed (in tension) and as heavy lines when they are in compression. To illustrate the arching effect, relative values of compressive forces, where acting across the joint elements, have been indicated by arrows. The figure is drawn after four approximations. As convergence has not yet been reached, the results are not symmetrical. However, it can readily be seen that in approaching the roof from above, the weight of the overlying rock is being transmitted to the abutments via the outer blocks in each row. Tensile failure of horizontal joint elements lead to partial separation of the rows. Thus, ultimately the main part of the lowest block row will act as a beam carrying only its own weight. It is stabilized through the shear strength mobilized in the upper part of the vertical joint elements by the development of lateral thrust. This beam effect decreases in the subsequent rows above the roof.

An interesting observation (not shown in Figure 2-36) is the occurrence of tensile stresses induced by the lateral thrust in beam block elements above the roof.

In conclusion it should be emphasized that we have not pretended to discuss all aspects of Trollope's problem, but have only used the model to give an illustration of the influence of the joint parameters on roof stability. It seems that the method of analysis can adequately handle such joint behavior features as failing in tension or shear, rotation of blocks, development of arches, and even, to a certain extent, the collapse pattern of structures in jointed rock.

2.4 DISCUSSION - THE DIFFERENT TYPES OF JOINTS AND THEIR RELATIVE SIGNIFICANCE

(1) Factors Influencing Joint Parameters - Joint Classification

The behavior of a jointed rock mass depends not only on the type and intensity of the applied loads and constraints, but on (1) the detailed properties of component joints -- stiffness and strength -- and (2) the fabric of the joint system as a whole -- joint spacing, orientation, persistence, etc. The finite element analysis procedures described in Section 2.3 allow these factors to be modelled if the requisite data of the prototype characteristics can be gathered. Much has been written on the methods for obtaining data on the fabric of the joint system so this will not be discussed here. The detailed stiffness and strength properties of individual joints will be discussed.

With the analysis techniques of Section 2.3, three distinct joint parameters must be introduced: (1) k_n, the unit stiffness across the joint; (2) k_s, the unit stiffness along the joint; and (3) S, the shear strength along the joint (described by c and φ). It is useful to characterize a joint by means of k_n, k_s, and S. This set of properties constitutes a necessary and, for the time being, sufficient description of joints to allow prediction of their "potential behavior" under load.*

It is recognized that the actual details of a joint may include ineffable or imponderable attributes, and moreover the characteristics are irregular and variable along the joint (see Fig. 2-37). Further, such features as the water content and degree of consolidation of the filling material, if present, may affect all three joint parameters. While joint stiffness and joint

---

*It may ultimately prove desirable to introduce off diagonal stiffness terms of the type $-k_{sn}$ to account for dilation during shearing in the analysis of Section 2.3.

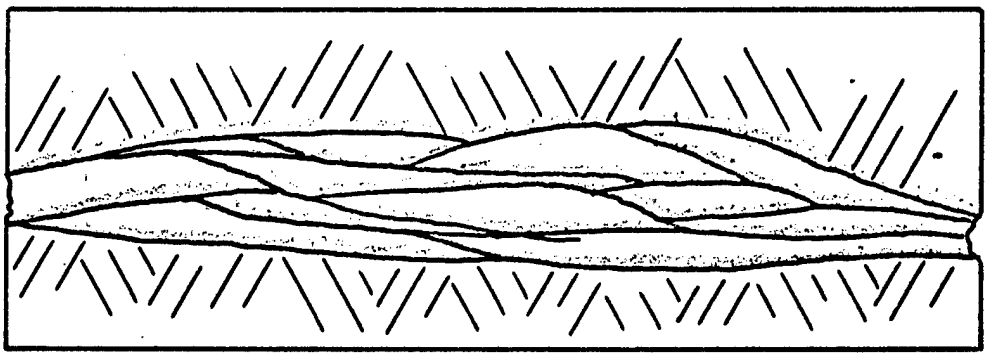

a. Sheared Zone

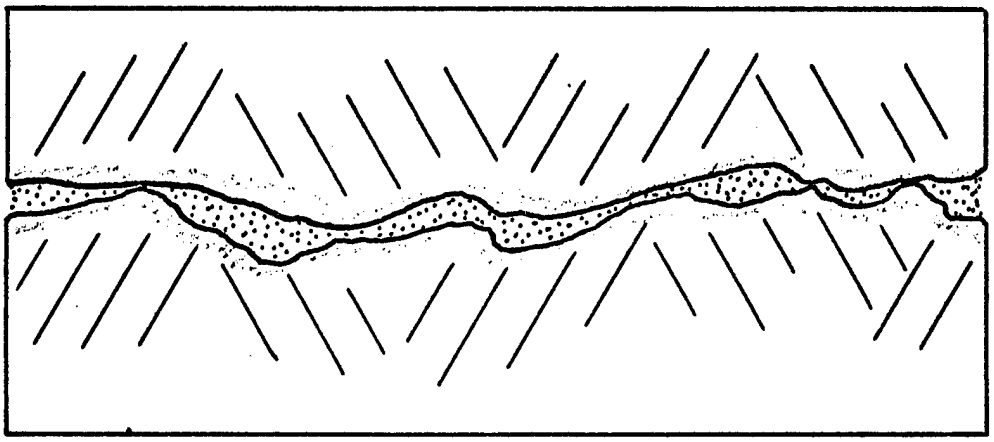

b. Irregular Filled Joint with Altered Wall Rock

Fig. 2-37. The complexity of Hypothetical Weakness Surfaces

strength may partially depend upon factors in common, however, the essential independence of these quantities must be recognized. The oft observed correlation between the Young's modulus and the unconfined compressive strength for many rock types should not lead to a misconception that a similar correlation exists between joint stiffness and joint strength. In an unfilled joint, the strength is primarily dependent on the description of the wall rock while the stiffness depends primarily on the description of the intervening space. The independence of these quantities is illustrated by Figure 2-38 in which idealized direct shear test curves give four extreme associations of tangential stiffness and shear strength. It should be emphasized that the mode of failure (tensile, shear) of a joint cannot be deduced from the stiffness values.

The most important factors influencing the joint parameters are as follows:

k_n will depend on

- the contact area ratio between the two joint walls
- the perpendicular aperture distribution and amplitude
- the relevant properties of the filling material (if present)

k_s will depend on

- the roughness of the joint walls determined by the distribution, amplitude, and inclination of asperities
- the tangential aperture distribution and amplitude
- the relevant properties of the filling material (if present)

S will depend on

- the friction along the joint
- the cohesion due to interlocking
- the strength of the filling material (if present)

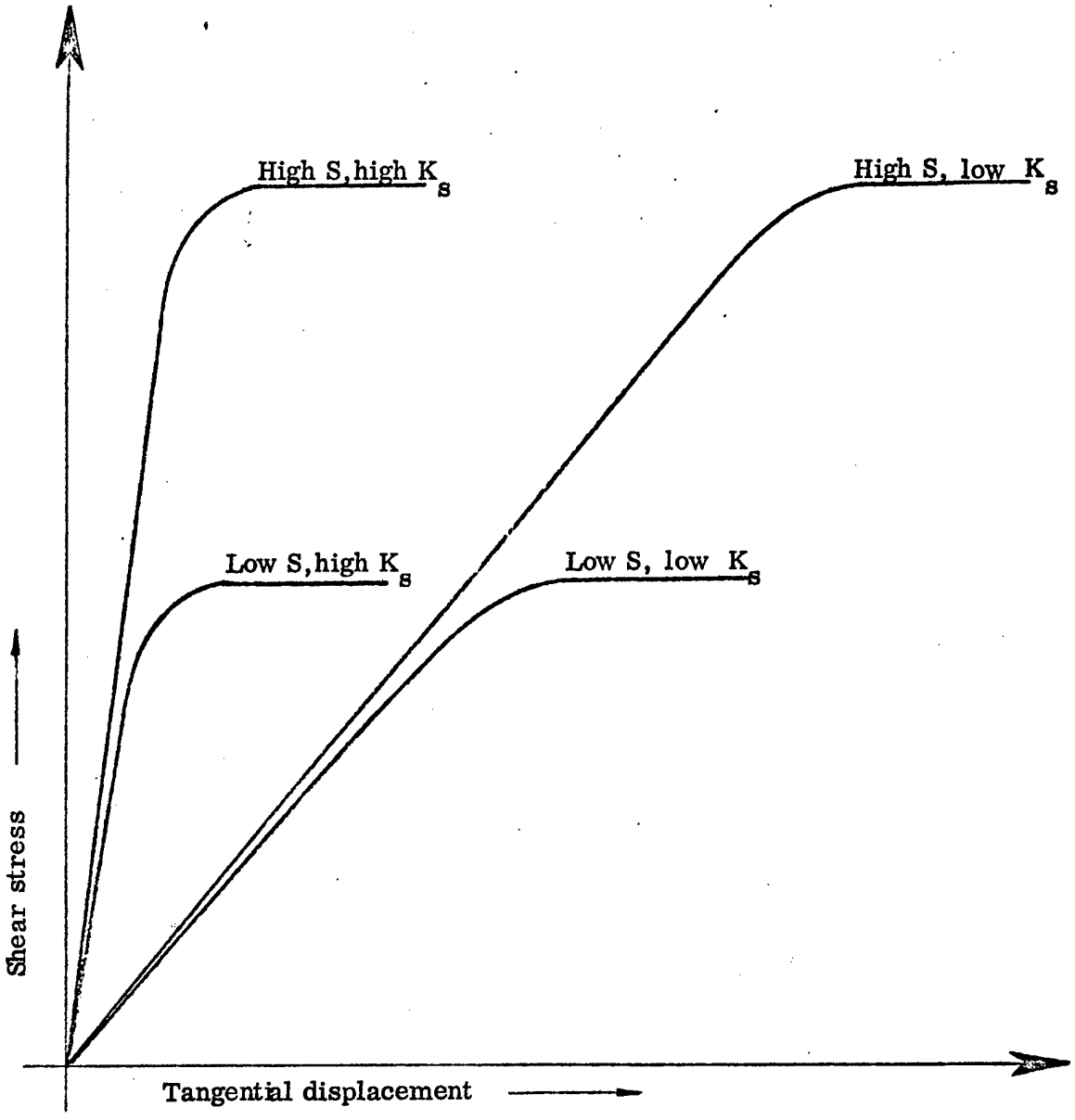

IDEALIZED CURVES ILLUSTRATING INDEPENDENCE OF STRENGTH (S) AND STIFFNESS (REPRESENTED BY K_s).

Fig. 2-38.

The strength of a joint referred to in this context is the strength in shear. The strength of joints in tension must usually be considered negligible. It should be emphasized that, through the cohesion due to interlocking, the joint strength is related to the wall rock strength.

Filling material present in the joint may have a decisive effect on all three parameters. Clay material will in general indicate low values of k_n and k_s. It will also indicate low strength values, except if an extensive interlocking necessitates shearing of strong wall rock asperities during failure. In particular, the montmorillonite group minerals can cause extremely slippery conditions with negligible shear strength of plane joints when the montmorillonitic clay material is wet, has a low consolidation, or is allowed to swell. Mobilized swelling pressures can pry the joint walls apart. If the joint walls are coated with chlorite, talc, graphite, etc., the joint will slip very easily especially when wet. Even if the strength in these cases is very low, the stiffness may be high.

A cementation of the joint, i.e. by quartz, calcite, or epidote, may give the joint properties that are as good or even better than the properties of the wall rock. In a stability context, these joints may therefore safely be ignored. An important exception is due to the possibility of calcite fillings dissolving with time especially when the calcite filling is porous or flaky.

Moisture in a joint will influence all three parameters indirectly through the influence on filling material properties and will also directly influence the strength of an unfilled joint through a reduction in frictional strength when the joint is wet. Water pressures play as great a role in jointed rock as in soils; the effective stress principle is considered to apply. Theoretically, pore water pressure can be included in the stiffness

k_n	S			k_s
	H	M	L	
H				H
H		x		M
H				L
M				H
M				M
M				L
L				H
L				M
L				L

k_n - is the stiffness perpendicular to the joint

k_s - is the tangential stiffness

S - is the joint shear strength

H - high value

M - moderate value

L - low value

Fig. 2-39. Classification of Joints by Means of k_n, k_s, and S.

matrix of the joint. However, it seems at present more relevant to regard the pore water pressure as an external pressure to be applied to both joint walls. (This can easily be done with the computer program used.) Thus, while the "wetness" of the joint is considered a joint property, pore water pressure is regarded as a system variable.

The factors influencing the values of the joint parameters k_n, k_s, and S are very difficult to quantitize for a given joint. Even if relevant data for each factor could be measured, the compilation to yield the parameters requires the dubious task of deciding on the relative influence of each factor. Therefore, the direct measurement of k_n, k_s, and S is necessary.

For the purpose of classification, each parameter may be rated high, moderate, or low. This yields a classification system of 27 joint parameter combinations. The classification system is shown as a diagram in Figure 2-39. A joint with high normal stiffness, moderate tangential stiffness, and moderate strength has been plotted as an example.

A high joint stiffness is a value which yields negligible joint displacements when compared to the elastic displacements of the rock blocks. Conversely a low stiffness is a value which leads to joint displacements that dwarf the elastic displacements of the blocks. A moderate joint stiffness corresponds to displacements of joints of the same order of magnitude as the elastic displacements. Similarly, the joint strength may be considered to be high, moderate, or low depending on whether the joints play a negligible, participating, or dominant role in the strength of the rock mass.

In Figure 2-40, eight idealized examples of interlocked joints are given to illustrate the influence of joint aperture and wall rock strength on the joint parameters. The examples of Figure 2-40 demonstrate again that the joint stiffness and the joint strength are independent. The figure also illustrates how the classification system mentioned may be used. In the examples, only high and low values are applied. For the wall rock

IDEALIZED DIAGRAMS ILLUSTRATING THE INFLUENCE OF JOINT APERTURE AND WALL ROCK STRENGTH ON JOINT PARAMETERS.

Example number.	Strength of wall rock.	Joint parameters : K_n	K_s	S
1.	H	H	H	H
2.	L	H	H	L
3.	H	H	L	H
4.	L	H	L	L
5.	H	L	H	H
6.	L	L	H	L
7.	H	L	L	H
8.	L	L	L	L

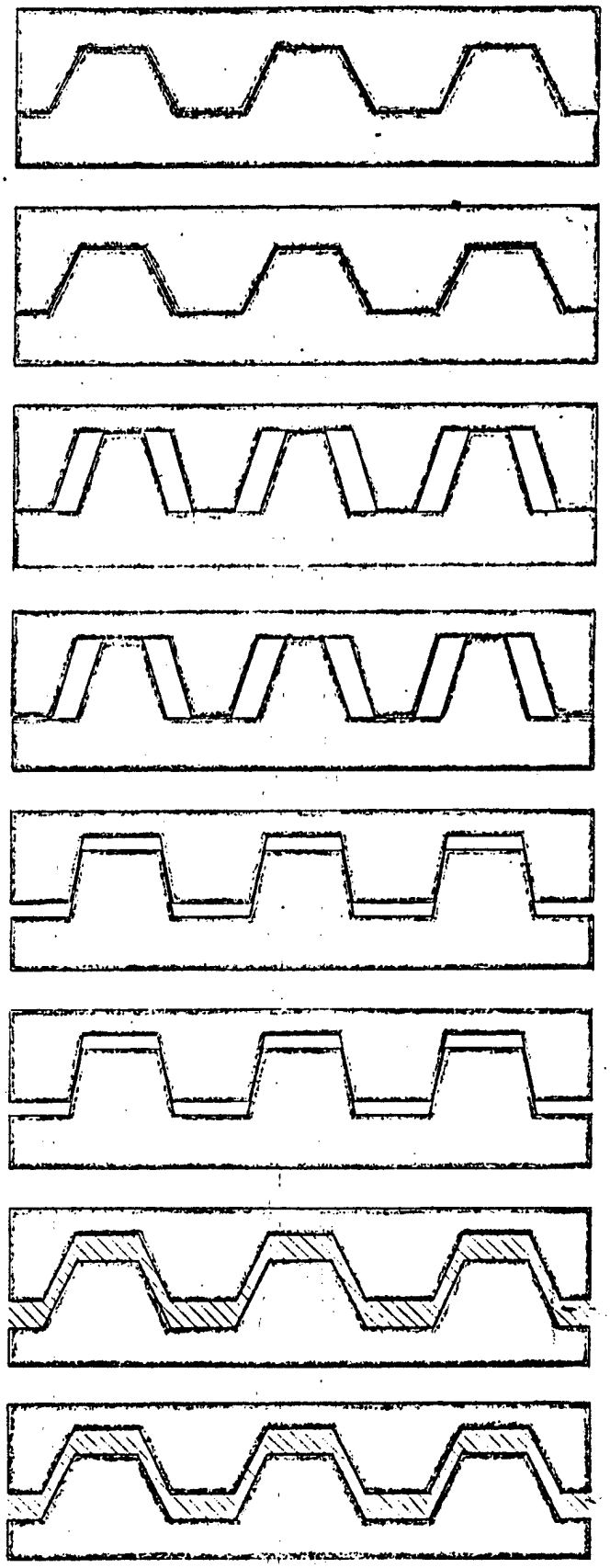

Fig. 2-40.

strength, a high value infers that the resistance to shearing of the asperities is high. A low wall rock strength indicates in reality highly altered wall rock.

Example 1 - Tight joint or plane cemented joint.

Example 2 - As 1, but with altered wall rock or plane, tight, and slippery joint.

Example 3 - Perpendicularly tight, but tangentially open joints.

Example 4 - As 3, but with altered wall rock.

Example 5 - Tangentially tight, but perpendicularly open joint.

Example 6 - As 5, but with altered wall rock.

Example 7 - Open joint with compressible filling.

Example 8 - As 7, but with altered wall rock or plane, open, and slippery joint.

(2) Values of the Joint Stiffness

While the adjectives high, moderate, and low may be understood in a relative sense when applied to joint stiffness, the joint stiffness concept is so new that no values are to be found in reports and publications about joint properties. The necessary data exist, however, in the results of direct shear tests, from around the world, on specimens with joints.

One of the most sophisticated joint test programs known to the author is a current investigation in the Department of Mining at Imperial College, University of London. A highly controlled, large direct shear test machine has been built and 9-inch width undisturbed specimens of natural joints are being tested*. As an illustration of the kinds of stiffness values associated with natural joints, the results of Test 1, performed in April 1967 on a joint in quartz porphyry from Rio Tinto, Spain, will be discussed.

*We are indebted to Dr. David Pentz for providing these data and allowing us to include them here.

The joint tested was 9 inches wide by 10 inches long. The angle of friction was 34^{o} and the cohesion was 150 psi. The slope of the pre peak portion of the shear stress - displacement curve gave a value of k_s = 3,780 psi/inch. The normal load - displacement data have not yet been supplied so k_n is not yet known to the writer. The elastic shear modulus of the solid rock was of the order of 3 million psi and the joint spacing is of the order of 5 feet. The elastic shearing displacement of a 5-foot thick joint bounded block of rock is thus given by a continuum unit stiffness of $\frac{1}{60 \text{ inches}}$ x 3 million psi = 50,000 psi/inch. Since the joint displacements are of the order of 13 times the elastic shearing displacements of the intervening joint blocks, the joint may be characterized as having low shear stiffness. It is classified as a low stiffness, moderate strength joint.

(3) The Relative Response of Different Classes of Joints

The wide range of possible joint conditions indicates the likelihood of extremely different response to applied load for joints of different classifications. To explore the possible range in behavior, a test problem has been selected -- the stresses and displacements of a 10 foot radius circular tunnel loaded horizontally with p_1 and vertically with $p_2 = 0.43\, p_1$. The Kirsch solution results have been compared with finite element solutions for: (I) a set of vertical joints, (II) a set of horizontal joints, and (III) a system of vertical and horizontal sets of joints. In each system joint spacing equals 3 feet. For each of the three systems, solutions were obtained for four extreme cases in which different joint properties were ascribed corresponding to the four permutations of high and low joint stiffness. Case 1 had high k_n and high k_s and Case 2 had high k_n and low k_s. Cases 3 and 4 had low k_n with high values and low values of k_s respectively (see Fig. 2-41). Selected results are presented in Table 2-5 and are summarized as follows.

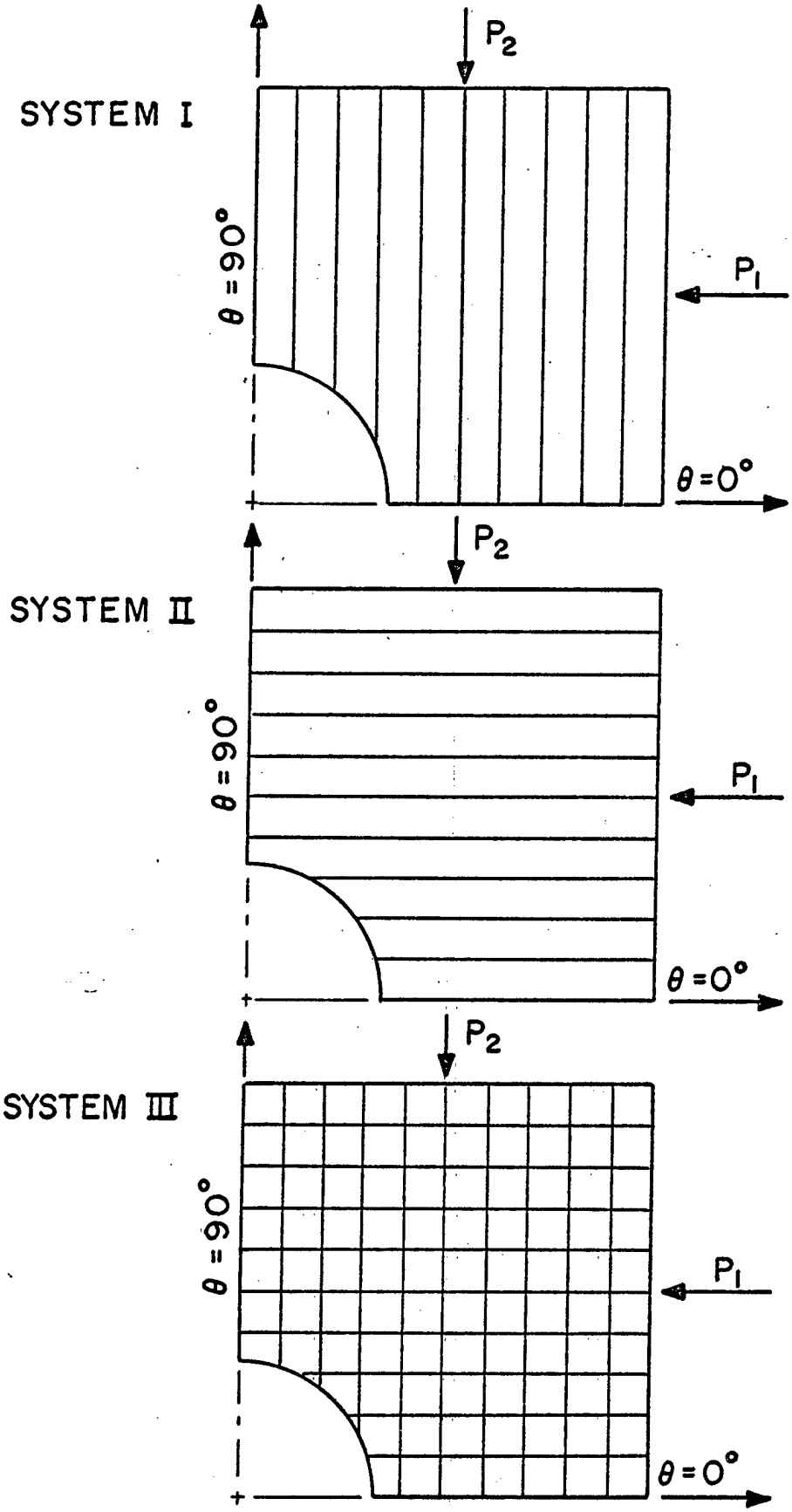

Case 1: High k_n High k_s
Case 2: High k_n Low k_s
Case 3: Low k_n High k_s
Case 4: Low k_n Low k_s

Fig. 2-41. Joint Systems and Cases Considered in Example.

TABLE 2-5. Effect of Joint Systems on Stresses Around a Circular Tunnel

Joint System	Case	Joint Parameters k_n	Joint Parameters k_s	Joint Parameters S	Tangential Stress Concentration σ_θ / p_1 At Roof Center $\theta = 90^o$	Tangential Stress Concentration σ_θ / p_1 At Springline $\theta = 0^o$	Relative Wall Deformation At Springline $\theta = 0^o$	Relative Wall Deformation At Roof Center $\theta = 90^o$
Homogeneous - Kirsch Solution	--	--	--	--	2.57	0.29	moderate inward	small downward
I	1	High	High	High	2.30	- 1.60	moderate inward	small upward
Vertical Joints at 3-foot Spacings	2	High	Low	High	6.20	0.60	large inward	large downward
	3	Low	High	High	- 0.30	1.60	large outward	small downward
	4	Low	Low	High	1.00	- 1.50	very large inward	moderate upward
II	1	High	High	High	2.60	- 0.70	moderate inward	small upward
Horizontal Joints at 3-foot Spacings	2	High	Low	High	5.10	1.30	very large inward	small downward
	3	Low	High	High	7.50	- 0.40	large inward	very large downward
	4	Low	Low	High	4.30	- 0.10	very large inward	large downward
III	1	High	High	High	2.30	- 1.2	moderate inward	small upward
Vertical and Horizontal Joints at 3-foot Spacings	2	High	Low	High	12.00	0.20	large inward	slight downward
	3	Low	High	High	1.30	- 3.30	very large inward	very large upward
	4	Low	Low	High	1.80	- 1.70	very large inward	large upward

(a) Wall Deformations - The pattern of wall deformations was markedly different for the tunnel in jointed rock than for the tunnel in continuous rock for each case in which one or both joint stiffness parameters was set low. The blocky structure results in a discontinuous pattern of deformations, each block moving independently of its neighbors. Greater deformations result when k_s is low than when k_n is set low.

The case in which the joints are assigned low normal stiffness and high tangential stiffness, Case 3, yields results quite unlike the other three cases considered. With the system of horizontal joints, the wall moves out rather than in and with the system of vertical joints the roof moves up rather than down.

(b) Wall Stresses in the Joint Blocks ($\theta = 0^o$) - Since p_1 is horizontal, the point where $\theta = 0^o$ is the wall of the tunnel. The Kirsch solution at this free field principal stress ratio predicts no tension anywhere, even in the wall. However, when the joint systems were considered, in certain cases significant tension developed in the wall.

(c) Roof Stresses in the Joint Blocks ($\theta = 90^o$) - The Kirsch solution predicts a tangential stress concentration in the roof ($\theta = 90^o$) of $2.6\ p_1$. The stresses were increased greatly for all three systems where the joints were assigned high normal stiffness and low tangential stiffness (Case 2). With a single set of either horizontal or vertical joints of this class, the maximum stress concentration in the wall was 5 and 6 respectively while with both vertical and horizontal joints of Case 2, the joint blocks suffered a compression stress of about $12\ p_1$. With a single

set of vertical joints having low normal stiffness and high shear stiffness (Case 3) the roof was, conversely, completely destressed. With horizontal Case 3 joints, however, just the opposite result was found, i.e. very high roof compression (6 p_1).

In summary this example shows the very great difference in the behavior of a tunnel under given loading conditions when the orientation and properties of the joints are varied. Stiff, strong joints do not alter the stress distribution around a tunnel; all other types of joints do. Direct measurement of joint quantities appears to be important, perhaps even more so than direct measurement of the rock block characteristics.

3. ANALYSIS OF THE ACTION OF ROCK BOLTS*

3.1 GENERAL

In this section, the states of stress due to single and multiple rock bolt installations are examined. In most of the cases, idealized rock bolt representations are used, these being point load representations of the anchor and bearing plate. The probable conditions in the immediate vicinity of the bearing plate and anchor are investigated in an attempt to determine the error introduced by the point load assumption. The beneficial or detrimental effects of a single rock bolt installed in a jointed medium are investigated and zones of various types of triaxial stress states are delineated both for single and multiple bolt installations. The material in which the rock bolts are installed is considered to be elastic, isotropic, and continuous. Elastic constants, where required, are chosen to be representative of a typical rock type in which rock bolts would be installed.

3.2 THE ROCK BOLT ANCHOR

The problem of evaluating the stress distribution in the vicinity of a rock bolt anchor has been considered by several investigators. Visual examination of actual rock faces which have been under anchor loadings, as well as examination of the anchors, reveals that the stresses at the interface between rock bolt anchor and wall rock are high enough to cause local plastic yielding of both substances. Models using photoelastic techniques have also helped define the probable stress distributions.

---

*This section was prepared by Dr. Hans Ewoldsen.

If a mathematical representation of the single rock bolt is desired, the usual assumption is to consider both anchor and bearing plate. The point load representation of the anchor requires a continuous, homogeneous medium. If continuity is assumed, tensile stresses are found to develop behind the rock bolt anchor which may exceed the tensile strength of the rock. In an in-situ situation it is most probable that these tensile stresses do not develop because of adjustments on joints behind the anchor. The problem of tensile stresses together with the uncertainties of using a point load assumption indicated that further study of the rock bolt anchor, as reported here, would be desirable.

In order to model the presence of joints in the physical system, a finite element type of solution is used with which it is possible to create zones weak in tension. Since the rock bolt anchor problem is an axisymmetric one, the axisymmetric finite element program was used. Restrictions inherent in this approach are only those which require symmetry about the axis of the rock bolt. The total 10,000 pound bolt load was sustained by a shearing force uniformly distributed over the inside of the bore hole. The anchor was 3 inches long and 2 inches in diameter. Assuming a friction coefficient of 0.8, a radial load of 12,500 pounds was also distributed over the rock wall.

In the first solution, there were no weak joints in the system; the stress distributions obtained are seen in Figures 3-1a, 3-1b, and 3-1c. As can be seen, tensile stresses develop behind the anchor. In the second solution, a joint was simulated, occuring immediately behind the anchor and perpendicular to the axis of the bolt. The resulting stress distributions are seen in Figures 3-1d, 3-1e, and 3-1f. In this case in the immediate vicinity of the anchor, the inclusion of the joint results in stresses being concentrated between the anchor and bearing plate with little stress being transmitted to the area behind the bolt. A comparison of the

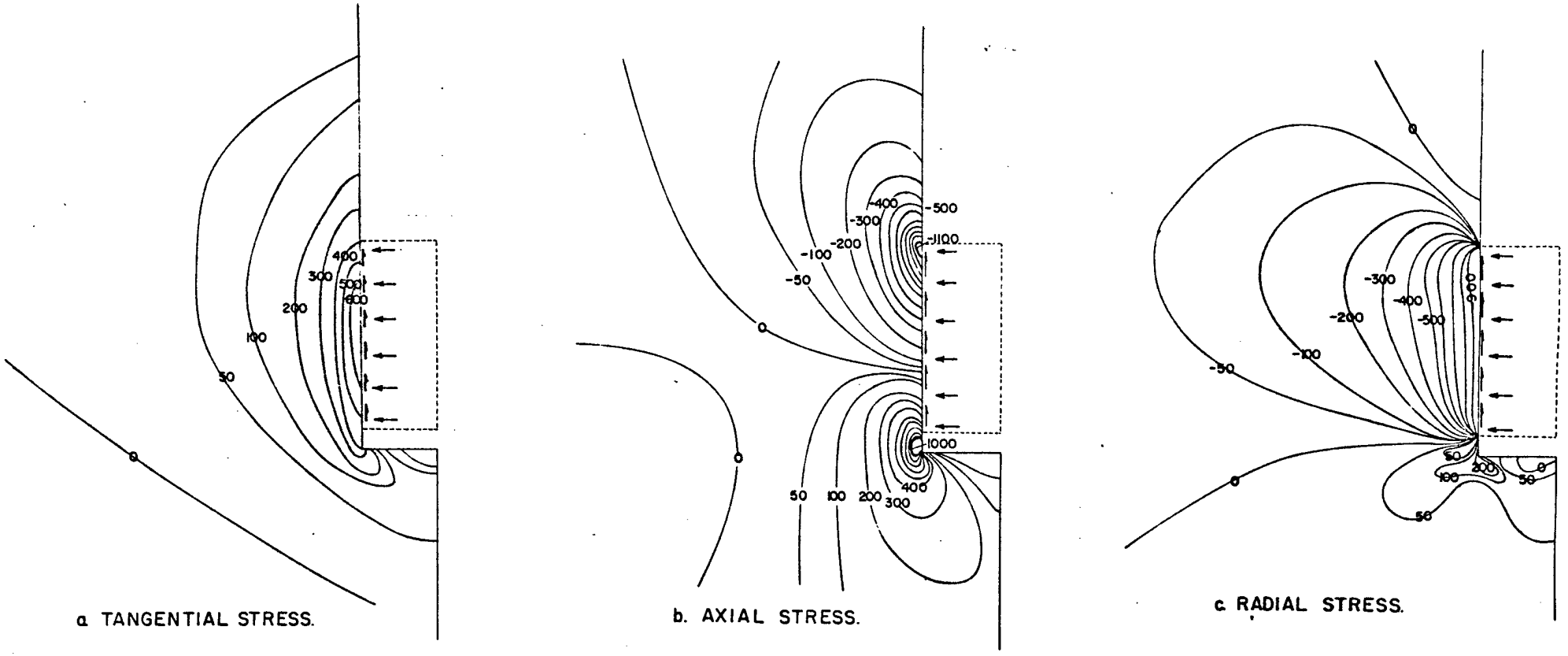

a. TANGENTIAL STRESS.

b. AXIAL STRESS.

c. RADIAL STRESS.

FIGURE 3-1 a, b, c STRESSES NEAR ROCK BOLT ANCHOR, NO JOINT BEHIND ANCHOR

ANCHOR FORCES:

NORMAL 12,500 POUNDS
SHEAR 10,000 POUNDS

(tension positive)

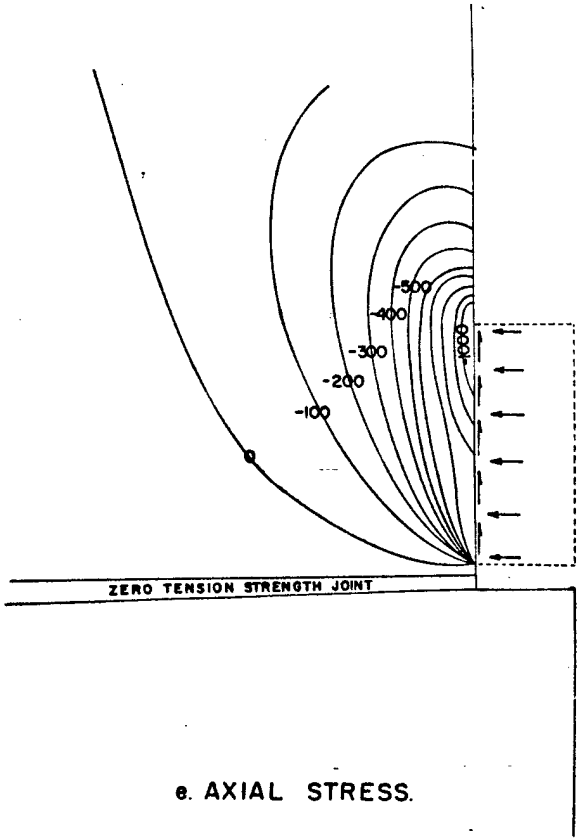

e. AXIAL STRESS.

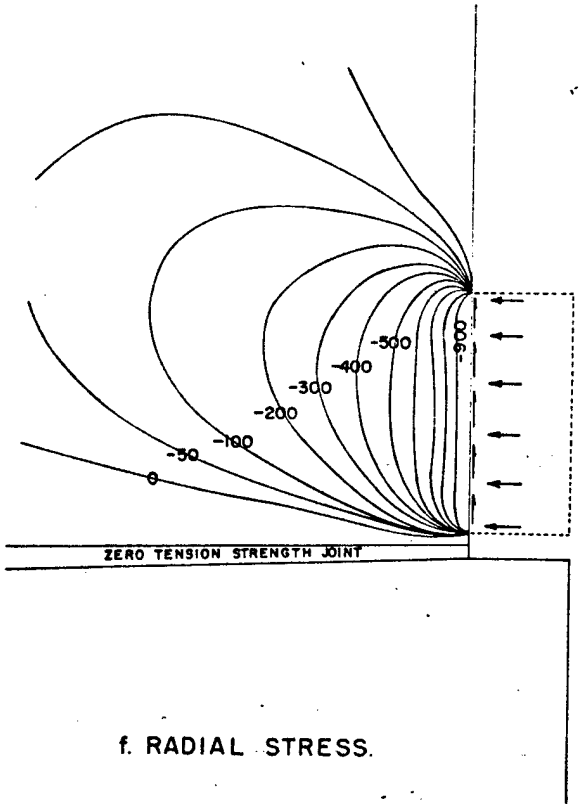

f. RADIAL STRESS.

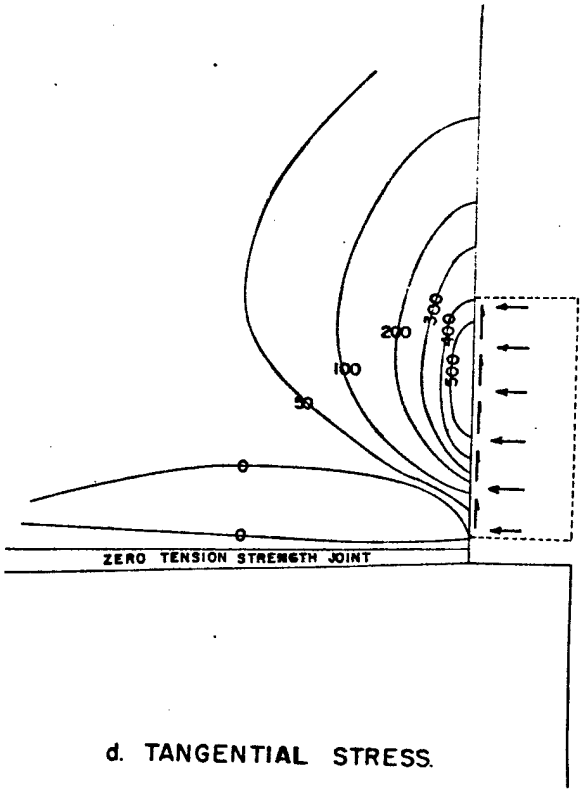

d. TANGENTIAL STRESS.

FIGURE 3-1 d, e, f STRESSES NEAR ROCK BOLT ANCHOR, ZERO TENSION STRENGTH JOINT BEHIND ANCHOR.

ANCHOR FORCE:

NORMAL	12,500 POUNDS
SHEAR	10,000 POUNDS

(tension positive)

stress distributions of the two cases for any single component (radial, axial, or tangential) reveals the interesting fact that the stress distributions are not appreciable different at points one or two anchor dimensions away from the anchor. This would indicate that it would make little difference in the zone of interest lying between the anchor and bearing plate whether a joint existed behind the anchor or the rock was continuous. Thus, the possibility of tension joints being created behind a line of rock bolt anchors does not appear to be of great importance as the resulting stress distributions will be almost identical. *

Comparison of Anchor and Point Load

A comparison was made between the finite anchor and point load representations of the anchor. The volume of rock considered in this comparison is limited in extent, thus stress equalities which would be expected at large radial distances were not found. Nevertheless, a trend toward equality was indicated by the comparison.

The axial stress distributions in the immediate vicinity of the rock bolt anchor are shown in Figure 3-2 for both point load and expansion anchor representations. The point load is applied at a point corresponding to the center of the expansion anchor. At points near the anchor, as would be expected, there is great difference in stress distributions. These arise from the greatly differing boundary conditions of the two solutions. As radial distance increase, stress contours of equal magnitude begin to coincide. Though the area included is not broad enough to include areas where stress contours from both solutions would coincide, St. Venant's principle and the trend shown in the present study indicate that coincidence would occur within several feet. Thus

* A zone of weakness existing behind an installation where closely spaced rock bolts of uniform short length are used may have adverse effects. In this case, bolts of varying lengths should be used.

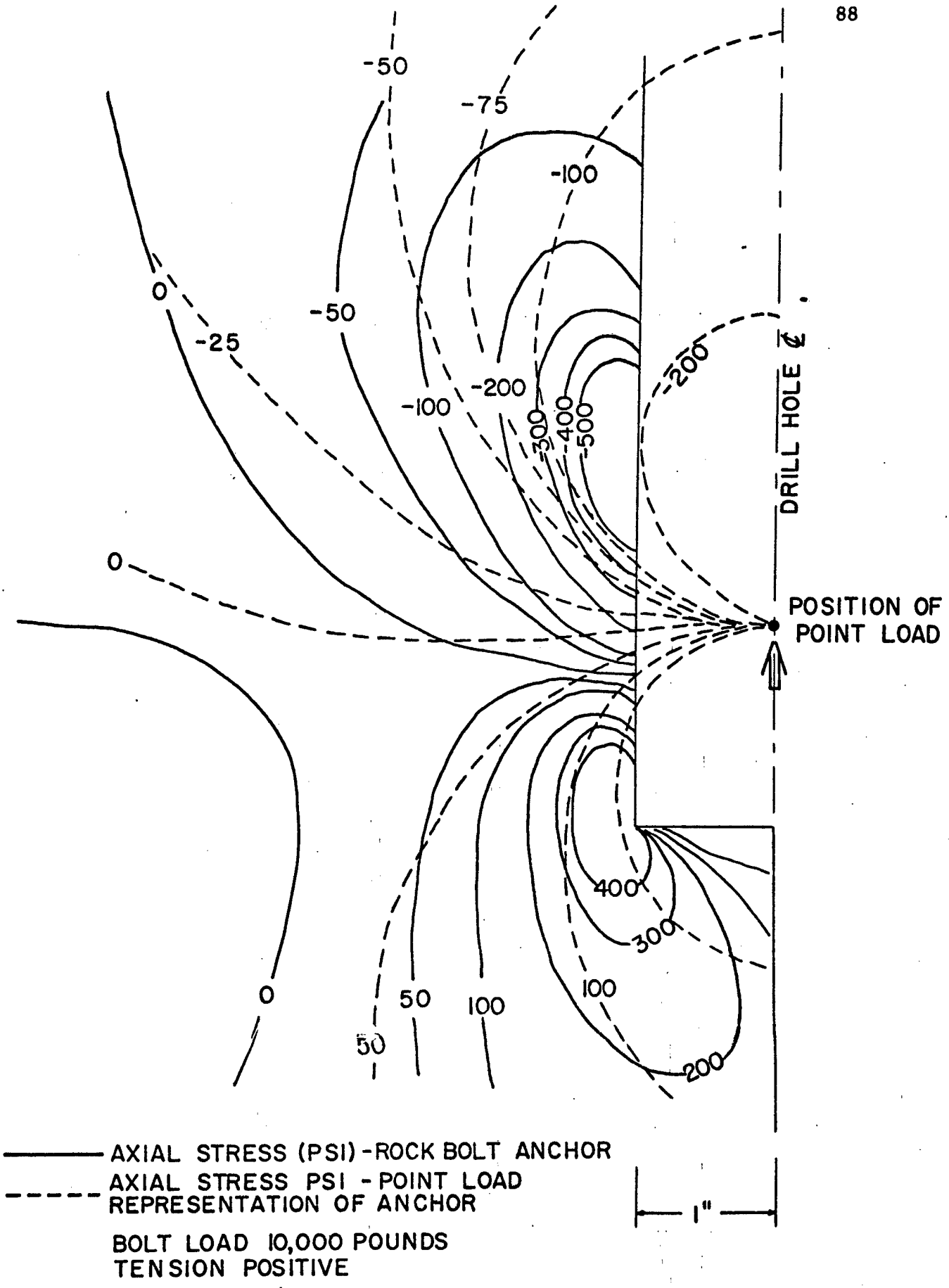

FIGURE 3-2 POINT-ANCHOR COMPARISON.

in conclusion, the simplifying assumption of point loadings is sufficient provided the area of interest is removed from the anchor. In the immediate vicinity of the anchor, a point load assumption is no longer valid.

3.3 ROCK BOLT BEARING PLATE

In most mathematical analyses of rock bolt stress distributions, using either analytic or finite element solutions, the usual assumption has been to consider the anchor and bearing plate loadings on the rock as point loads. The previous section considered the error introduced by replacing the actual anchor load distribution by an interior point load. This section considers the error of replacing the actual load distribution under the bearing plate by a point load at the surface.

The stress variation between a surface point loading and a surface square plate loading was examined. The dimensions of the square plate (8" x 8") were chosen to correspond to the usual bearing plate dimensions. Stresses in either solution are linearly dependent upon loading, thus a nominal total load of 10,000 pounds was used for both solutions.

The point loading solution is the familiar Boussinesq surface load on the half space. The solution for a surface normal load over a rectangular domain (uniform load intensity) is obtained through integration of the Boussinesq solution.

The stresses were obtained on a plane containing the point of load application. The stress variation between the two solutions was examined using the vertical stress component σ_{zz} as this is the component of greatest magnitude. The stress difference, $\sigma_{zz_{plate}} - \sigma_{zz_{point}}$, is

shown in Figure 3-3. As can be seen, there are two domains, one is which the stresses of the point loading are higher than the plate, and one in which they are lower. At points more than 1-1/2 feet from the point of load application, the difference between the two solutions becomes less than 10%. For most purposes, a point load assumption should result in sufficient accuracy.

3.4 STRESS DISTRIBUTION FROM A SINGLE ROCK BOLT

The mathematical approximation of a rock bolt may be represented by the superposition of an interior point load and a surface rectangular loading. It was shown in Section 3.3 that for normal rock bolt dimensions, there is little difference between the plate and point loadings; therefore in the following, the rock bolt is represented by the superposition of normal surface and interior point loads. A nominal load of 10,000 pounds was used. Stresses for other loadings may be found through multiplication of the 10,000 pound stresses by a linear factor.

The radial, tangential, and axial stress components (referred to a cylindrical coordinate system referenced to the bolt) are shown in Figures 3-4 a, b, and c for a rock bolt 10 feet in length.

If a single rock bolt is installed, it is evident that the primary beneficial effect will be to increase the normal stress on planes perpendicular to the bolt axis between the anchor and bearing plate. Stresses in directions normal to the bolt axis may be either tensile or compressive depending on position. The rock bolt stresses were indicated to be a linear function of load. Thus an increase or decrease in bolt loading will not alter the position of zero stress contours but will result in change of intensity of tensile or compressive stresses.

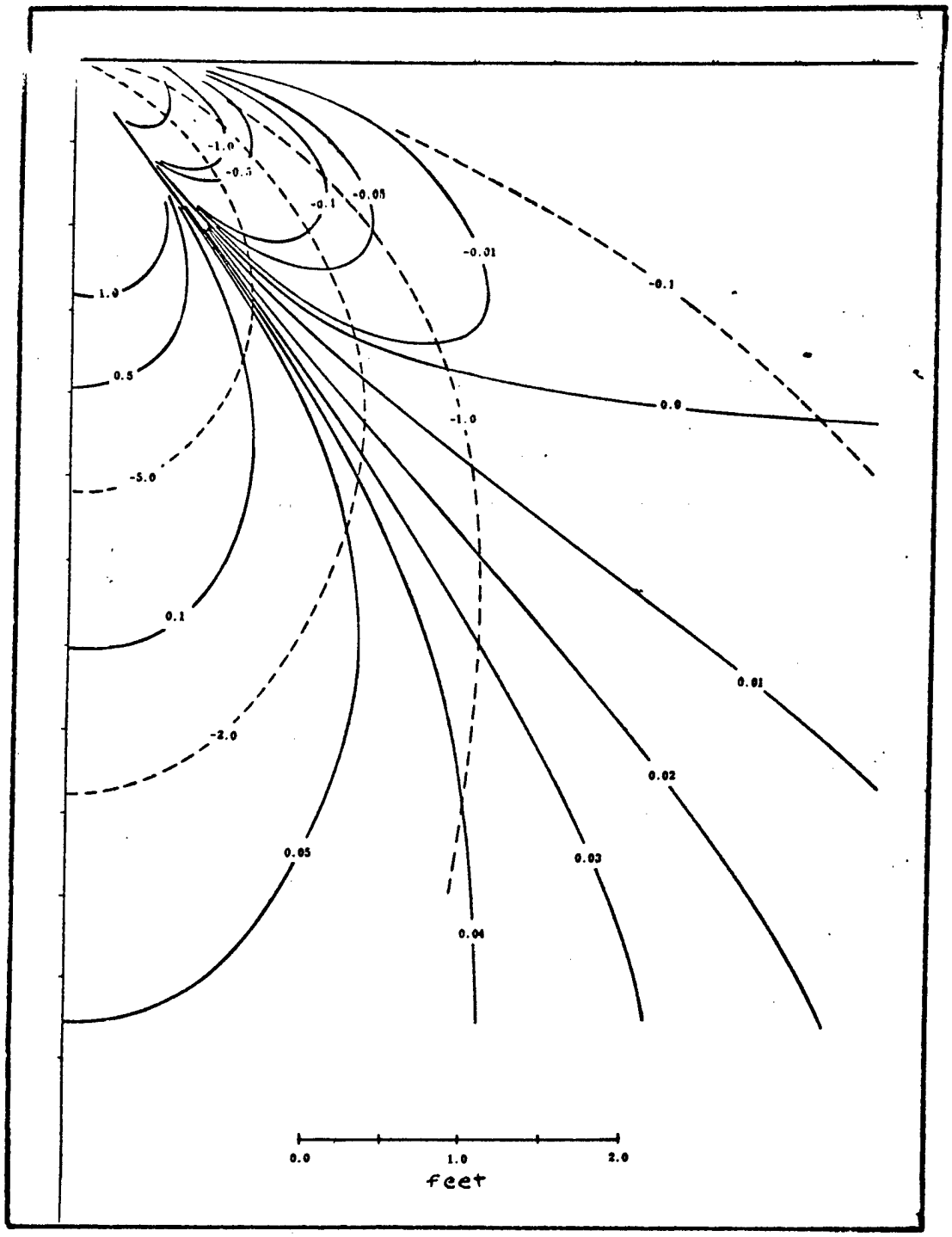

FIG. 3-3 POINT - PLATE COMPARISON

10,000# total bolt load 10 foot bolt length

Dashed contours give axial stress, psi, under rock bolt with 8" x 8" bearing plate;

Solid contours give axial stress difference, psi, between solutions for rock bolt with bearing plate, and for point load representation.

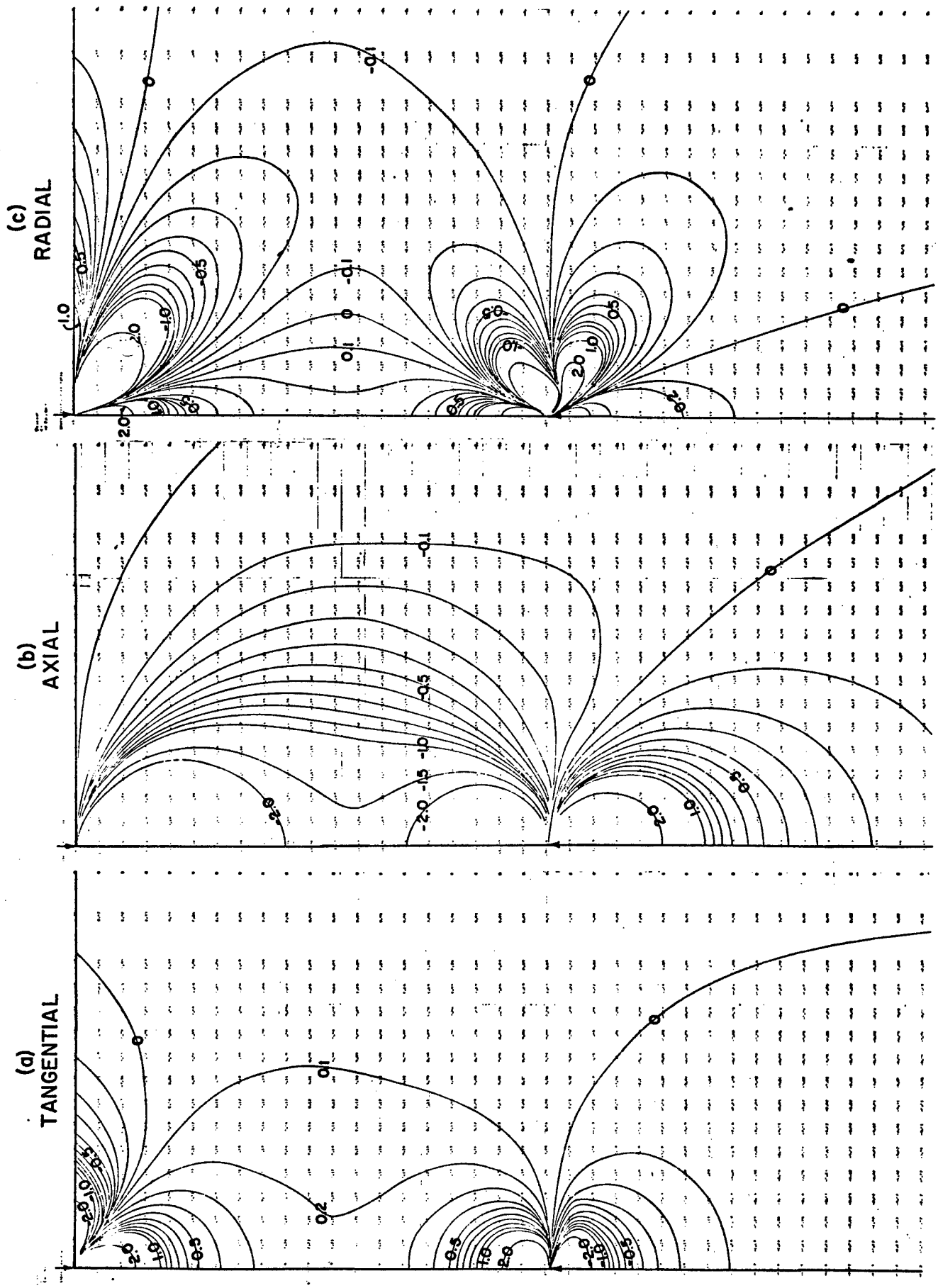

FIGURE 3-4. STRESSES (PSI) DUE TO A SINGLE ROCK BOLT.
LOAD 10,000 POUNDS; LENGTH 10 FEET; TENSION POSITIVE.

Looking at the individual stress components, it is seen that the tangential stress is tensile between anchor and bearing plate, compressive behind the anchor, and compressive in a surface lobe. Axial stresses are compressive between bearing plate and anchor and tensile behind the anchor. The radial stress distribution is complex with lobes of tension and compression extending away from both bearing plate and anchor. Stress magnitudes of all components fall off rapidly away from the bearing plate and anchor.

3.5 ROCK BOLT TRIAXIAL CONDITIONS

Superposition of the respective normal stress components allows the various states of triaxial stress to be delineated. These triaxial stress zones are presented in Figure 3-5. It is seen from the figure that there are in general no large areas of triaxial tension or compression. The most common triaxial stress state is that of two compressive and one tensile normal stresses.

Triaxial tension does exist in an annular lobe at the surface. The triaxially tensile zones of several bolts may merge to form a surface "pit" in which it is impossible to stabilize material through rock bolting. These triaxially tensile zones may be seen in rock bolted models using crushed rock.

Triaxial compression exists in an annular lobe near the surface and a very small lobe near the anchor. The surface compressive lobe is of definite benefit as lobes of several bolts may merge to form a zone near the surface in which all normal stresses are compressive; thus joints will be less likely to open.

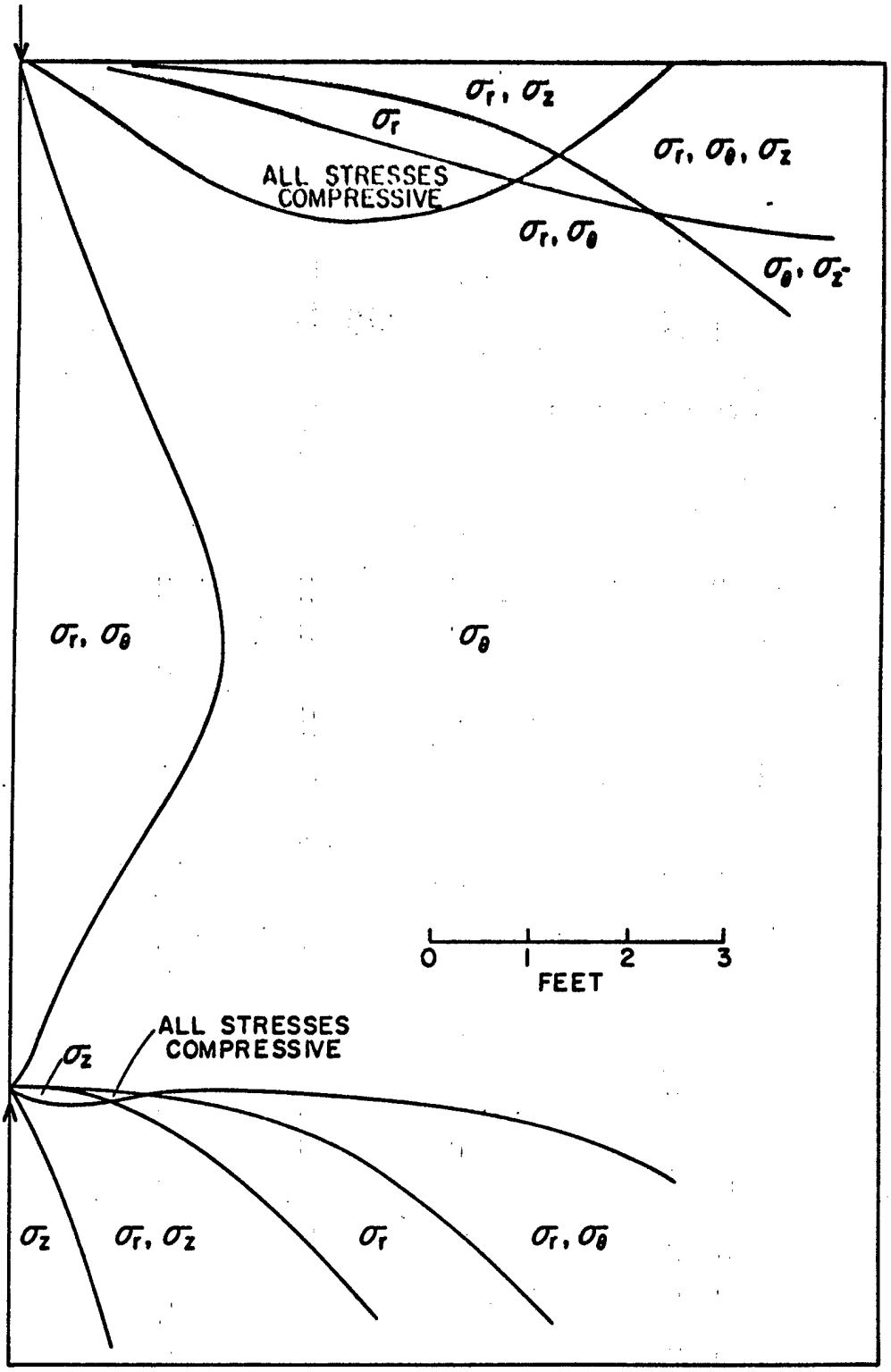

FIGURE 3-5. VARIABLE CONDITIONS OF CONFINEMENT OWING TO A SINGLE ROCK BOLT.

TOTAL LOAD 10,000 POUNDS; BOLT LENGTH 10 FEET; STRESSES INDICATED ARE TENSILE.

A point to note is the fact that in the major portion of the zone between anchor and bearing plate, only the tangential stress is tensile. The radial and axial stresses are compressive.

3.6 THE EFFECT OF JOINTS

Ideally, if a rock bolt is installed in a tunnel perimeter, the stresses resulting from the rock bolt should increase the stability of the rock surrounding the rock bolt. As the stress state of a single rock bolt is a complex one, there is no a priori way in which to determine what the effect of the rock bolt will be on joint planes at points removed from the bolt.

It is important to distinguish the regions in which the effect of a single rock bolt is detrimental from those in which it is beneficial. For this purpose a ubiquitous joint system (see Section 2.2) was considered in the region around the bolt. A sector of tunnel perimeter encompassing 80^{o} of arc was considered with the bolt length equal to the tunnel radius. Joint orientations with respect to the tunnel axis were considered at every 10^{o} in the range 0^{o} - 90^{o}. Joint planes were restricted to those parallel to the axis of the tunnel (two dimensional ubiquitous joints).

Using a criterion of $\tau = N \tan \phi$, ranges of friction angle ϕ necessary to prevent slip were determined at points in the rock mass. The series of plots obtained is shown in Figures 3-6a to j. From these figures it is seen that for sets of joints at low angles to the bolt axis, very high friction angles are required in the immediate vicinity of the bolt if slip is to be prevented. Zones in which the required friction angle is 30^{o} or less are confined to areas more than 20^{o} of arc away from the rock bolt. As the joint orientation angle is increased, the zones of low required friction angle migrate towards the bolt axis, until at 90^{o} the low friction angle zone is centered on the bolt axis.

Required Friction to Prevent Slip on Joints

Tunnel Radius - 10 feet

Single Rock Bolt

Bolt Length - 10 feet

Slip Criterion - $\tau = N \tan \phi$

Rock Bolt Stresses Only Are Utilized in Deriving the Required Friction Angle

Geometry of problem as shown:

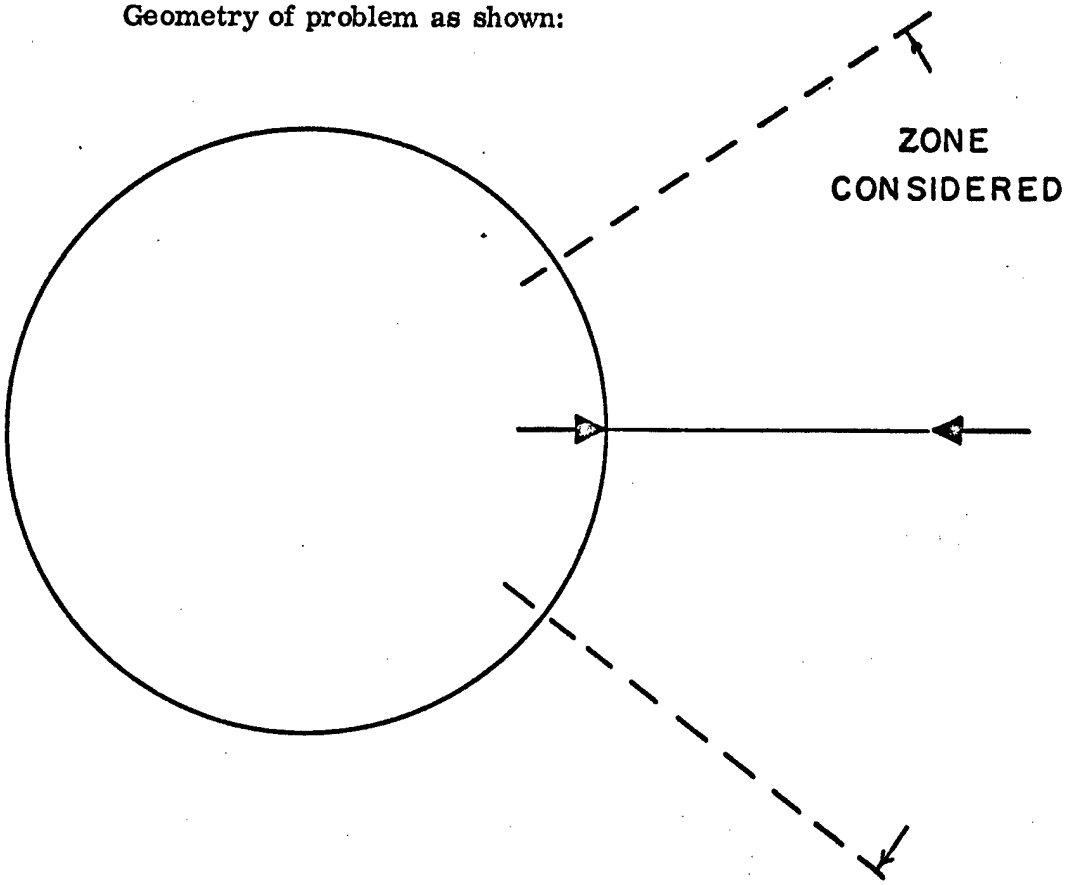

Explantion of Figures 3-6 a - j.

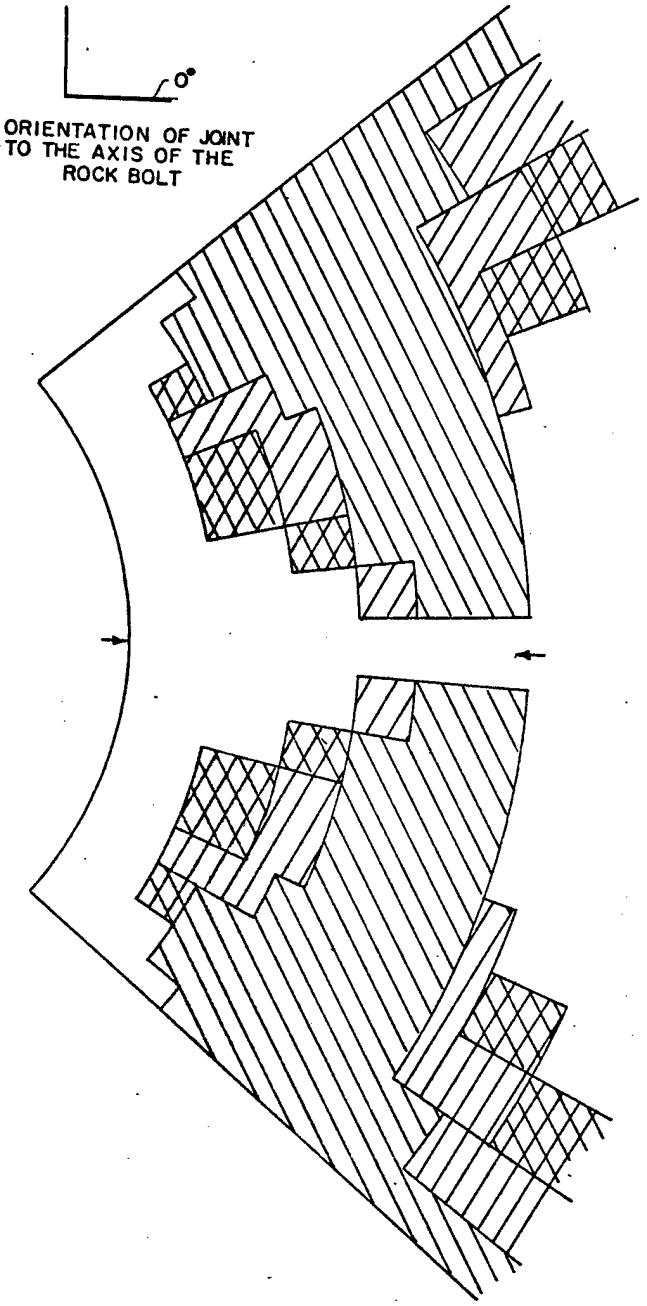

FIGURE 3-6a 0° JOINTS.

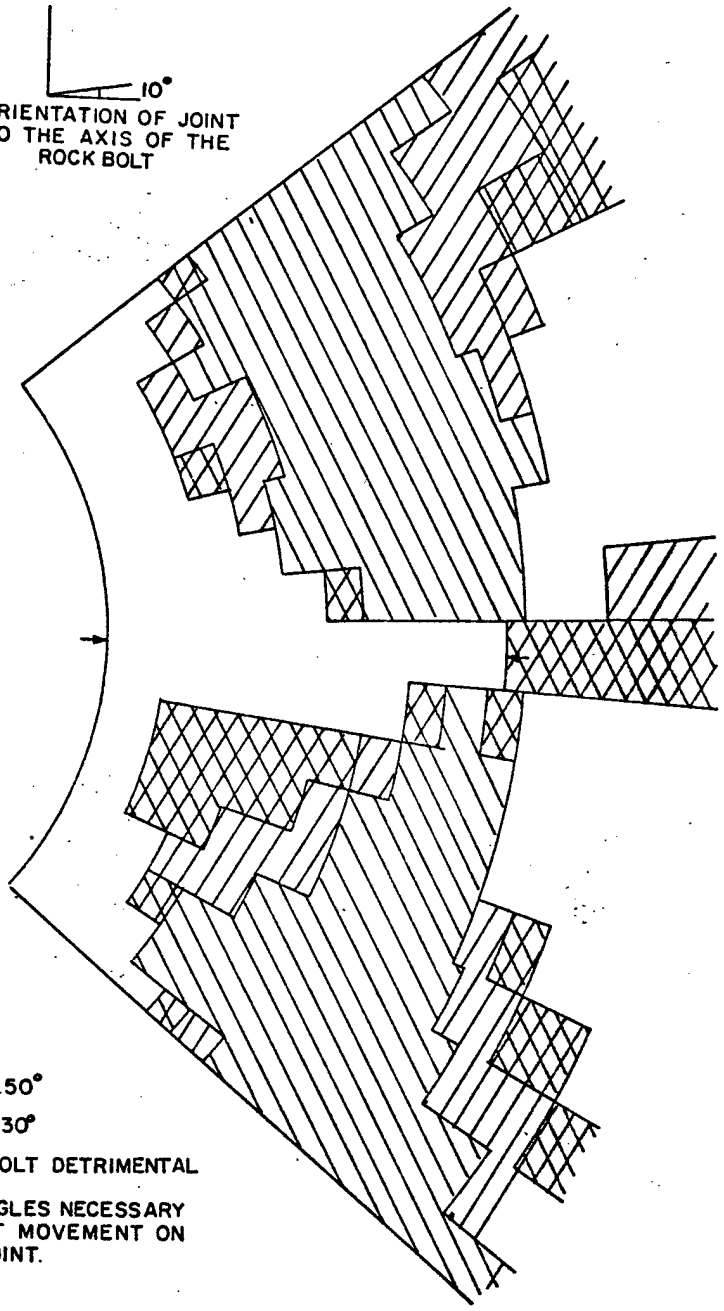

$\phi > 50°$

$30° < \phi < 50°$

$0° < \phi < 30°$

ROCK BOLT DETRIMENTAL

FRICTION ANGLES NECESSARY TO PREVENT MOVEMENT ON JOINT.

FIGURE 3-6b 10° JOINTS.

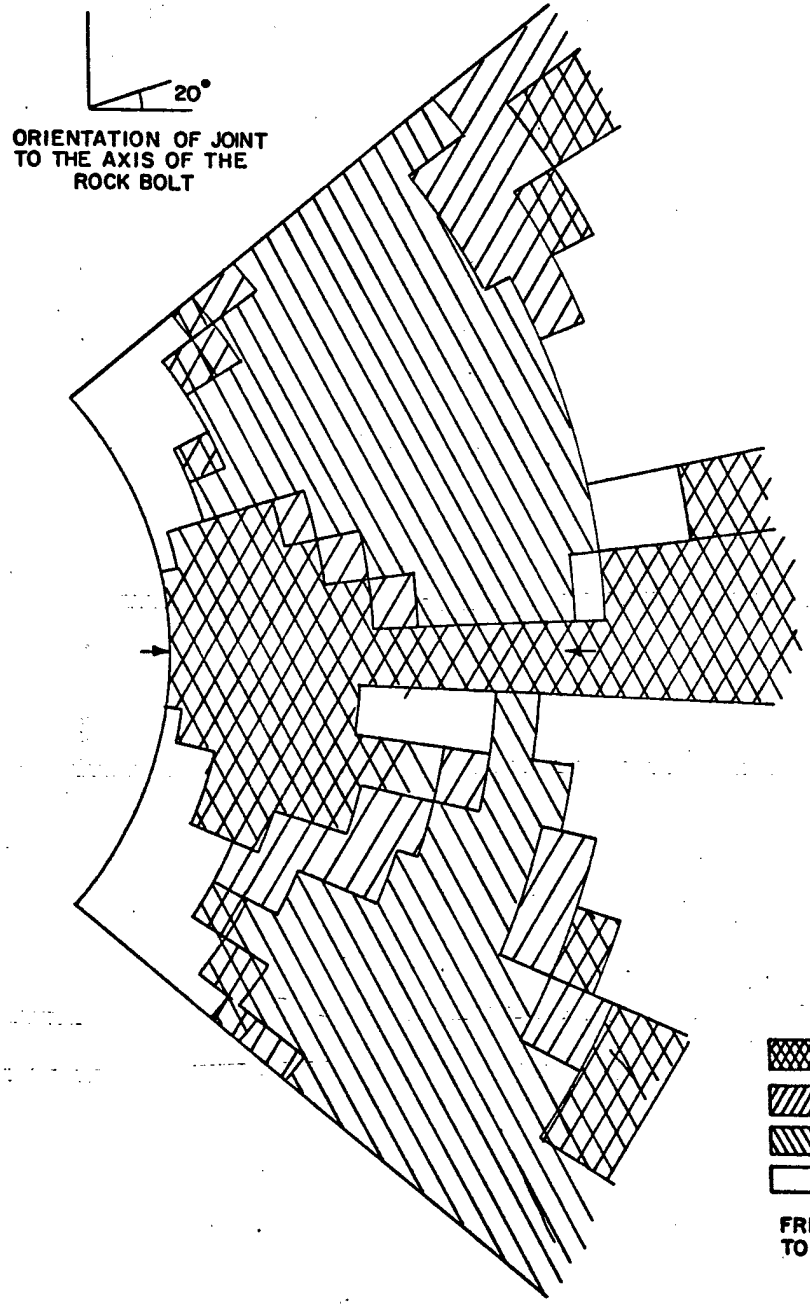

FIGURE 3-6c 20° JOINTS.

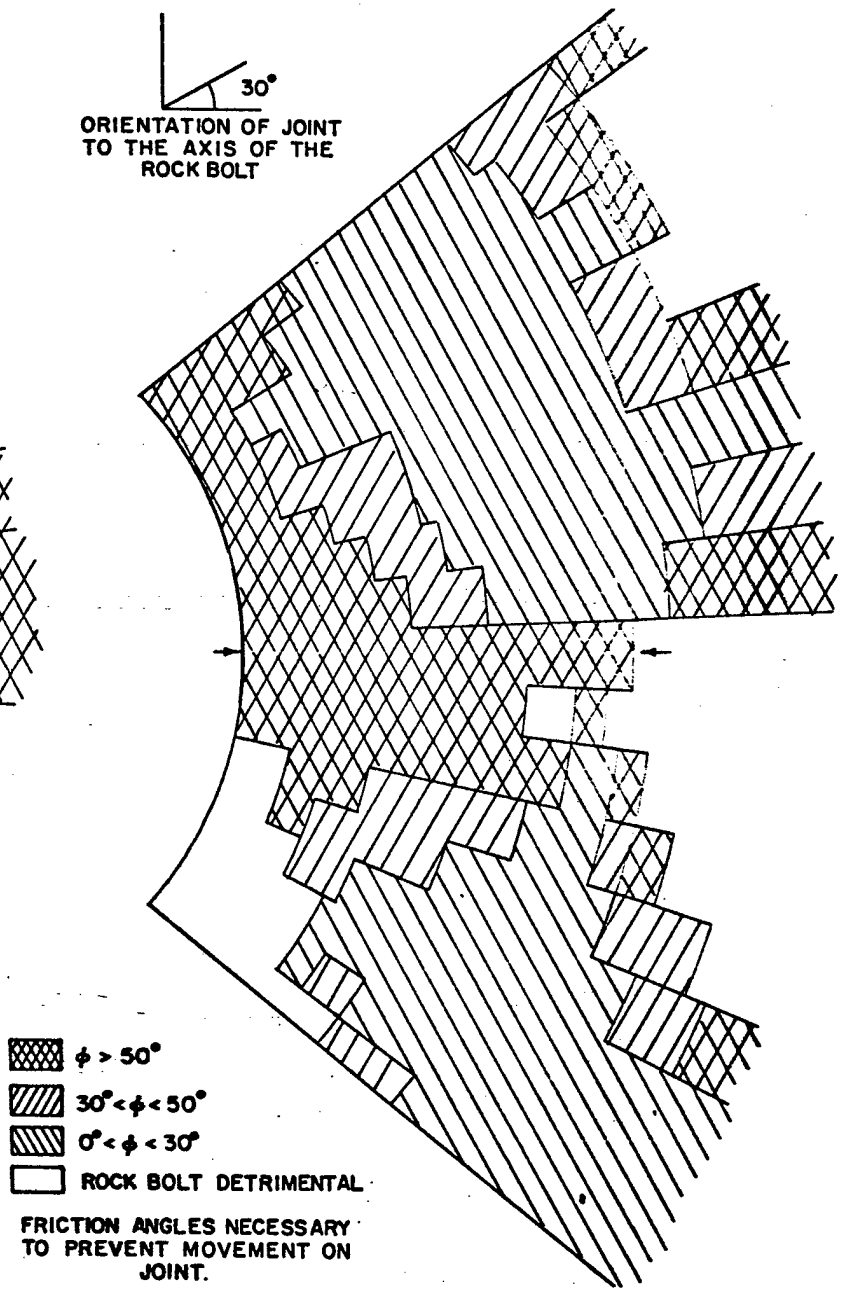

FIGURE 3-6d 30° JOINTS.

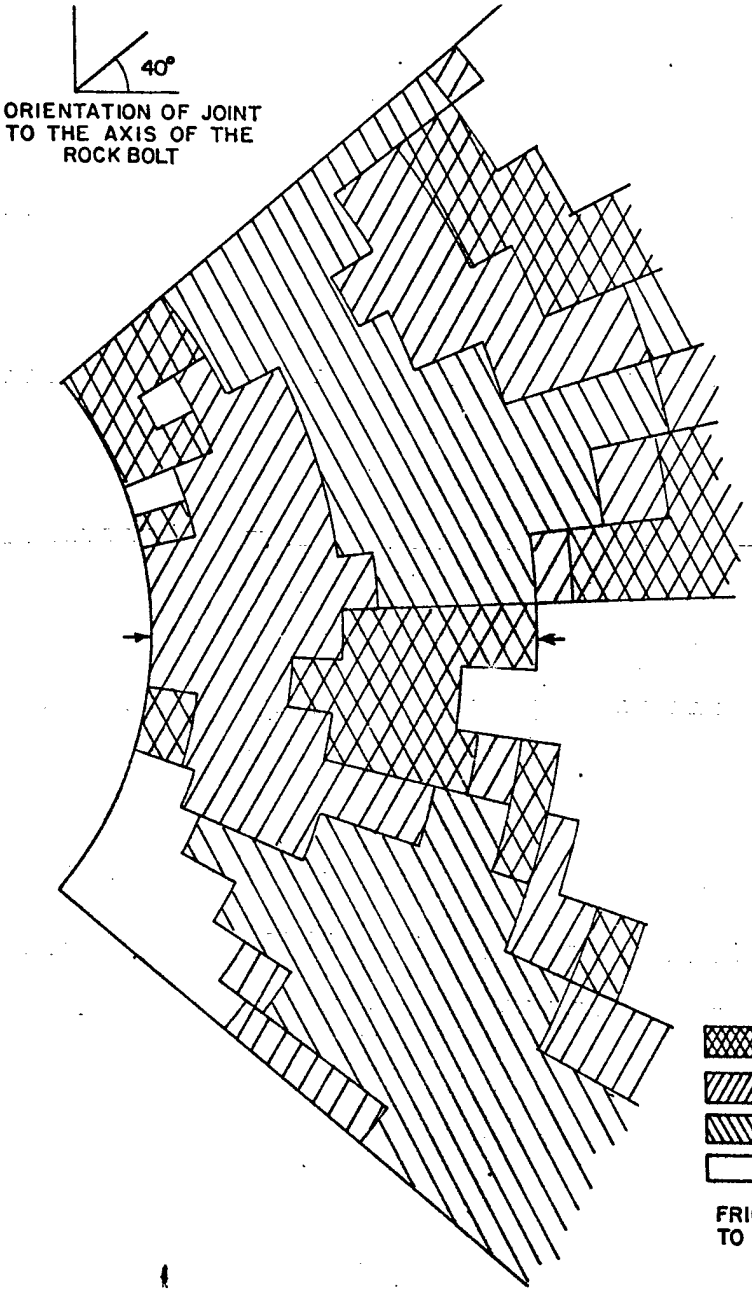

FIGURE 3-6e 40° JOINTS.

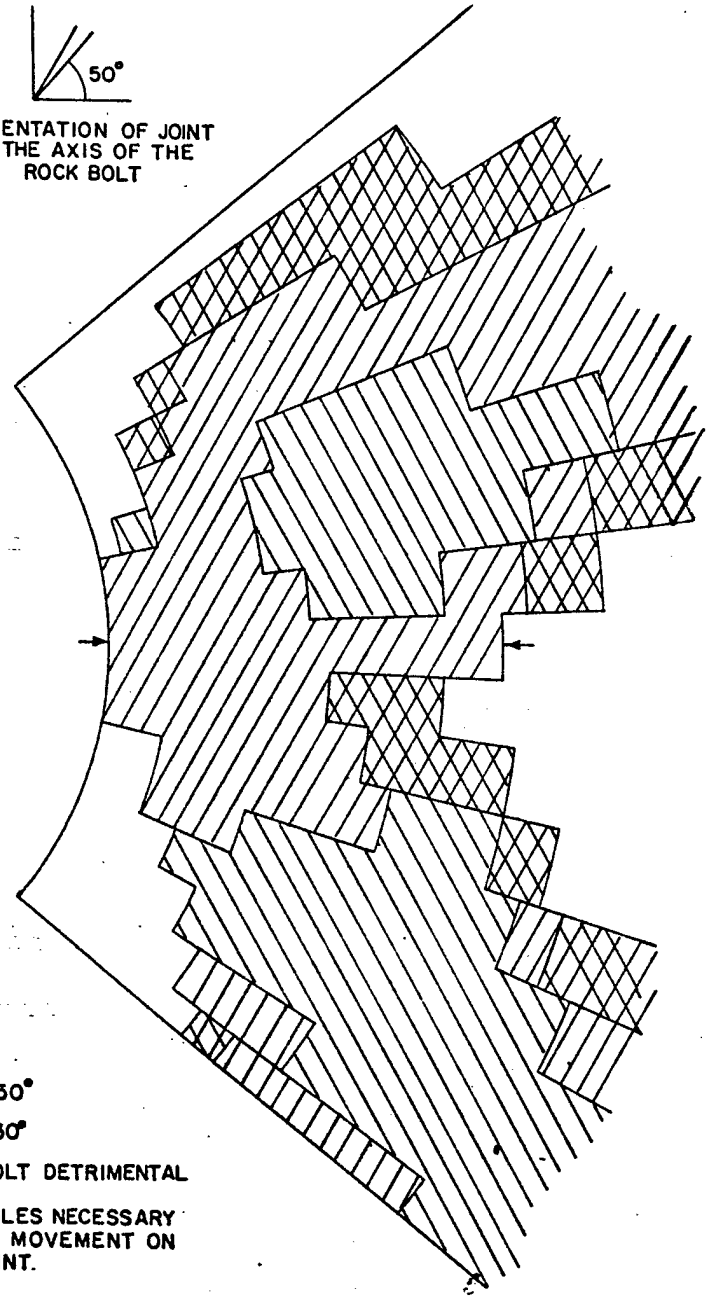

FIGURE 3-6f 50° JOINTS.

$\phi > 50°$

$30° < \phi < 50°$

$0° < \phi < 30°$

ROCK BOLT DETRIMENTAL

FRICTION ANGLES NECESSARY TO PREVENT MOVEMENT ON JOINT.

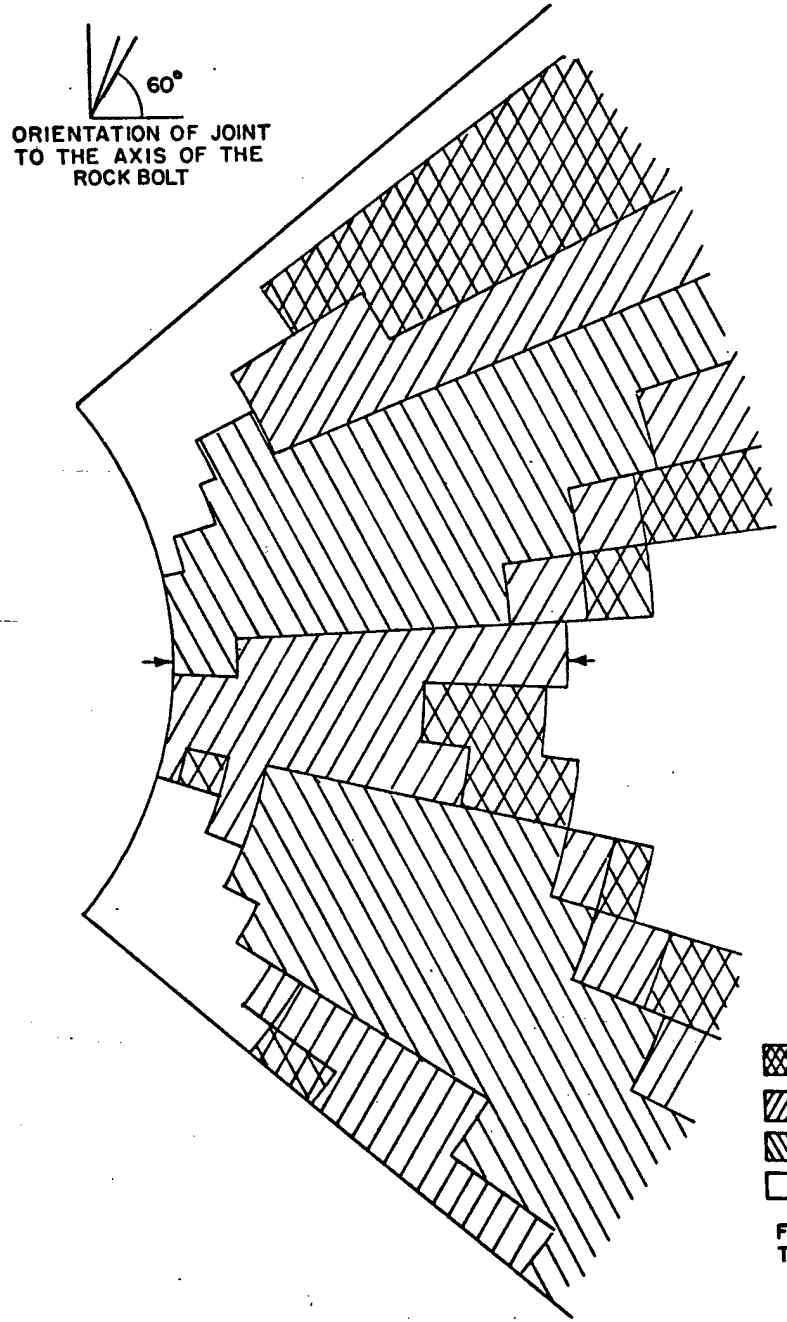

FIGURE 3-6g 60° JOINTS.

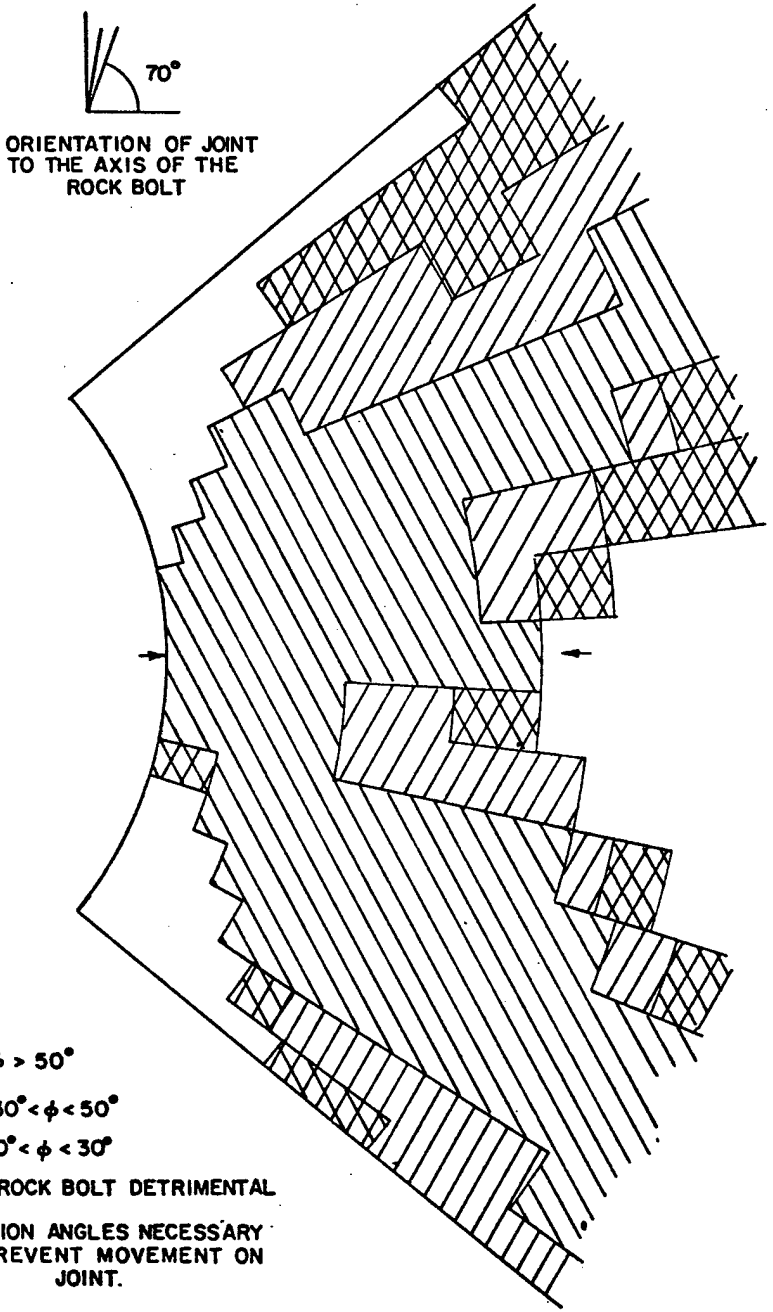

FIGURE 3-6h 70° JOINTS.

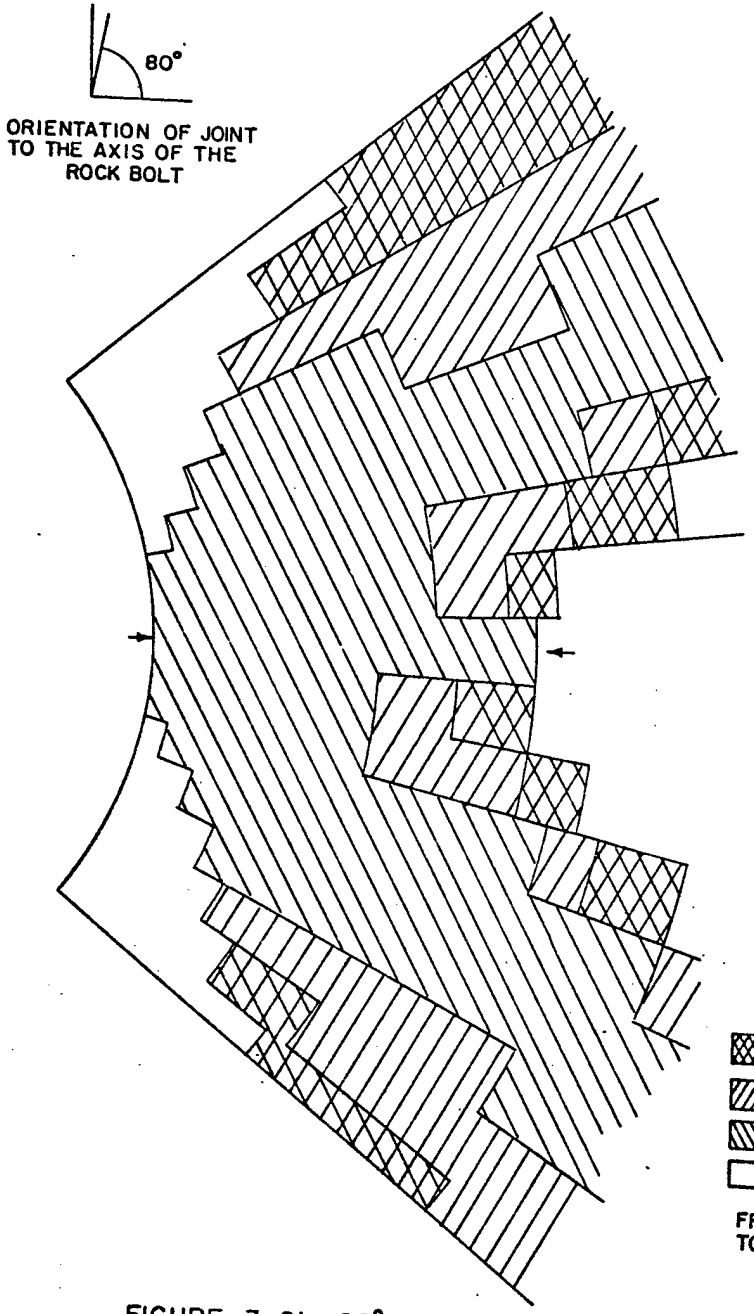

FIGURE 3-6i 80° JOINTS.

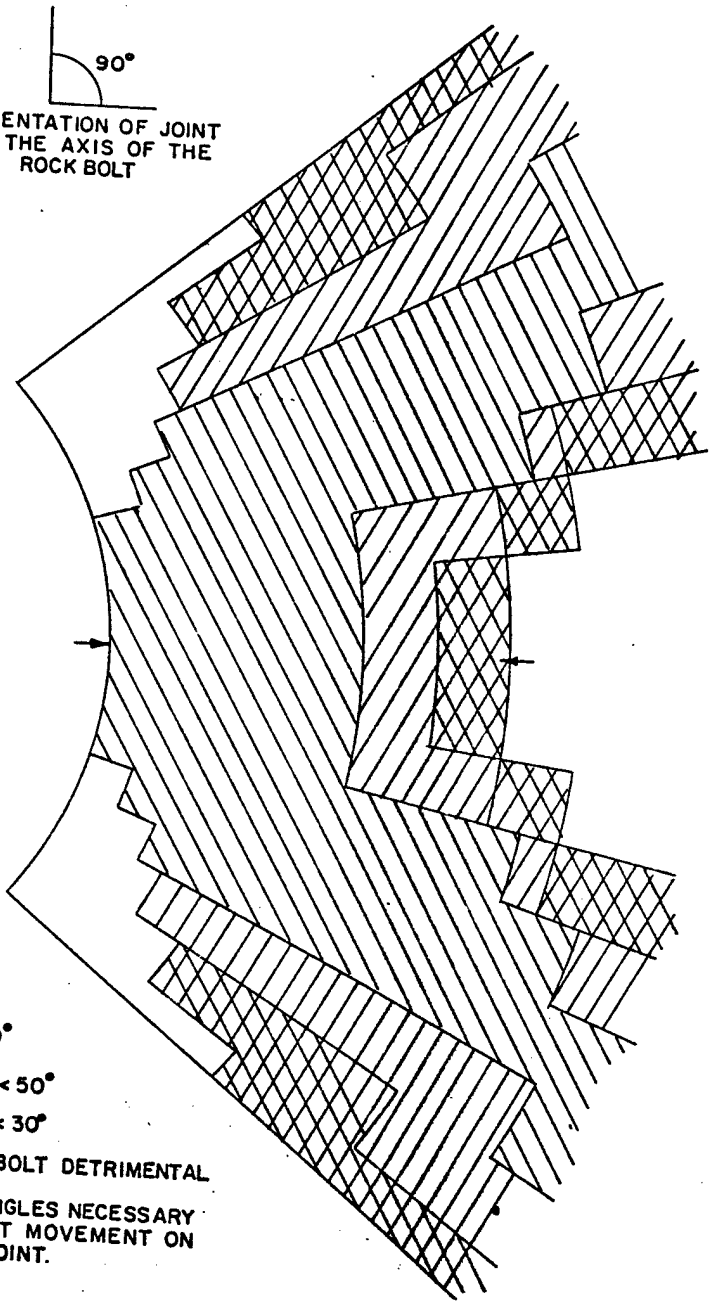

FIGURE 3-6j 90° JOINTS.

3.7 MULTIPLE BOLT STRESSES

Single rock bolt installations are rare; the more common usage finds rock bolts installed in a regular patterned arrangement, the maximum distance between adjacent bolts being on the order of one half the bolt length. The stresses resulting from two patterned arrays were examined -- the first pattern a rectangular array and the second a staggered array. These arrays are shown in Figure 3.7 and 3.8. Loads on all bolts were set at 10,000 pounds, the length of bolts at 10 feet, and spacing at 5 feet. Stresses were examined on cross sections A -A' with the stress distributions shown in Figures 3-7 and 3-8.

For the parameter values chosen, which are generally representative of rock bolt installations, the stress distributions obtained show:

(a) Axial stress relationships are relatively unchanged by bolt pattern installation. Superposition of compressive components from adjacent bolts increase the magnitude of the compressive stresses found in the central two-thirds of the bolt length. At the spacing chose, there is very little axial tension at the surface. Axial tension exists behind the plane of anchors, unless of course it is relieved by joint block movements.

(b) In the central portion of the bolt, both radial and tangential tensions are removed through compressive components from adjacent bolts. Tensile zones are retained around the anchor and bearing plate, but the tensile stress magnitudes of the single bolt are reduced.

If the spacing between bolts is reduced to 2.5 feet, the stress distributions of Figures 3-9a, b, and c are obtained. It is seen that the stress contour patterns are similar; the major difference resulting from a decrease in bolt spacing is an increase in the stress intensity in all zones considered.

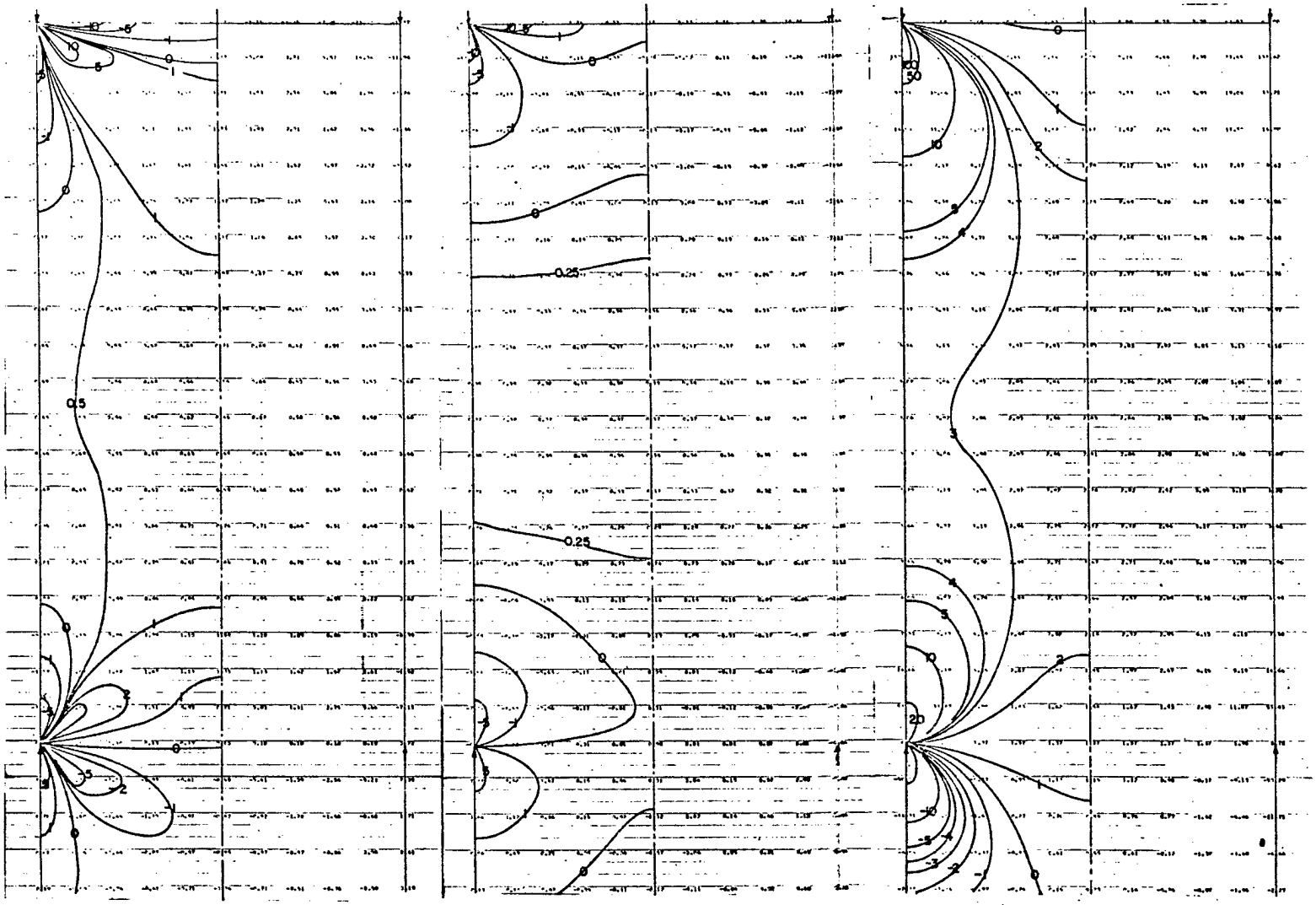

COMPRESSION POSITIVE

SECTIONS TAKEN ALONG xx

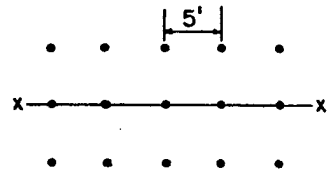

Rectangular Array

FIGURE 3-7 STRESSES DUE TO A RECTANGULAR PATTERN OF ROCK BOLTS.
BOLT LOAD 10,000 POUNDS; BOLT LENGTH 10 FEET; SPACING 5 FEET.

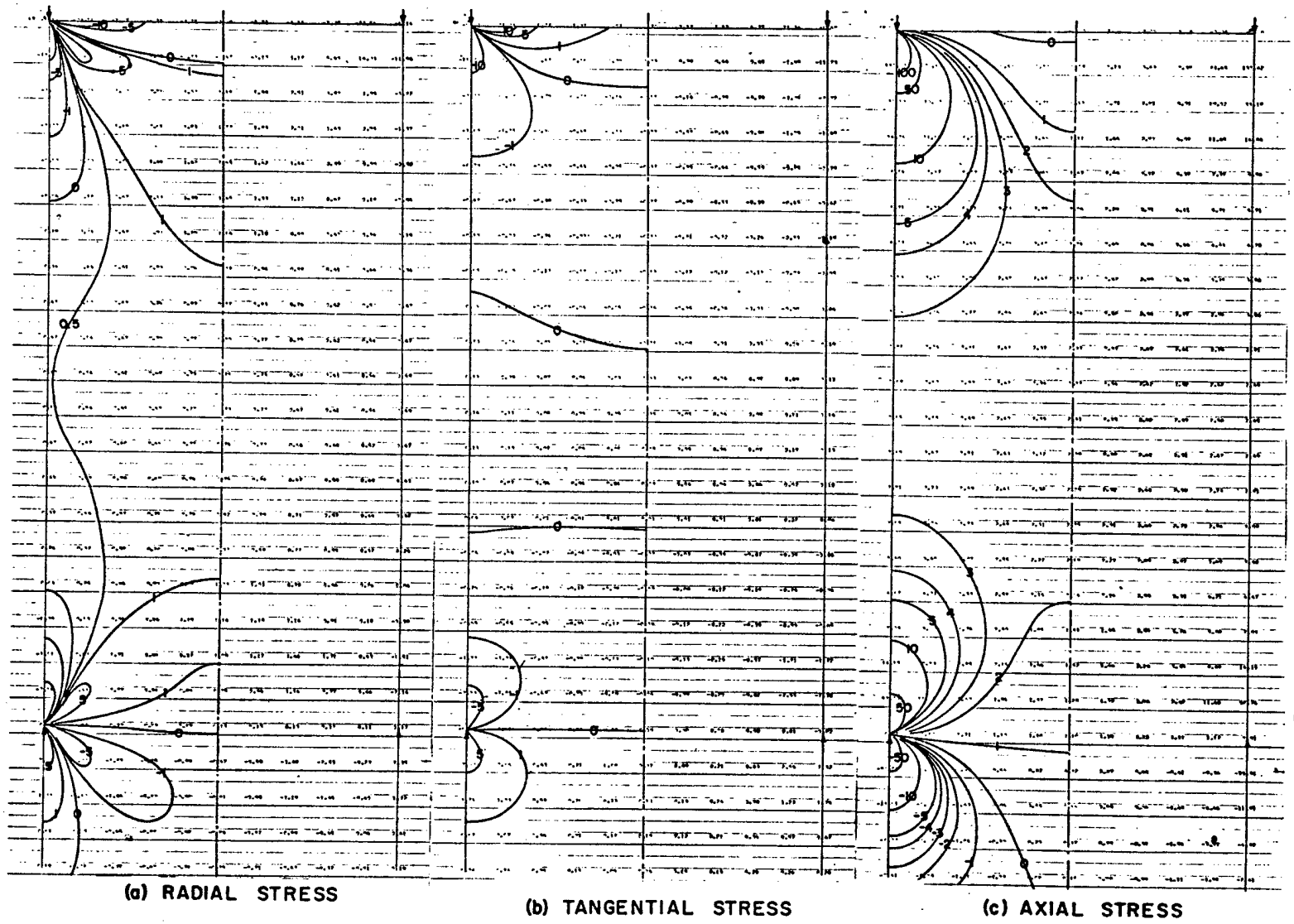

COMPRESSION POSITIVE

SECTIONS TAKEN ALONG xx

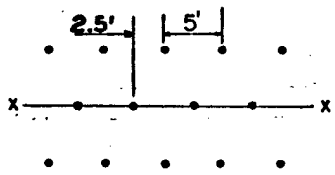

STAGGERED ARRAY

FIGURE 3-8 STRESSES DUE TO A STAGGERED PATTERN OF ROCK BOLTS.
BOLT LOAD 10,000 POUNDS; BOLT LENGTH 10 FEET; SPACING 5 FEET.

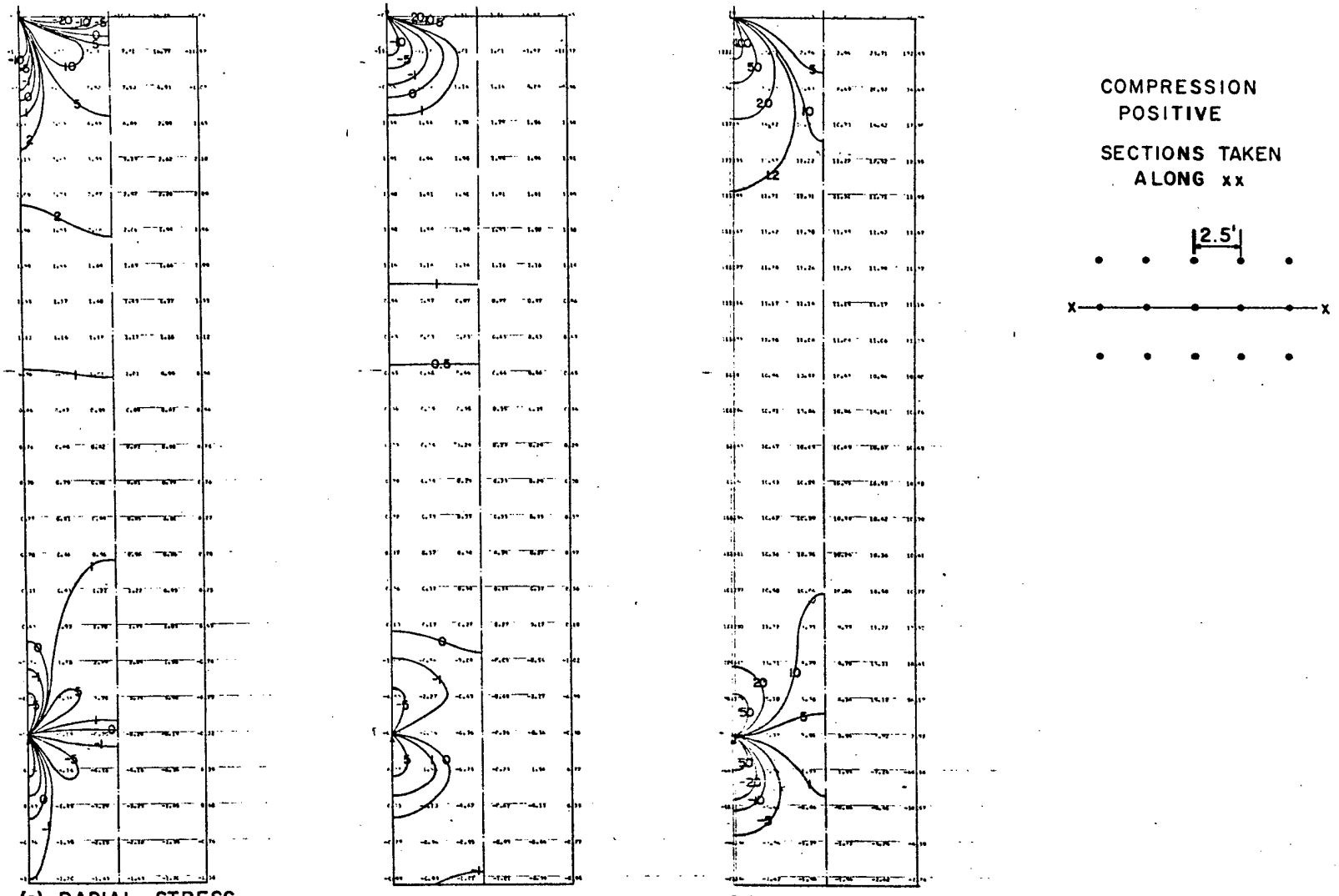

FIGURE 3-9 STRESSES DUE TO A RECTANGULAR PATTERN OF ROCK BOLTS.
BOLT LOAD 10,000 POUNDS; BOLT LENGTH 10 FEET; SPACING 2.5 FEET.

3.8 ROCK CONFINEMENT CONDITIONS RESULTING FROM MULTIPLE BOLT PATTERNS

Superposition of the normal stress components resulting from a patterned array of bolts results in a triaxial stress distribution for the patterned array. These rock bolt pattern triaxial zones are of interest as they indicate where the rock bolts tend to do the most in rock stabilization.

The triaxial zones existing on section A - A' for the three cases of Figures 3-7, 3-8, and 3-9, are shown in Figures 3-10 a, b, and c. The most apparent change from the single bolt triaxial distribution is the development of a broad zone of triaxial compression over the central portion of the bolt. This zone is seen to be greater for the rectangular array than for the hexagonal array. If an arbitrary scale is set up in which tensile stresses are rated as minus factors, axial tension then most unfavorable, it is seen that the staggered array produces a "better" surface zone than the rectangular array along the section investigated.

3.9 SUMMARY

Rock bolts introduce a complex state of stress governed by the lengths of the rock bolt and the loading. For a fixed rock bolt geometry, the stress intensity at any point varies linearly with the loading magnitude.

Triaxial stress zones of single bolts are seen to be, in general, not triaxially compressive. If patterned bolt arrays are installed, zones of triaxial compression become larger due to interaction between adjacent bolts.

a. RECTANGULAR ARRAY - 5' SPACING

b. HEXAGONAL ARRAY - 5' SPACING

c. RECTANGULAR ARRAY 2½' SPACING

BOLT LENGTH 10 FEET.
BOLT SPACING AND PATTERN AS INDICATED.

SECTION
TAKEN ALONG X AXIS

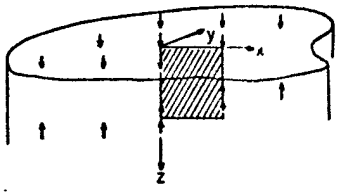

CONFINEMENT CODE
T=TENSION; C=COMPRESSION

σ_x	σ_y	σ_z	CODE
T	T	T	1
T	T	C	2
T	C	T	3
T	C	C	4
C	T	T	5
C	T	C	6
C	C	T	7
C	C	C	8

rad. tang. axial

FIGURE 3-10. VARIABLE CONFINEMENT OWING TO MULTIPLE BOLTS.

If a given friction angle is assumed, it is seen that the prevention of slip on joint planes is dependent both on position and joint orientation. As a rule of thumb, high angle joints are stabilized near the bolt axis and low angle joints are stabilized far from the bolt axis.

4. ANALYSIS OF SUPPORTS AND LININGS *

4.1 GENERAL

Linings and supports for tunnels are shell type structures, in which rotations as well as displacements must be considered. In the previous report, a ring of continuum elements was used to represent the lining of a tunnel. To improve the representation, in this section shell theory will be developed and coded for introduction in the computer solution to the problem of support of tunnels in jointed rock.

*This section was prepared by Dr. Robert L. Taylor.

4.2 SHELL ELEMENT - PLANE STRAIN ANALYSIS

(1) General

The shell segment is treated according to layered orthotropic shell theory (1,2,3). In this way the effect of closely spaced hoop or longitudinal stiffeners placed on one side of the shell can be incorporated into the analysis. (Also the concrete layer can be combined provided the thin shell theory still applies -- $t/R < \frac{1}{20}$.)

The analysis for the tunnel liner and the surrounding rock is modeled, at present, by a finite element plane strain representation. Thus, the shell analysis to follow is similarly restricted to the plane strain condition. A typical shell is shown in Figure 4-1a and the finite element representation in Figure 4-1b. In the analysis used herein, the shell is approximated by a series of straight segments joined at nodes (4,5). Experience has shown that provided L_i is much less than R, straight elements introduce no appreciable error. (The additional stored energy can easily be computed as a measure of this error.) The shell and element behavior is deduced from the principle of minimum potential energy. To this end, consider a typical element as shown in Figure 4-2. The end nodes of the element are denoted by I and J; their positions are given by the Cartesian coordinates x,y.

---

1. Ambartsumyan, S. A., Theory of Anisotropic Shells, NASA Tech. Transl. TT F-118, May 1964.
2. Dong, S. B., Pister, K. S., and Taylor, R. 1., Jour. Aerospace Sciences, Aug. 1962.
3. Reissner, E. and Stavsky, Y., Jour. Applied Mechanics, v. 28, 1961.
4. Graffton, P. E., and Strome, D. R., AIAA Jour., v. 1, Oct. 1963.
5. Percy, Pian, et.al., AIAA Jour., v. 3, Jan. 1965.

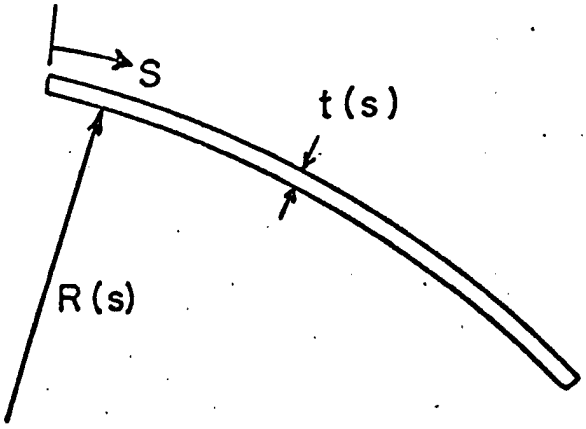

Fig. 4-1a. Typical Shell

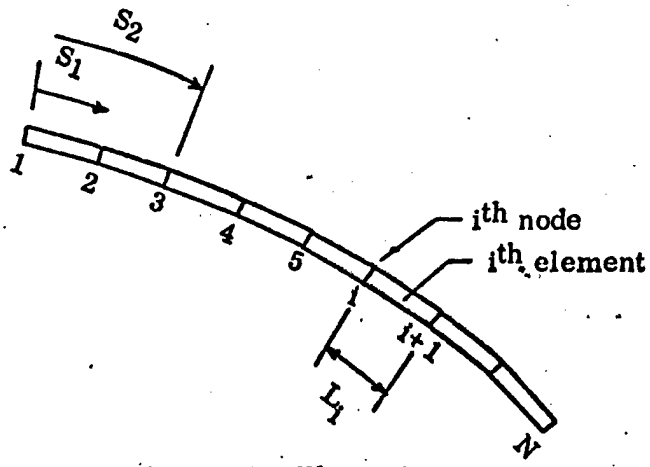

Fig. 4-1b. Finite Element Representation

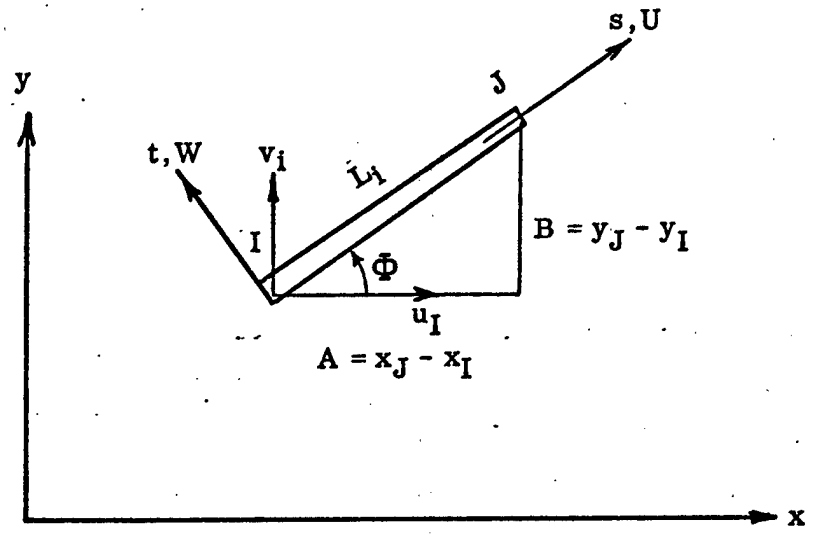

Fig. 4-2. Typical Shell Element

(2) Analysis of Element Stiffness

Using Love's first approximation, the strain energy density is given for the shell by

$$V = \frac{1}{2} \int_V \left[\sigma_s \varepsilon_s + \sigma_z \varepsilon_z \right] dv \tag{4-1}$$

where s is the shell coordinate and z is the normal to the x y plane.

For an orthotropic material

$$\begin{aligned} \sigma_s &= c_{11} \varepsilon_s + c_{12} \varepsilon_z \\ \sigma_z &= c_{12} \varepsilon_s + c_{22} \varepsilon_z \end{aligned} \tag{4-2}$$

Through the Kirchhoff-Love assumption the strains may be expressed as

$$\begin{aligned} \varepsilon_s &= \varepsilon_{s_0} + t \chi_s \\ \varepsilon_z &= \varepsilon_{z_0} + t \chi_z \end{aligned} \tag{4-3}$$

where ε_{s_0} and ε_{z_0} are the strains at some reference surface in the shell, i.e. $t = 0$, (In homogeneous shells this is taken for convenience at the shell middle surface.) and χ_s and χ_z are the change in curvature of the shell reference surface.

Using Equations 4-2 and 4-3, Equation 4-1 may be rewritten as

$$\begin{aligned} V &= \frac{1}{2} \int_V \left[c_{11} \varepsilon_s^2 + 2 c_{12} \varepsilon_s \varepsilon_z + c_{22} \varepsilon_z^2 \right] dv \\ &= \frac{1}{2} \int_V \left[c_{11} (\varepsilon_{s_0} + t \chi_s)^2 + 2 c_{12} (\varepsilon_{s_0} + t \chi_s) \right. \\ &\qquad \left. (\varepsilon_{z_0} + t \chi_z) + c_{22} (\varepsilon_{z_0} + t \chi_z)^2 \right] dt \, da \end{aligned} \tag{4-4}$$

Let the shell properties be defined as:

$$A_{ij} = \int_h c_{ij}\, dt \tag{4-5a}$$

$$B_{ij} = \int_h c_{ij}\, t\, dt \tag{4-5b}$$

$$D_{ij} = \int_h c_{ij}\, t^2\, dt \tag{4-5c}$$

where h is the total shell thickness. Then Equation 4-4 becomes

$$\begin{aligned} V = \frac{1}{2} \int_A \Big[& A_{11}\, \varepsilon_{s_0}^{\,2} + 2\, A_{12}\, \varepsilon_{s_0}\, \varepsilon_{z_0} + A_{22}\, \varepsilon_{z_0}^{\,2} \\ & + 2\, B_{11}\, \varepsilon_{s_0}\, \chi_s + 2\, B_{12}\, (\varepsilon_{s_0}\, \chi_z + \varepsilon_{z_0}\, \chi_s) \\ & + 2\, B_{22}\, \varepsilon_{z_0}\, \chi_z + D_{11}\, \chi_s^{\,2} + 2\, D_{12}\, \chi_s\, \chi_z \\ & + D_{22}\, \chi_z^{\,2} \Big]\, da \end{aligned} \tag{4-6}$$

For a cylindrical shell (with an infinite radius of initial curvature - flate plate) the strain displacement temperature measures are given by

$$\varepsilon_{s_0} = \frac{\partial U}{\partial S} - \alpha_{11}\, \Delta T \tag{4-7a}$$

$$\varepsilon_{z_0} = -\alpha_{22}\, \Delta T \tag{4-7b}$$

$$\chi_s = -\frac{\partial^2 W}{\partial S^2} \tag{4-7c}$$

$$\chi_z = 0 \tag{4-7d}$$

where ΔT is the temperature change in the element.

Thus Equation 4-6 reduces to

$$V = \frac{1}{2}\int_A \Big[A_{11}(U_{,s} - \alpha_{11}\Delta T)^2 - 2(A_{12}U_{,s} + B_{12}W_{,ss})\alpha_{22}\Delta T + D_{11}W_{,ss}^2 + 2B_{11}(U_{,s} - \alpha_{11}\Delta T)W_{,ss}\Big]\, da \quad * \qquad (4\text{-}8)$$

In order to maintain compatibility between contiguous shell elements, it is necessary to match nodal displacements and rotations. To facilitate this match U must have at least two degrees of freedom, W must have at least four degrees of freedom. To this end we select the element displacements in the form

$$U = \frac{1}{2}\Big[U_I(1-p) + U_J(1+p)\Big] \qquad (4\text{-}9a)$$

$$W = \frac{1}{4}\Big[W_I(2 - 3p + p^3) + W_J(2 + 3p - p^3) + \frac{\theta_I L}{2}(1 - p - p^2 + p^3) + \frac{\theta_J L}{2}(-1 - p + p^2 + p^3)\Big] \qquad (4\text{-}9b)$$

where $-1 \le p \le 1$ and

$$p = -1 + \frac{2}{L_i}S \qquad 0 \le S \le L_i \qquad (4\text{-}10)$$

In the above θ_I and θ_J are the nodal rotation $\frac{\partial W}{\partial S}\Big|_I$ and $\frac{\partial W}{\partial S}\Big|_J$ respectively. The strain energy may now be expressed in terms of the assumed displacement functions with

$$U_{,s} = U_{,p}\frac{\partial p}{\partial S} = \frac{1}{L_i}\Big[U_J - U_I\Big] \qquad (4\text{-}11)$$

---

*Some square terms in ΔT are deleted since they drop out when variations of V are taken.

$$W_{,ss} = W_{,pp} (p_{,s})^2$$

$$= \frac{1}{L_i^2} \left[W_I \cdot 6p - W_J \cdot 6p + \frac{\theta_I L}{2} (6p - 2) + \frac{\theta_J L}{2} (6p + 2) \right] \quad (4\text{-}11b)$$

In order to match shell displacements with the rock displacements (continuum elements), the shell displacements U_I, W_I, etc., are expressed in terms of u_I and v_I by the transformation equation (see Fig. 4-2).

$$U_I = \frac{A}{L} u_I + \frac{B}{L} v_I \quad (4\text{-}12a)$$

$$W_I = -\frac{B}{L} u_I + \frac{A}{L} v_I \quad \text{(etc. for } U_J \text{ and } W_J) \quad (4\text{-}12b)$$

Equation 4-8 is expressed finally in terms of u_I, v_I, θ_I, u_J, v_J, and θ_J as :

$$V = \int_{-1}^{+1} \frac{1}{2} S_i F_{ij} S_j - T_i S_i \, dp \quad (4\text{-}13)$$

where

$$F_{11} = A_{11}, \quad F_{12} = F_{21} = B_{11}, \quad F_{22} = D_{11} \quad (4\text{-}14a)$$

$$T_1 = A_{11} \alpha_{11} \Delta T + A_{12} \alpha_{22} \Delta T$$

$$T_2 = B_{11} \alpha_{11} \Delta T + B_{12} \alpha_{11} \Delta T + B_{12} \alpha_{22} \Delta T \quad (4\text{-}14b)$$

and

$$S_1 = U_{,s} \qquad S_2 = W_{,ss} \quad (4\text{-}14c)$$

The S_i are related to the nodal displacements through

$$S_i = G_{ijk} X_k \alpha_j \quad (4\text{-}15a)$$

where

where

$$\alpha_j = \langle u_I, v_I, \theta_I, 0, u_J, v_J, \theta_J, 0 \rangle * \tag{4-15b}$$

$$X_k = \left\langle -\frac{A}{L^2}, -\frac{B}{L^2}, \frac{A}{L^2}, \frac{B}{L^2}, -\frac{6Bp}{L^3}, \frac{6Ap}{L^3}, \right.$$

$$\left. \frac{3p-1}{L}, \frac{6Bp}{L^3}, -\frac{6Ap}{L^3}, \frac{3p+1}{L} \right\rangle \tag{4-15c}$$

The non zero G_{ijk} are

$$G_{111} = G_{122} = G_{153} = G_{164} = G_{215} = G_{226}$$

$$= G_{237} = G_{258} = G_{269} = G_{2,7,10} = 1 \tag{4-15d}$$

Thus Equation 4-13 becomes

$$V = \frac{1}{2} \alpha_j G_{ijk} F_{i\ell} H_{kn} G_{\ell mn} \alpha_m - \alpha_j G_{ijk} T_i Y_k$$

$$= \frac{1}{2} \alpha_j k_{jm} \alpha_m - \alpha_i f_j$$

where **

$$H_{kn} = \int_{-1}^{+1} X_k X_n \cdot \frac{L}{2} \, dp$$

$$Y_k = \int_{-1}^{+1} X_k \cdot \frac{L}{2} \, dp$$

---

*Numbering is for computer coding applications.

**It is to be noted that the above development depends on use of the computer to perform the indicated operations and construction is such that Gaussian quadriture may be used for the integrations. The number of operations does not excessively surpass the steps necessary to compute the element stiffness by hand explicity before programming is attempted (see listing) but greatly simplifies the coding.

The k_{jm} is the element stiffness and f_j the thermal load vector. Assembly into the shell structure stiffness proceeds in the usual manner by the direct stiffness method.

(3) Shell Properties

The shell properties for layered shells are obtained from Equation 4-5 by changing the c_{ij} for each layer. Accordingly one may write

$$A_{ij} = \sum_{k=1}^{N} \int_{h_k}^{h_{k+1}} c_{ij}^{(k)} \, dz = \sum_{k=1}^{N} c_{ij}^{(k)} \left[h^{k+1} - h^{k} \right]$$

where N is the number of layers in the shell, $c_{ij}^{(k)}$ are the properties of the "k" layer, h_k is the distance to the most negative surface of the k layer; and h_{k+1} is the distance to the most positive surface. Similarly

$$B_{ij} = \frac{1}{2} \sum_{k=1}^{N} c_{ij}^{(k)} \left[h_{k+1}^{2} - h_k^{2} \right]$$

$$D_{ij} = \frac{1}{3} \sum_{k=1}^{N} c_{ij}^{(k)} \left[h_{k+1}^{3} - h_k^{3} \right]$$

For a single layer, the above definitions reduce to those conventionally used in shell theory.

(4) Shell Forces

The forces in each element may be computed from the values of the nodal displacements and rotation using the constitutive equations together with Equations 4-7 and 4-11. The constitutive equations consistent with Love's first approximations are given by

$$N_s = A_{11}\,\varepsilon_s + A_{12}\,\varepsilon_z + B_{11}\,\chi_s + B_{12}\,\chi_z$$

$$N_z = A_{12}\,\varepsilon_s + A_{22}\,\varepsilon_z + B_{12}\,\chi_s + B_{22}\,\chi_z$$

$$M_s = B_{11}\,\varepsilon_s + B_{12}\,\varepsilon_z + D_{11}\,\chi_s + D_{12}\,\chi_z$$

$$M_z = B_{12}\,\varepsilon_s + B_{22}\,\varepsilon_z + D_{12}\,\chi_s + D_{22}\,\chi_z$$

For cylindrical shells in plane strain the most important shell forces are N_s and M_s which are, with aid of Equation 4-7, given by

$$N_s = A_{11}\,\varepsilon_s + A_{12}\,\varepsilon_z + B_{11}\,\chi_s$$

$$M_s = B_{11}\,\varepsilon_s + B_{12}\,\varepsilon_z + D_{11}\,\chi_s$$

Now Equation 4-11 completely defines each shell force over each element in terms of the nodal displacements. In the computer codes these are evaluated only at the midlength of each element. In addition the shear is evaluated from the equilibrium requirement

$$Q_s = \frac{\partial M_s}{\partial S}$$

with the displacement expansion used. The above expression reduces to

$$Q_s = -D_{11}\,W_{,sss}$$

(5) Computer Code

The above development has been coded in FORTRAN IV language. Preliminary debugging was accomplished for simple beam type configurations. The program was then used for a comparative study of the performance of stiffened shell linings as described below.

4.3 SHELL LINERS - EVALUATION OF ALTERNATE DESIGNS

To assess the effectiveness of tunnel linings in resisting loads, five tunnel liners were analyzed. The sections selected for analysis are alternate designs incorporating different types of stiffeners (see Fig. 4-3). Section A is an unstiffened steel liner. In Section B a 5/8 inch plate has been welded to the steel to make 7.2 inch deep stiffeners 12 inches on centers. In Section C, similar stiffeners have been added; they are 2-1/2 inches deep on 6 inch centers and are formed of 1/4 inch plate. All sections contain equivalent weights of steel.

The finite element mesh used in the analysis is shown in Figure 4-4. The liner appears as the circular line segment and has an inner radius of 42 inches. Under the loading it is assumed that a portion of the rock and concrete liner fail and will carry no load. The failed portion is then accelerated against the liner as in the example of Section 2.2-(5). The analysis utilized a pressure load on the shell to simulate the rock acceleration load. The same load has been used for each shell configuration, hence, the relative effectiveness of each liner with respect to the others may be assessed. During this preliminary investigation, only the displacement profiles have been computed. Also, only elastic shell behavior is included. The cases analyzed are listed in Table 4-1 and described in Figure 4-3.

The displacement plots for Cases 1-A1, 1-A2, and 1-B are shown in Figure 4-5 and for Cases 1-A2 and 1-C in Figure 4-6. From these figures it is observed that stiffeners will decrease displacements in the liner appreciably. The chances of complete collapse of the 1-A1 and 1-A2 configurations by the formation of plastic hinges in the region of high curvature should be considered in future analyses.

TABLE 4-1

Case	Tunnel Liner No.	Liner Section	Thickness (in.)	Concrete f'_c - (psi)
1-A1	1	A	1.000	3500
2-A1	2	A	1.000	9000
1-B	3	B	0.625	3500
1-A2	5	A	0.375	3500
1-C	7	C	0.375	3500

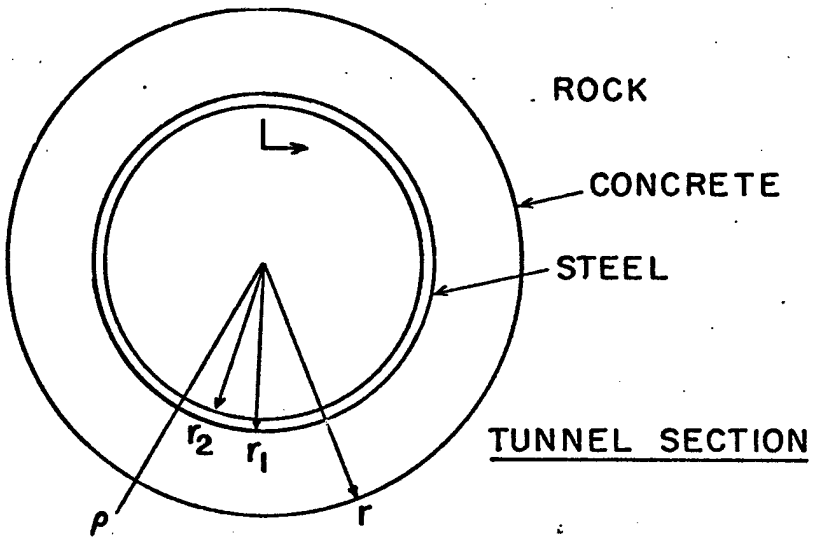

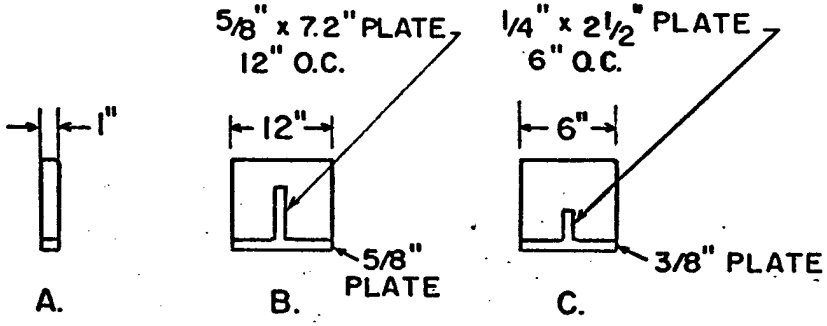

Tunnel Liner No.	Liner Section	Radii r in.	Radii r_1 in.	Radii r_2 in.	Concrete f'_c psi	Steel Thickness in.	Steel F_y psi	Steel ASTM
1	A	55.000	43.000	42	3500	1.000	36000	A 36
2	A	55.000	43.000	42	9000*	1.000	46000	A242
3	B	54.775	42.775	42	3500	See Sec. B	36000	A 36
5	A	50.375	42.375	42	3500	0.375	36000	A 36
7	C	50.250	42.375	42	3500	0.375	36000	A 36

*Assume that the addition of fine, chopped wire to the concrete increases the unconfined compressive strength from f'_c = 6000 psi to f'_c = 9000 psi. Refer to "Fibrous Reinforcements for Portland Cement Concrete" Technical Report No. 2-40, May 1965, ORDL.

Fig. 4-3. Shell Details

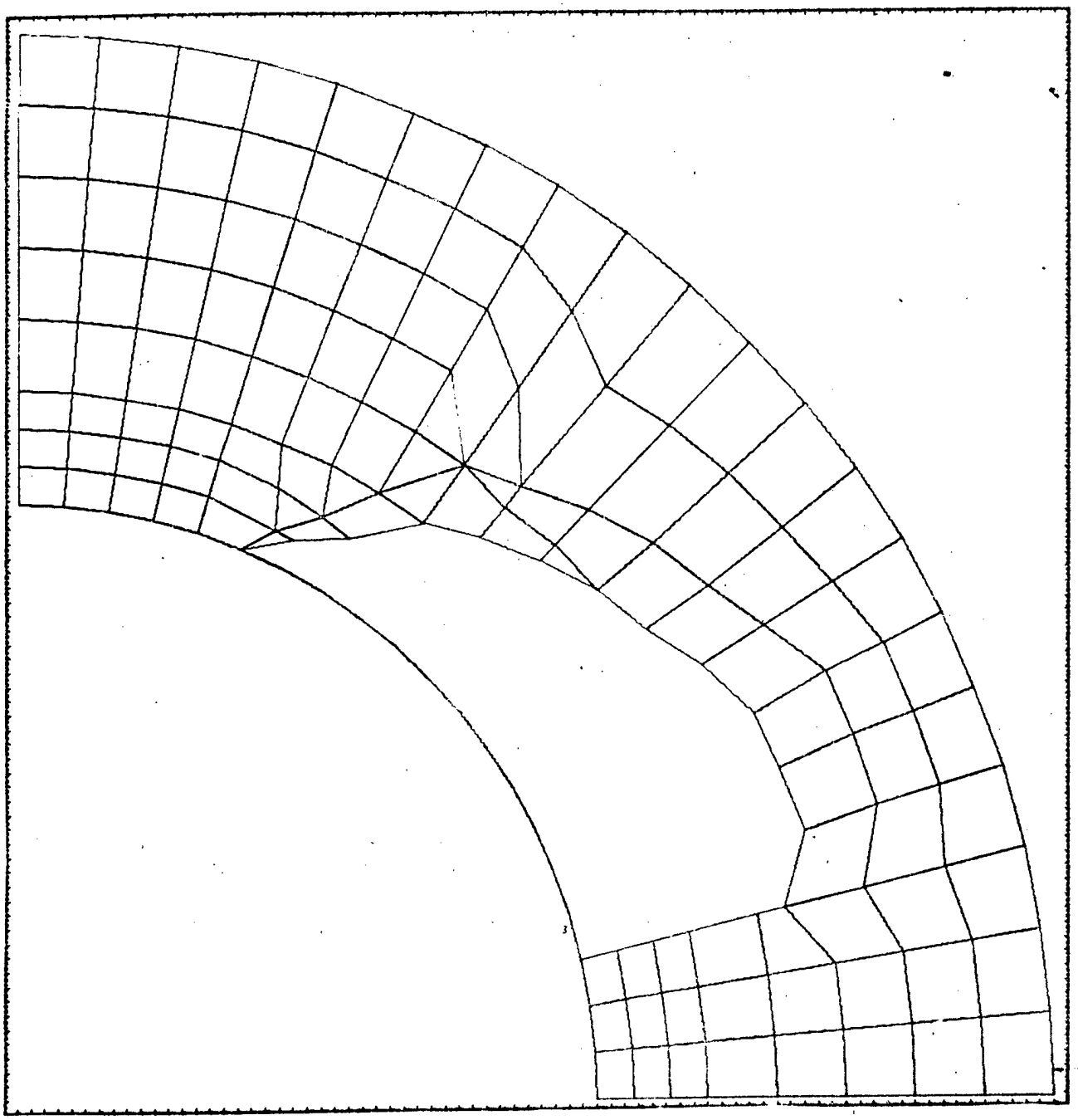

Fig. 4-4. Finite Element Mesh Used in Shell Lining Comparisons

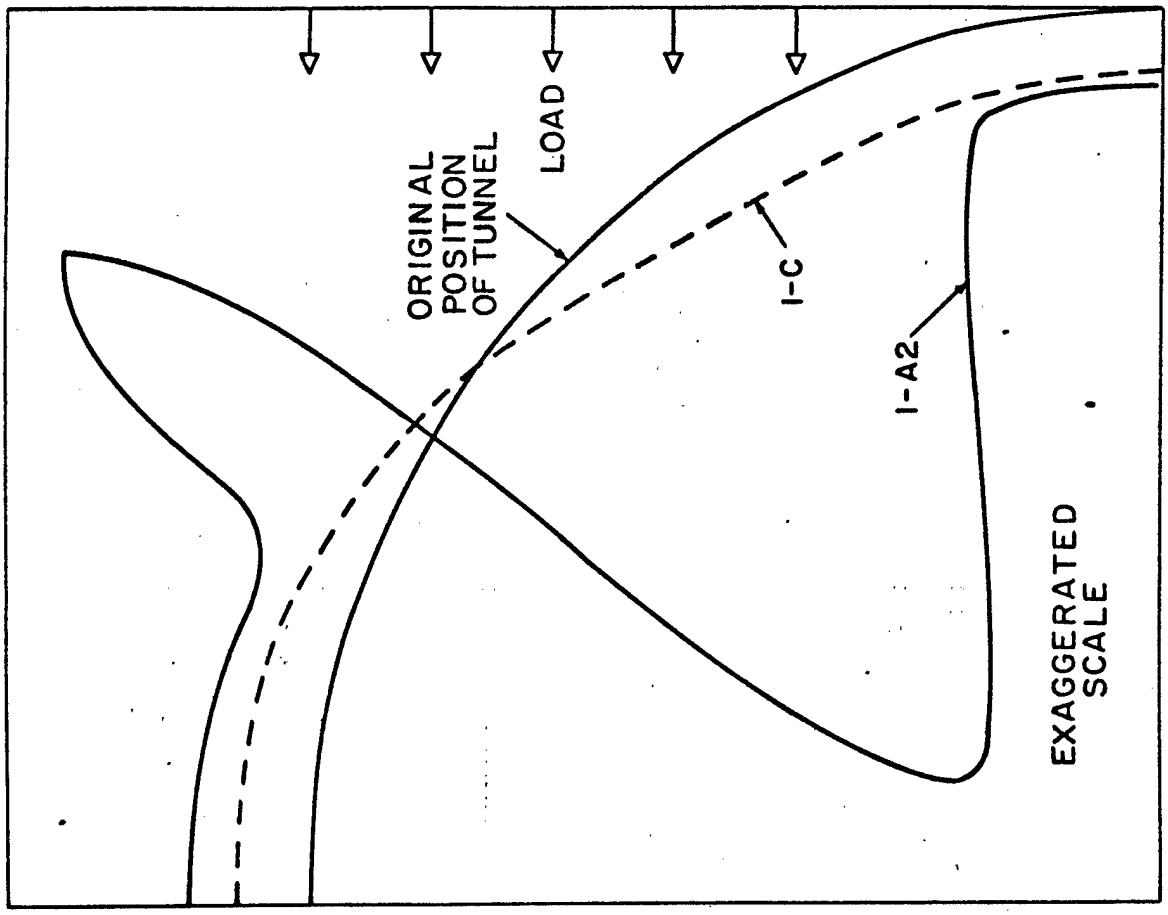

FIGURE 4-6 LINER DISPLACEMENTS. CASES I-A2 AND I-C.

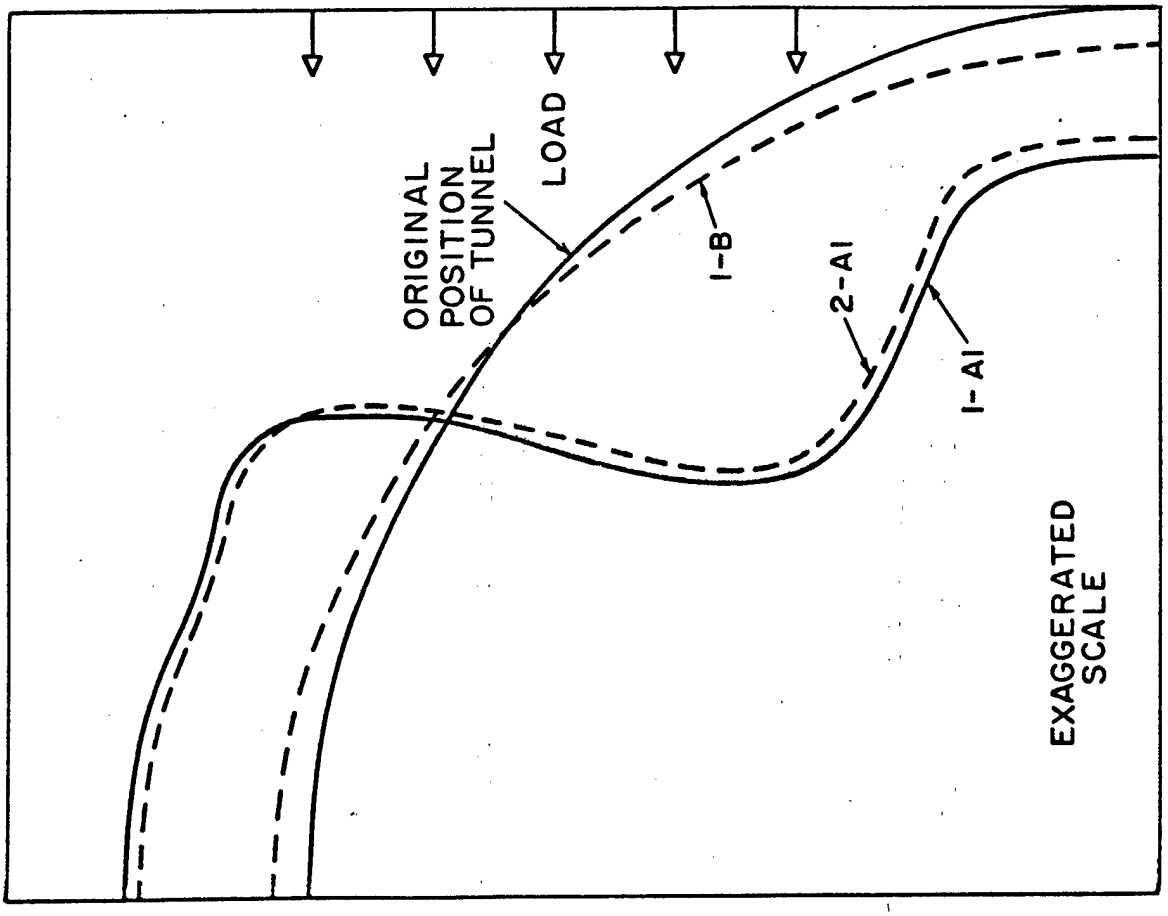

FIGURE 4-5 LINER DISPLACEMENTS. CASES I-A1, I-B AND 2-A1.

5. PERSONNEL AND ACKNOWLEDGEMENTS

Dr. Richard E. Goodman served as Principal Investigator and prepared Section 2 of this report. Dr. Tor Brekke contributed to Section 2.4 and to the development of the examples described in Section 2.3-(6). Also participating in work described in Section 2 were Michael Cleary, Jan Roggeveen, and Fred Sage. Dr. Robert L. Taylor and Dr. Goodman collaborated on the joint stiffness development. Section 3 of this report was prepared by Dr. Hans Ewoldsen. Dr. Taylor prepared Section 4 with the assistance of Mr. Gerald Goodreau.

The Principal Investigator served as coordinator of all aspects of the work and editor of the report and thus takes responsibility for its contents -- good and bad. He is indebted to Gloria Pelatowski, Ann Finucane, and Charles Bale for considerable help in preparing the final draft.

DISTRIBUTION LIST

(Number of Copies Shown in Parentheses)

Defense Documentation Center (20)
Building 5, Cameron Station, Alexandria, Virginia 22315

Director, Defense Atomic Support Agency (5)
P. O. Box 2610, Washington, D. C. 20305

Commander, Test Command, Defense Atomic Support Agency (3)
ATTN: TCDT-B, Sandia Base, New Mexico 87115

Chief of Engineers, Department of the Army, Washington, D. C. 20315

ATTN:	ENGMC-D (1)		ENGCW-E (1)
	ENGMC-E (1)		ENGCW-Z (1)
	ENGMC-M (1)		ENGCW-EG(1)
	ENGMC-EM(1)		ENGTE-E (1)

Division Engineers, U. S. Army Engineer Divisions

Lower Mississippi Valley	(1)	North Pacific	(1)
Missouri River	(1)	Ohio River	(1)
New England	(1)	South Atlantic	(1)
North Atlantic	(1)	South Pacific	(1)
North Central	(1)	Southwestern	(1)

District Engineers, U. S. Army Engineer Districts

Alaska	(1)	Nashville	(1)
Albuquerque	(1)	New Orleans	(1)
Baltimore	(1)	New York	(1)
Buffalo	(1)	Norfolk	(1)
Canaveral	(1)	Omaha	(1)
Charleston	(1)	Philadelphia	(1)
Chicago	(1)	Pittsburgh	(1)
Detroit	(1)	Portland	(1)
Fort Worth	(1)	Rock Island	(1)
Galveston	(1)	Sacramento	(1)
Huntington	(1)	St. Louis	(1)
Jacksonville	(1)	St. Paul	(1)
Kansas City	(1)	San Francisco	(1)
Lake Survey	(1)	Savannah	(1)
Little Rock	(1)	Seattle	(1)
Los Angeles	(1)	Tulsa	(1)
Louisville	(1)	Vicksburg	(1)
Memphis	(1)	Walla Walla	(1)
Mobile	(1)	Wilmington	(1)

Director, U. S. Army Engineer Waterways Experiment Station (5)
P. O. Box 631, Vicksburg, Mississippi 39180

Director, Ohio River Division Laboratories (2)
5851 Mariemont Avenue, Cincinnati, Ohio 45227

Director, U. S. Army Engineer Nuclear Cratering Group (1)
P. O. Box 808, Livermore, California 94551

Chief of Research and Development, Department of the Army (1)
ATTN: Atomic Division, Washington, D. C. 20310

Commanding General, U. S. Army Materiel Command (3)
ATTN: AMCRD-DE-N, Washington, D. C. 20310

Commander, Air Force Weapons Laboratory (2)
ATTN: Library, Kirtland AFB, New Mexico 87117

Air Force Ballistics Missile Division (1)
ATTN: WDGN, P. O. Box 262, Inglewood, California 90300

Headquarters, Ballistic System Division (1)
Air Force Systems Command, Norton AFB, California 92409

Director of Civil Engineering, Headquarters, U. S. Air Force (1)
ATTN: AFOCE Washington, D. C. 20330

Aeronautical Research Laboratory (1)
Wright-Patterson AFB, Ohio 45433

Director of Defense Research and Engineering (1)
ATTN: Technical Library, Washington, D. C. 20330

Ballistics Research Laboratory, Terminal Ballistics Laboratory
ATTN: Mr. W. J. Taylor (1)
Mr. A. A. Thompson (1), Aberdeen, Maryland 21005

Commanding Officer and Director, U. S. Naval Civil Engineering Lab. (1)
ATTN: Code L31, Port Hueneme, California 93041

Chief of Naval Operations, Department of the Navy (1)
ATTN: OP-71, Washington, D. C. 20350

Chief, Bureau of Yards and Docks, Department of the Navy (1)
ATTN: Code, Washington, D. C. 20370

U. S. Bureau of Mines, Office of Program Coordination (1)
ATTN: J. E. Crawford, Department of the Interiof,
Washington, D. C. 20240

U. S. Bureau of Mines
ATTN: Dr. Leonard Obert (1), Bldg. 20, Denver Federal Center,
Denver, Colorado 80225

U. S. Bureau of Reclamation
ATTN: Mr. W. H. Wolf (1)
Mr. George B. Wallace (1), Bldg. 66, Denver Federal Center,
Denver, Colorado 80225

U. S. Geological Survey (1)
Denver Federal Center, Denver, Colorado 80225

Colorado School of Mines
ATTN: Dr. John J. Reed (1), Golden, Colorado 80401

Dr. Richard S. Culver (1)
4020 Evans Drive, Boulder, Colorado 80302

University of Illinois, Civil Engineering Department
ATTN: Dr. Don U. Deere (1), 207 Talbot Laboratory
Dr. W. J. Hall (1), 111 Talbot Laboratory
Dr. A. J. Hendron (1), 207 Talbot Laboratory
Dr. N. M. Newmark (1), 1114 Civil Engineering Bldg.
Dr. J. L. Merritt (1), 2122 Civil Engineering Bldg.
Urbana, Illinois 61803

Pennsylvania State University, Department of Mining (1)
ATTN: Dr. R. Stefanko, University Park, Pennsylvania 16802

Texas A&M University (1)
ATTN: Dr. J. W. Handin, College Station, Texas 77843

South Dakota School of Mines (1)
ATTN: Professor E. M. Oshier, Rapid City, South Dakota 57701

Massachusetts Institute of Technology
ATTN: Dr. R. C. Hirschfeld (1)
Dr. W. F. Brace, Cambridge, Massachusetts 02139

University of Minnesota, Mining and Metallurgical Building (1)
ATTN: Dr. Charles Fairhurst, Minneapolis, Minnesota 55455

University of California, Department of Mineral Technology
ATTN: Dr. Richard E. Goodman (10)
Dr. Robert L. Taylor (2), Berkeley, California 94720

University of Missouri, Rock Mechanics Research Group (1)
ATTN: Dr. G. B. Clark, Rolla, Missouri 65401

University of Idaho, Department of Mining Engineering and
Metallurgy (1), ATTN: Dr. Samuel S. M. Chan, Moscow, Idaho 83843

American Cyanamid Company, Engineering-Chemical Research Center (1)
ATTN: Mr. R. H. Karol, P. O. Box 672, Princeton, New Jersey 08540

Illinois Institute of Technology Research Institute (1)
ATTN: Library, 10 West 35th Street, Chicago, Illinois 61816

Stanford Research Institute, Physical Sciences Division (1)
ATTN: Mr. F. M. Sauer, Menlo Park, California 94025

Rand Corporation (1)
ATTN: Dr. Harold Brode, 1700 Main Street, Santa Monica, Calif. 80401

Bechtel Corporation (1)
ATTN: Mr. Thomas A. Lang, 220 Bush Street, San Francisco, Calif. 94104

California State Department of Water Resources (1)
ATTN: Mr. J. A. Wineland, P. O. Box 388, Sacramento, Calif. 95802

Dr. Walter P. Moore, Jr. (1)
No. 2 Pinedale, Houston, Texas 77006

The Boeing Company, Missile and Information Systems Division (1)
ATTN: Mr. S. L. Strack, Seattle, Washington 98124

Aerospace Corp., WS 120A Basing and Ground Systems, Weapon System Division, ATTN: Mr. Martin Goldsmith (1), San Bernardino Operations, San Bernardino, California

UNCLASSIFIED

Security Classification

DOCUMENT CONTROL DATA - R & D

(Security classification of title, body of abstract and indexing annotation must be entered when the overall report is classified)

1. ORIGINATING ACTIVITY *(Corporate author)*
Omaha District, Corps of Engineers
Omaha, Nebraska 68102

2a. REPORT SECURITY CLASSIFICATION
UNCLASSIFIED

2b. GROUP

3. REPORT TITLE
Analysis of Structures in Jointed Rock

4. DESCRIPTIVE NOTES *(Type of report and inclusive dates)*
Interim

5. AUTHOR(S) *(First name, middle initial, last name)*
Richard E. Goodman

6. REPORT DATE	7a. TOTAL NO. OF PAGES	7b. NO. OF REFS
September, 1967	124	10

8a. CONTRACT OR GRANT NO.
Contract No. DACA45-67-C-0015

b. PROJECT NO.
Military Construction Investigational Program, O&MA Sub-Projects I-4 and II-2; DASA Subtask NWER 13.191 D.2 and

d. NWER 13.191 E.3

9a. ORIGINATOR'S REPORT NUMBER(S)
Technical Report No. 3

9b. OTHER REPORT NO(S) *(Any other numbers that may be assigned this report)*

10. DISTRIBUTION STATEMENT
This document has been approved for public release and sale; its distribution is unlimited.

11. SUPPLEMENTARY NOTES
Reference: Technical Report No. 2, Sept., 1966, same originating agency, "Geologic Factors in Design of Blast Resistant Tunnels".

12. SPONSORING MILITARY ACTIVITY
Department of the Army and Defense Atomic Support Agency, Washington, D. C. 20305

13. ABSTRACT

Two approaches to finite element analysis of the effects of rock joints and fractures on underground unlined, lined, or reinforced tunnel openings are considered. First, a three dimensional ubiquitous joint analysis is described and applied to tunnel design. Although this approach allows an estimate of the weakening effect of closely spaced joint sets, it is based on the assumption that the existence of a joint does not alter the stress distribution significantly. Since this may not always be a satisfactory assumption and because it may sometimes be desirable to model the action of individual joints occurring in determined locations, a new rock joint representation is developed and a joint stiffness analysis applied to a series of basic problems. The different types of rock joints and their relative significance are discussed and a classification system based on shear strength of the joint, stiffness perpendicular to the joint and tangential stiffness of the joint is suggested.

Using a finite element axisymmetric program, states of stress in the rock due to single and multiple rock bolt installation are examined and iso-stress maps of the triaxial compression zones are shown. States of stress in the vicinity of the rock bolt anchor and bearing plate are investigated. The effectiveness of a single rock bolt installation to strengthen rock joints of various orientations is investigated.

In a very preliminary study, the theory of a layered orthographic shell was coded using a finite element plane strain representation. An evaluation of the load resisting capability of various tunnel linings incorporating different types of stiffeners was made. Further analytical work is recommended.

DD FORM 1 NOV 65 1473 REPLACES DD FORM 1473, 1 JAN 64, WHICH IS OBSOLETE FOR ARMY USE.

UNCLASSIFIED

Security Classification

14. KEY WORDS	LINK A		LINK B		LINK C	
	ROLE	WT	ROLE	WT	ROLE	WT
Jointed Rock						
Rock						
Rock Bolts						
Composite Tunnel Liners						
Rock Bolt Reinforcement						
Rock Mechanics						
Rock Stress						
Finite Element						